Multi-Decadal Stochastic Streamflow Projections and Application to Water Resources Decision Making in the Colorado River Basin

by

Solomon Tassew Erkyihun

B. Sc. Addis Ababa University, 2000

M. Sc., Norwegian University of Science and Technology, 2004

A thesis submitted to the

Faculty of the Graduate School of the

University of Colorado in partial fulfillment

of the requirements for the degree of

Doctor of Philosophy

Department of Civil, Environmental and Architectural Engineering

2015

This thesis entitled:

Multi-Decadal Stochastic Streamflow Projections and Application to Water Resources Decision Making in the Colorado River Basin

written by Solomon Tassew Erkyihun

has been approved for the Department of Civil, Environmental and Architectural Engineering

_____

Dr. Edith Zagona

_____

Dr. Rajagopalan Balaji

_____

Dr. Roseanna Neupauer

_____

Dr. Joseph Kasprzyk

_____

Dr. Kenneth Nowak

Date_____

The final copy of this thesis has been examined by the signatories, and we find that both the content and the form meet acceptable presentation standards of scholarly work in the above mentioned discipline.

Erkyihun, Solomon Tassew (Ph.D., Civil, Environmental, and Architectural Engineering)

Multi-Decadal Stochastic Streamflow Projections and Application to Water Resources Decision Making in the Colorado River Basin

Thesis directed by Dr. Edith Zagona

Effective water resources planning and management requires skillful decisions on multi-year or decadal timeframes. In basins such as the Colorado River Basin (CRB), streamflow is not stationary but exhibits variability that reflects teleconnections with large scale climate indices such as Atlantic Multi-decadal Oscillation (AMO) and Pacific Decadal Oscillation (PDO). This research addresses this problem with four main contributions: It develops a stochastic streamflow simulation model and decadal scale streamflow projections based on these climate indices, compares this with other models recently developed, identifies and quantifies periods of unpredictability, and demonstrates the value of adding decadal scale projections to existing decision criteria in the CRB Supply and Demand Study (Basin Study).

The novel WKNN model identifies and reconstructs dominant signals in the AMO and PDO using wavelet analysis, simulates each using block K-nearest neighbor (K-NN) bootstrap, then simulates the streamflow using a K-NN bootstrap conditioned on the simulated climate forcings. Traditional methods develop similar models on the flow timeseries and have limited skill in projections. Here, the climate indices are modeled and streamflow generated conditionally, exploiting the skill in climate indices. Our WKNN model is compared with other recently developed methods – Conditional Hidden Markov Model and the enhanced wavelet autoregressive model – with respect to skill of projections over a range of lead times.

To understand and quantify the time-varying predictability of streamflow, we recover the underlying dynamics using a nonlinear dynamical system based approach. Time varying

predictability is assessed by quantifying the divergence of trajectories in the phase space with time, using Local Lyapunov Exponents (LLE). Ensembles of projections from a current time are generated by block resampling trajectories from the K-nearest neighbors of the current vector in the phase space.

Decadal scale WKNN projections and time varying predictabilities indicated by LLE are demonstrated to enhance existing decision criteria in the CRB Study that identify system vulnerability and invoke options and strategies to increase water availability or reduce demand through conservation or efficiency. Based on projections being wet, dry or unpredictable, improved decisions may reduce cost or reduce shortage and are illustrated by tradeoff curves of risk of shortage vs. cost.

Dedication

To my wife, Tigist and my three kids: Solyana, Bemnet and Hallalujah

Acknowledgement

I wish to thank my committee members with their expertise and precious time. A special thanks to my co-advisors Dr. Edith Zagona, my committee chairman and Dr. Balaji Rajagopalan for their reflection, guidance, and encouragement throughout the entire process. Thanks to Dr. Roseanna Neupauer, Dr. Joseph Kasprzyk, and Dr. Kenneth Nowak for serving on my committee.

I thank Dr. Kenneth Nowak, Dr. Jim Prairie and Alan Butler for devoting your time especially for details about the Colorado River Basin Water Supply and Demand Study. I am grateful for the Center for Advanced Decision Support for Water and Environmental Systems (CADSWES) staff, a special thanks to Jim Pasquotto.

I sincerely acknowledge the Bureau of Reclamation Lower Colorado Regional Office grant R12AC30023 “Inter-Decadal Streamflow Projection Research and Application to Operational Decision-making” for funding this research.

I am very grateful and thankful my family for their encouragement and support.

Contents

Figures

Tables

1 Introduction

1.1 Background and Research Objective

Modeling and simulation of streamflow timeseries is vital for any water resources planning and management [*Loucks & van Beek*, 2005]. Hydrological timeseries are characterized in terms of seasonality, trends, intermittency, and randomness [*Salas,* 1980]. Modeling hydrologic timeseries has a wide range of applications: generation of synthetic hydrological scenarios, determining the likelihood of extremes, forecasting, gap filling, trend analysis, etc. Stochastic timeseries modeling in water resources planning and management is a key ingredient of robust water resources planning [*Walker et al.,* 2003; *Lempert and Collins,* 2007; *Lempert and Groves,* 2010]. In the context of robust water resources plannng, timeseries models have been developed to i) generate ensembles of synthetic sequences that reflect the statistical characteristics of the observed record to portray the range of possible hydrologic scenarios and ii) predict (project) timeseries sequences on inter-annual to multi-decadal time scales for skillful planning and management [*Salas,* 1980]. Stationary timeseries models such as Auto Regressive Moving Average (ARMA) models assume parameters such as mean and auto correlation function of the timeseries do not change through time [*Salas,* 1980] and are the staple of traditional modeling approaches. Often streamflow timeseries exhibit a change in the mean and variance of the streamflow; the Colorado River flow at Lees Ferry (Figure 1.2) is a good example. This change in mean and variance with time in this research is referred as the non-stationary characteristic. The Colorado River water apportionment made in the early 1900s between the upper and lower basins was made during the "wet" epoch of Lees Ferry streamflow [*The Colorado River Compact,* 1922]. As this apportionment assumes higher average flows (a Lees Ferry mean flow of ~18MAF), meeting this demand during times of normal flow and dry epochs is a challenge.

Had the nonstationarity of the Colorado River flow been known during the early 1900s, adaptive decisions could have been made – e.g., to apportion the river flow based on water availability rather than fixed volume [*The Colorado River Compact,* 1922; *Minutes and Records of the Colorado River Commission,* 1922]. To this end, ability to model nonstationarity is crucial for efficient water resources planning decisions [*United States Department of the Interior,* 2001]. Recent wavelet spectral based methods offer attractive alternatives for modeling nonstationarity and also nonlinearity [*Kwon et al.,* 2007; *Nowak et al.,,* 2011].

Water resources planning and management in any river basin are directly or indirectly related to human activity, the environment, institutional policies and regulations and cultures. Beneficial use of the available water depends on its timing and magnitude along with the physical infrastructure (such as dams) used to manage it [*Gupta et al.,* 2011]. Particular water resources management decisions are made to meet the specified objectives of the river basin system such as water supply, flood control, power generation, navigation, recreation, environmental services, etc., subject to constraints such as policies and physical conditions.

Long term (multi-decades to century scale) plans for the physical infrastructure and operating policies of a basin should be made with consideration of the long term variability of hydrology and demands such that risks and reliabilities can be quantified [*Hallegatte,* 2009; *Yohe et al.,* 2004]. For short term (seasonal) decision making, e.g., decisions about reservoir releases on daily or seasonal timescales, a wide range of forecasting techniques are in use that rely on information about current and forecasted weather/climate conditions and may also rely in part on timeseries models, to determine operations that best meet system objectives [*Raff et al.,* 2013]. Between long and short term is multi-year to decadal scale decisions to implement changes that would take effect over several years and could benefit from projections based on understanding

of multi-year to decadal scale variability [*Nowak,* 2011]. This is an area that has recently gained traction among hydro climate scientists based on insights that relate streamflow variability at seasonal to multi-decadal time scales to climate forcings such as the El Nino Southern Oscillation (ENSO) [*Ropelewski and Halpert.,* 1986, 1989; *McCabe and Dettinger,* 1999; *Rajagopalan et al.,* 2000], the Pacific Decadal Oscillation (PDO) [*Latif and Barnett,* 1994; *Hidalgo,* 2004; *McCabe et al.,* 2007], and the Atlantic Multi-decadal Oscillation (AMO) [*Enfield,* 2001; *Tootle et al.,* 2005; *Timilsena et al.,* 2009]. Furthermore, these forcings are nonstationary and thus impart nonstationarity to the variability of precipitation and flow – this has been identified for Colorado River flows [e.g., *Nowak et al.,* 2012]

Water managers in the Colorado River Basin (CRB) anticipate increasing water demands in the coming decades [*Reclamation,* 2012]. This, along with the recent decade long dry spell and future drying from a warmer climate in the basin, leaves users at risk of unmet demands in the future. Under such circumstances, mid-term decisions may be considered either to increase the water availability through infrastructure development, transfers, etc., or to reduce demands through conservation and other options to use the available water more efficiently. The Bureau of Reclamation (Reclamation) recently undertook a major study, the Colorado River Basin Supply and Demand Study (henceforth referred as the Basin Study) to project future supply/demand imbalances in the CRB; in this they developed a decision making framework to explore the possibility of implementing options and strategies when the system shows signs of being vulnerable to the risk of not meeting demands [*Reclamation*, 2012]. The Basin Study decision algorithm identifies vulnerable states – when shortage is anticipated – using indictors such as streamflow and reservoir pool elevations based on the current and past states of the system. To mitigate the vulnerable states, options and strategies, which either increase the basin

water supply through infrastructure development or decrease demand through conservation, are identified for implementation. Since options and strategies always incur costs, effective decisions depend on accurate identification of vulnerable states so that appropriate options and strategies are implemented when needed but unnecessary costs are avoided.

This research seeks to improve decisions at the multi-year to decadal time scales by incorporating skillful projections of flow into the decision algorithm. Although we base this research on the CRB, the techniques and results can potentially be applied to other basins in the world. An important premise is that the flow variability exhibits periodicity at these time scales that provide a basis for skillful projections; recent literature on the CRB affirms this (*Nowak et al.,* 2011; *Bracken et al.,* 2014). Streamflow timeseries exhibit sustained multiyear (or decade long) wet and dry epochs determined from some threshold (such as mean and median of the timeseries). The early 1920s wet flow (sustained high flow based on the reference mean flow of 15 MAF) of the Colorado River flow and the recent drought in the southwestern US are good examples. In this research such variability is referred to as the nonstationarity characteristic *Read and Vogel* [2015].

1.2 Flow Characteristics of CRB and Role of Large Scale Climate Indices

The Lees Ferry flow gauge is a key station that divides the CRB into upper and lower basins used in operating policies (Figure 1.1). Located downstream of Lake Powell, the Lees Ferry station represents about 90% of the Colorado River flow [*Rajagopalan et al.,* 2009].

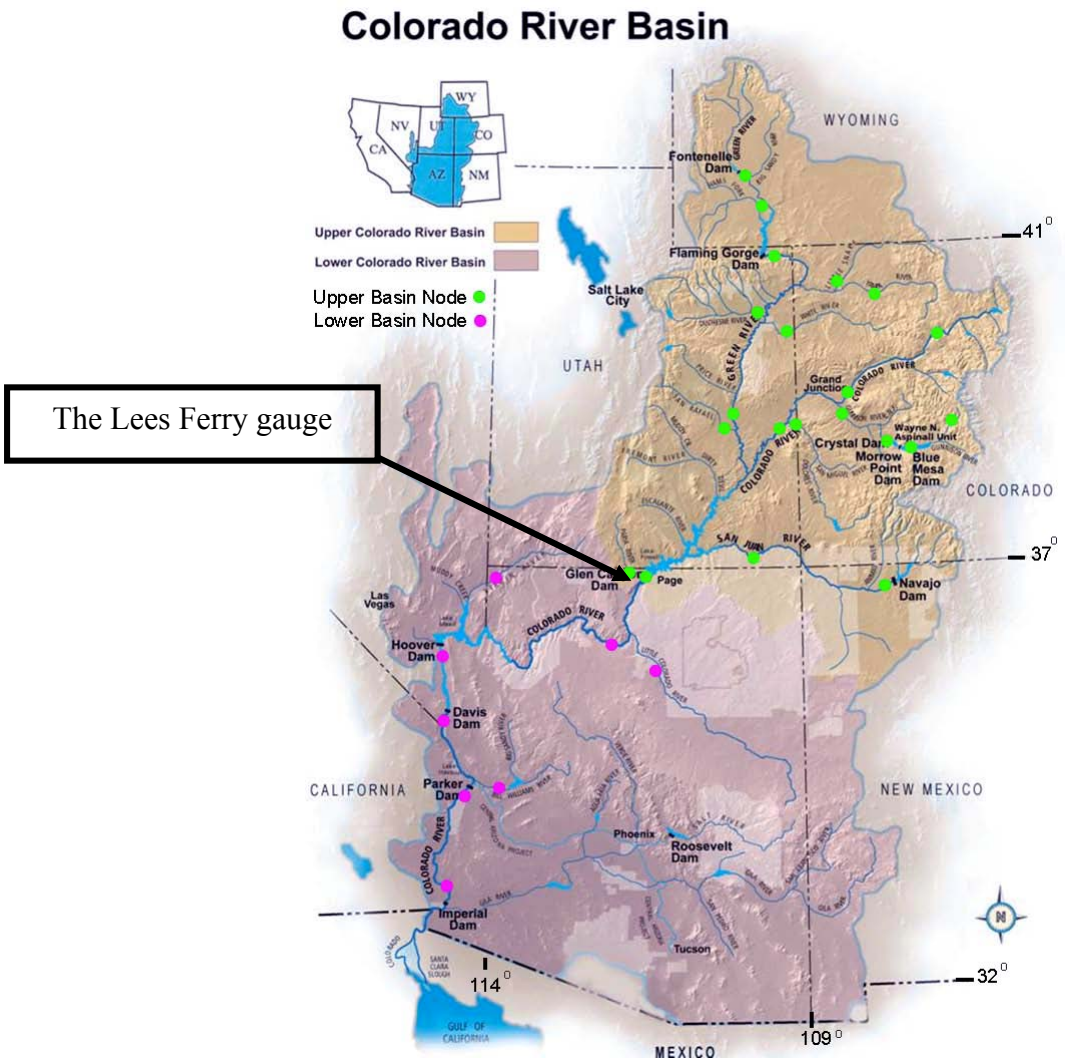

Figure 1.1 The Colorado River Basin and the basin states including Mexico. The green and purple dots are the natural flow nodes of the upper and lower Colorado River basins, respectively (adapted from Nowak [2011])

By removing anthropogenic effects such as regulation and diversions, the naturalized flow is regularly updated by Reclamation [*Prairie and Callejo,* 2005]. As can be seen in Figure 1.2, the annual variability of the naturalized Lees Ferry streamflow is very high with epochs of wet periods in the early 1900s and mid-1980s. To understand the long term variability, the Lees Ferry streamflow is reconstructed based on tree- ring chronologies [*Woodhouse et al.* 2006],

which show similar inter annual variability and a rich history of the non-stationary characteristics of the streamflow.

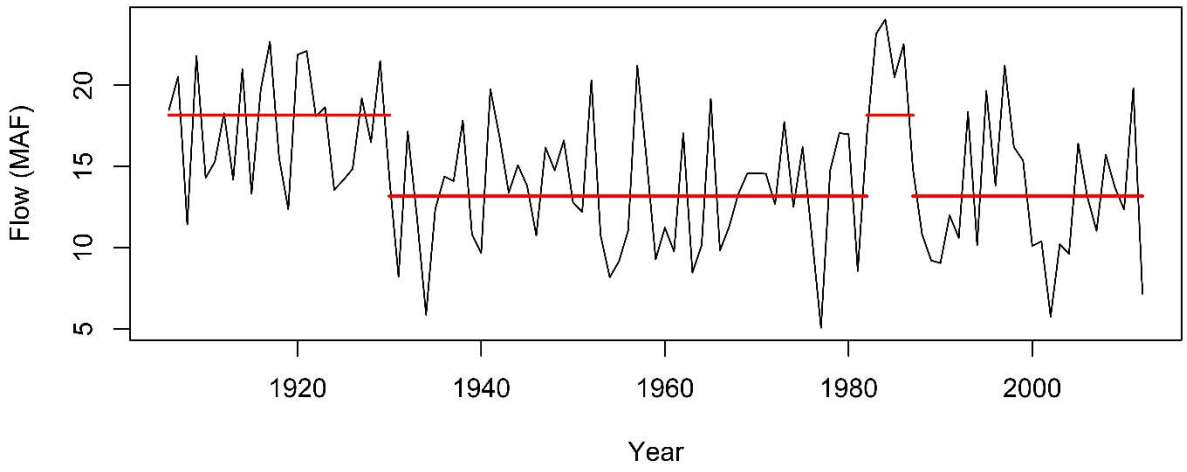

Figure 1.2: Timeseries plot of the naturalized streamflow at Lees Ferry (1906 – 2012) in the CRB. The horizontal lines show the mean flow values of the wet epochs (in in the early 1900s and mid 1980s with) and flow sequences for the rest of the time period with mean values of 18.2 MAF and 13.2 MAF respectively (Adapted from *Bracken et al.*,2014)

Large scale Sea Surface Temperature (SST) anomalies corresponding to large climate forcings defined earlier – AMO, PDO and ENSO – have been studied extensively to understand their connections with precipitation and streamflow over the United Sates (US) [*Ropelewski and Halpert,* 1986; *Redmond et al.,* 1991; *Dracup and Kahya*, 1994; *Latiff and Barnett,* 1994; *Rajagopalan et al.,* 2000; *Thomson et al.,* 2003; *Hidalgo,* 2004; *McCabe et al.*, 2007]. ENSO refers to the warm and cool phases of the El Nino and La Nina events in the tropical pacific, respectively, and is characterized by SST-based indices which are average of SST anomalies over different regions of central and eastern equatorial Pacific. The index, NINO3 (bounded by 90°W-150°W and 5°S- 5°N) is widely used to study the effects of ENSO on the hydro climatology of the US. During El Nino events, for example, the subtropical jet stream is

intensified bringing more moisture to the southwestern US, and vice versa during La Nina [*Redmond et al.,* 1991; *Timilsena et al.,* 2009; *Dracup and Kahya*, 1994; *Thomson et al.,* 2003]. ENSO has strong correlations with the surface climate of northwestern and southeastern parts of the United States [*Ropelewski and Halpert,* 1986]. However, it has a poor signal in the CRB [*Hidalgo and Dracup,* 2003; *Kahya and Dracup,* 1993; *McCabe and Dettinger,* 2002; *Grantz et al.,* 2005; *Regonda et al.,* 2006].

The recent drought since 2000 in the CRB fuels most of the recent research to describe the variability of the Colorado River flow through the observation of the PDO. PDO is defined as the first principal component of the northern pacific SST anomalies pole ward of 20^{o} N [*Zhang et al.,* 1997; *Mantua et al,* 1997] and typically shows ~50 years ~ 70 years of periodicity [*MacDonald and Case,* 2006; *Minobe,* 1997] and persists in the warm and cool phases in the range of 15 years-25 years [*Chao,* 2000]. There is strong evidence that the PDO has influence on the hydro climatology of the western US including the CRB at decadal time scales [*McCabe et al.,* 2004, 2007, 2008]. The warm phases of PDO with increased SST in the northern Pacific correlates with increased flow in the central and western US and vice versa when it is cold [*Tootle et al.,* 2005; *Hidalgo,* 2004; *Timilsena et al.,* 2009].

AMO is the variability of the SST in the North Atlantic Ocean (0 to 70^{o} N) with a period ranging from 60 to 80 years. The periodicity of the AMO index [*Enfield et al.,* 2001] compared to the PDO and ENSO, is the longest. The teleconnection of the AMO index with streamflow across the United States [*Enfield et al.,* 2001] and with the upper CRB at decadal and multi decadal timescales [*McCabe et al.* 1999*,* 2007; *Hidalgo,* 2004; *Nowak et al.* 2012] are well demonstrated. *Nowak et al.* [2012] showed the correlation of the low frequency variability of the Lees Ferry streamflow with the dominant frequency of the AMO index. In this, the Lees Ferry

streamflow tends to show increased flow with the warm phases of AMO and vice versa. Understanding the influence of climate indices (AMO and PDO) on the variability of the streamflow (for example the Lees ferry flow in the upper CRB), a stochastic streamflow simulation and projection model is developed conditioned on the variability of climate indices.

1.3 Stochastic Timeseries Models

The Auto Regressive (AR) models, a special case of ARMA models, have been the traditional approach of choice [*Thomas and Fiering* 1962; Salas, 1980] for the simulation of annual and seasonal streamflow. In this modeling framework, the process at a current time is modeled as a linear function of the process at previous time steps which captures the mean of the process, plus a noise or residual term which is normally distributed. Thus, normality of the process is a strong requirement. Flow series are rarely normal and in such cases the data is transformed before the AR model is fitted. This model has the ability to reproduce statistical characteristics of the streamflow such as mean, variance, skewness and lag correlations. If relationship with past values is nonlinear and data is not normally distributed, these models perform poorly. The introduction of non-parametric stochastic timeseries modeling approaches like the kernel density estimators [*Sharma et al.,* 1997] and K- Nearest neighbor (K-NN) time series bootstrap [*Lall and Sharma,* 1996*; Lall* 1995; *Rajagopalan et al.,* 2010] have to a large extent addressed the above drawbacks of linear AR models.

However, the nonparametric models cannot capture nonstationarity in spectral characteristics, an indicator of multi-decadal variability. These features are important for producing wet and dry spell characteristics and multi-year variability. Recent timeseries modeling approaches demonstrated on hydrologic series using Hidden Markov Model (HMM)

[e.g., *Bracken et al.,* 2014] and the wavelet spectrum based auto regressive models (WARM) [e.g., *Kwon et al.,* 2007, *Nowak et al.,* 2011] are significant additions to hydrologic timeseries simulation and prediction repertoire. In the HMM modeling approach, the observations are assumed to be a realization from hidden state sequences with a Transition Probability Matrix (TPM) and each state with its unique probability distribution [*Zucchini & MacDonald,* 2009; *Ibe* 2009]. The number of hidden states and the associated distribution parameters are estimated using objective methods such as the Expectation Maximization (EM) algorithm [*Zucchini & MacDonald,* 2009., 2009, *Bracken net al.,* 2014]. The HMM model uses the Markov chain for simulation. In this, the TPM is used recursively to simulate the next n time steps based on the current state. This recursive use brings the TPM it into a constant matrix after say n time steps. Simulating beyond the nth time step will produce a constant value, limiting the HMM simulations to the nth timestep. A timeseries for example with 2 hidden states (2 by 2 TPM) simulates shorter time steps compared to a timeseries of 3 hidden states (3 by 3 TPM). Therefore, nonstationary features of a timeseries can be better captured few years using the HMM model relative to ARMA models but are limited in their ability to capture multidecadal variability. However, they can be augmented with climate information to model multidecadal features well, as shown by *Bracken et al.,* [2014]. The WARM modelling approach [*Kwon et al.,* 2007] decomposes the timeseries into significant orthogonal periodic (or 'signal') components using wavelets and the residual is 'noise' [*Torrence and Compo*, 1998]. The significant components are modeled separately, as they are orthogonal, by AR models, and the noise, which is mostly White, is modeled as a Normal distribution. Simulation and prediction are obtained by adding the signal components from their respective AR models and the noise. This modelling

approach has been shown to skillfully reproduce the distributional properties -mean, variance, skewness and lag 1 correlation and also stationary spectral characteristics [*Kwon et al.,* 2007].

To capture nonstationarity in the spectrum, which is important for capturing long wet and dry epochs, Nowak *et al.* [2011] proposed an enhancement to the WARM by making the signal components stationary by normalizing them with the Scaled Average Wavelet Power (SAWP). This approach captures all the features of WARM and the time varying spectral characteristics – as shown for the CRB flows by *Nowak et al., [*2012].

The timeseries models described above (AR, WARM and HMM) are applied directly to the streamflow. Given the strong teleconnection of the large scale climate forcings of AMO and PDO with the CRB flows, this research seeks to find a new approach to incorporate these forcings in the stochastic streamflow simulation and projection approach. As mentioned earlier, based on the literature, it is becoming increasing clear that periodic and nonstationary characteristics of climate forcings translate into the teleconnected streamflow. Thus, we propose a new approach to simulate the climate forcings first and consequently simulate streamflow. For this, the wavelet based block bootstrap model, or Wavelet K- nearest neighbor (WKNN, *Erkyihun et al.,* 2015) is proposed to simulate the signal of the climate forcings using wavelets and block bootstrap and, conditionally simulate the streamflow using KNN bootstrap. Details of this of this new method are presented in Chapter 2.

A complementary novel approach using HMM is also proposed as an alternative simulation and projection model. In this, the climate forcings are modeled and simulated from HMM and the streamflow are conditionally simulated, as above. The performance of the three stochastic timeseries simulation and projection models – WARM [*Kwon et al.,* 2007], WKNN [*Erkyihun et al.,* 2015] and conditional HMM – are evaluated with respect to their ability to

capture the nonstationarity features of the streamflow. The projection skills of the models for lead times ranging from one to twenty years are evaluated; their results serve as a guide to identify appropriate simulation/projection modelling techniques for use in decision making purposes. These are described and presented in Chapter 3.

1.4 Streamflow Predictability and Simulation

Streamflow processes are realizations of nonlinear dynamical systems with coupled components – large scale climate forcings, precipitation, temperature, land surface properties of the watershed etc. - thus, the predictability of the streamflow varies over time. Stochastic time series models are not capable of reconstructing epochal behavior of predictability which strongly influences the simulation skill. Nonlinear dynamical systems based time series modeling approach provides ways to reconstruct the underlying dynamics of the system via reconstruction of phase space from the observed time series [*Kennel et al., 1992; Abarbanel and Lall, 1996*]. Utilizing the reconstructed phase space, the time varying predictability of the timeseries can be determined through Local Lyapunov Exponents (LLE) [*Abarbanel et al.,* 1992; *Bailey et al.,* 1995; *Guégan and Leroux, et al.,* 2011]. Applying this to CRB streamflow interesting epochal variations of predictability are identified. Furthermore, time series projections based on the phase space show that the skill varies with the epochal predictability [*Rajagopalan et al.,* 2015]. The application of this nonlinear dynamical modeling approach is demonstrated on the Lees Ferry streamflow and the results are presented in Chapter 4 along with the details of the method and its potential applications in water resources management.

1.5 Enhanced Decision Framework with Decadal Projections for the CRB

The Basin Study [1] recently conducted by Reclamation, was made to understand the possible future supply-demand imbalances over the 50 year planning period and also to identify possible ways to alleviate the future risks of shortage through scenario analysis. The scenarios are developed by considering the future demand, supply, legal, technical, climate change and environmental conditions of the Basin, simulated in the long term planning model, the Colorado River Simulation System (CRSS). CRSS is a complex object oriented model implemented using the RiverWare modeling tool at monthly time scale [*Zagona et al.,* 2001]. "It simulates the operation of the major Colorado River system reservoirs and generates information regarding the future state of the system such as: reservoir storage volume, reservoir water levels, and release from dams, diversions and return flows" [*Reclamation,* 2012]. The study identified a comprehensive list of options and strategies to alleviate possible shortfalls which can be broadly categorized into options that increase the basins water supply through infrastructure development, and strategies that reduce demand through conservation and those increasing the efficiency of existing system through operational modifications.

A decision making framework was developed that simulates the operations of the CRB for a wide range of hydrologic scenarios, and implements appropriate options and strategies based on the values of signposts. Signposts are indicators of vulnerability to shortage; they are typically a combination of current and recent past flow magnitudes and pool elevations. If for example, the Lake Mead pool elevation falls below a predefined level and the average Lees Ferry 10 years running flow volume (mean) is below a given threshold, vulnerability will be detected and the

[1] http://www.usbr.gov/lc/region/programs/crbstudy/finalreport/)

signpost informs the system to implement appropriate options and strategies to address this risk of shortage. Currently the decisions to implement options and strategies are made entirely based on the risk indicators at the current state of the system or in the past. This research proposes that better decisions can be made if skillful projections of future flow conditions were considered. For example, if vulnerability is detected, but a wet future flow condition is projected, that would mitigate the demand supply imbalance and the unnecessary cost of implementing an option would be avoided.

This research seeks to develop an approach to integrate the decadal scale streamflow projections with the decision making framework. The proposed approach will be tested first on a single historic data set to compare the performance of the decision with and without the projections with respect to resulting shortages and to the cost of implemented options and strategies. Then, an ensemble of future hydrologic scenarios will be generated using the appropriate timeseries model, and the decisions will be compared with the existing decision model to demonstrate improvements over the range of possible hydrologic scenarios.

1.6 Summary of Research Objectives

The overall goal of this research is to develop techniques to improve water resources planning decisions by incorporating skillful streamflow projections at decadal timescales on the CRB. The specific objectives of this research are listed below.

- To develop a stochastic streamflow simulation and projection model using large scale climate indicators which is capable of reproducing the non-Gaussian and nonstationarity characteristics of streamflow.

- To compare recently developed timeseries simulation models (Conditional HMM, WARM and WKNN), and investigate the suitability of these models for streamflow projection at different lead-times. This will help provide guidance in selecting the appropriate models for planning and management of water resources.
- To understand and quantify the time varying predictability of the CRB flow. Thus, identify predictable and less predictable epochs and incorporate the epochal streamflow projections with their predictability skill.
- To integrate the flow projections and the epochal predictability within an existing decision making framework to demonstrate the potential value of using decadal scale projections.

1.7 Outline of Thesis Chapters

This dissertation consists of six chapters. This introduction is followed by four chapters presented in a format suitable for submission to academic journals. Chapter six summarizes and concludes the dissertation with remarks for future work. An overview of the last five chapters are briefly presented as follows.

Chapter 2 develops the WKNN, the new conditional timeseries simulation/projection model that utilizes the strong teleconnection of large climate indices with streamflow. This modelling approach is a three-step process: (i) identify and reconstruct dominant signals in the climate indices with established teleconnections to streamflow using wavelet analysis [*Torrence and Compo.* 1998; *Kwon et al.,* 2007; *Nowak et al.,* 2011], (ii) simulate each climate signal using a block K-NN bootstrap [*Efron and Tibishirani*, 1993] and, (iii) simulate the streamflow using a K-NN bootstrap [*Lall and Sharma*, 1996] conditioned on the simulated climate forcings. The

application of this model is demonstrated by using the Lees Ferry streamflow and the large scale climate indices, AMO and PDO. Depending the decadal scale projection skill, this modeling approach will be used to improve the baseline decision making framework. Chapter 2 has been submitted to Water Resources Research and is in revision.

Chapter 3 seeks to identify the suitability of the WKNN model and recently developed timeseries simulation models the Conditional Hidden Markov Model (CHMM) and the WARM [*Kwon et al.,* 2007] for simulation and projection at inter annual, decadal and multi-decadal time scales. The comparison is mainly to identify the relative performances of the models in simulation and more on the performances of the three models in projection at different projection lead times. For example, for decadal scale planning, the model that performs well both in simulation and projection at decadal scale is appropriate. This chapter is in preparation for submission to an academic journal.

To determine the credibility of the decadal scale streamflow projections, Chapter 4 presents a nonlinear dynamical system based time series approach to understand and recover the underlying dynamics and time varying predictability of CRB flows. Time varying predictability is determined through LLE [*Abarbanel et al.,* 1992; *Bailey et al.,* 1995; *Guégan and Leroux, et al.,* 2011]. The phase space is the representation of the "true space" in which the dynamics unfolds. It is determined from the observation timeseries sequences through the process of embedding [*Kennel et al.,* 1992; *Abarbanel and Lall,* 1996]. Timeseries projections within the predictable epoch are credible and can be used in water resources planning to improve the baseline decision making process. This chapter has been submitted to Journal of Geophysical Research and is in review.

Chapter 5 presents the integration of the decadal scale timeseries projections in the Basin Study decision making framework. Integration of the projections and the predictability information is performed in two broad steps. (i) Identification of the predictable and less predictable epochs through the nonlinear dynamical modeling approach as described in Chapter 4. In the low predictable epochs the projections are not used in the decisions. (ii) Integration of the projections in the predictable epochs with the existing decision making framework. The integration is performed in such a way that the existing decision framework is informed about the future state of the flow through ensemble projections. The projections are then interpreted as wet or dry. If dry, the decision framework is informed about the future state of the flow to implement options and strategies as described earlier. However, if the future flow is "wet" the existing decision framework is informed to suppress decisions to avoid unnecessary cost in the implementation of options and strategies as the future "wet" flow could satisfy the demand supply imbalances. The results of the enhanced decision logic are reported and compared with the results of the original logic with respect to cost and shortages. This Chapter is in preparation for submission to an academic journal.

Chapter 6 summarizes the methodologies implemented and provides conclusions about the results. It also presents recommendations for future work to expand the methodological frontier to better address the possible future demand supply imbalances in the planning and management of water resources in the CRB.

2 Wavelet-based Time Series Bootstrap Model for Multi-decadal Streamflow Simulation Using Climate Indicators

A version of this chapter has been submitted as a paper to Water Resources Research and is in review.

Abstract

A novel model to generate stochastic streamflow projections conditioned quasi-oscillatory climate indices – such as the Pacific Decadal Oscillation (PDO) the Atlantic Multi-decadal Oscillation (AMO), and the El Nino Southern Oscillation (ENSO) is presented. Recognizing that each climate index has underlying band-limited components that contribute most of the energy of the signals, we first pursue a wavelet decomposition of the signals to identify and reconstruct these features from an annually resolved, proxy based, paleo-reconstruction of each climate index and, the historical data covering the period from 1650-2012. A k-nearest neighbor, block bootstrap approach is then developed to simulate each of these climate index series, while preserving their time-frequency structure, and marginal distributions. Finally, given the simulated climate index time series, a k-nearest neighbor bootstrap is used to simulate annual streamflow series, conditional on the joint state space defined by the climate index for each year. We demonstrate this method by applying it to simulation of streamflow at Lees Ferry gauge on the Colorado River using indices of two large scale climate forcings: Pacific Decadal Oscillation (PDO) and Atlantic Multi-decadal Oscillation (AMO) which are known to modulate the Colorado River Basin hydrology at multi-decadal time scales. Skill in stochastic simulation of multi-decadal projections of flow using this approach is demonstrated.

2.1 Introduction

Understanding streamflow variability and the ability to generate realistic scenarios at multi-decadal time scales is important for robust water resources planning and management in any river basin, especially in semi-arid basins such as the Colorado River Basin. It is increasingly evident that large scale climate forcings such as El Nino Southern Oscillation (ENSO), Pacific Decadal Oscillation (PDO) and Atlantic Multi-decadal Oscillation (AMO) modulate the hydroclimatology of the Western United States at multi-decadal time scales [*Tootle* et al., 2005*, Timilsena et al.,* 2009*; Enfield et al.,* 2001; *McCabe and Dettinger,* 1999, 2007 *Hidalgo*, 2004; *Nowak et al.,* 2012]. The influence of ENSO on the variability of precipitation and flows in western United States has been well documented [*Redmond and Koch.* 1991; *Timilsena et al.,* 2009; *Dracup and Kahya*, 1994; *Thomson et al.,* 2003]. The subtropical jet stream that funnels storms to this region during winter, which is the major source of moisture, is intensified over the southwestern US during El Nino events, bringing more rain and snow to this region while drying the northwestern US – vice-versa during La Nina events. This causes significant inter-annual variability in precipitation and stream flow. However, its direct impact on the Colorado Basin is weaker [e.g*., Regonda et al.,* 2006*; Grantz et al.,* 2005]. The PDO is a decadal phenomenon [*McCabe et al.,* 2004, 2007, 2008] that has been shown to influence western United States hydroclimatology along with ENSO over inter-annual and multi-decadal time scales [*Gershunov and Barnett,* 1998, *Rajagopalan et al., 2000*]. The positive phase of PDO with increased sea surface temperatures over the northern Pacific is generally associated with increased flow in the central and western United States and the negative phase with decreased flow [*Tootle et al.,* 2005; *Hidalgo,* 2004; *Timilsena et al.,* 2009]. Recent research indicates strong connections between AMO and hydroclimatolgy over the US. The warm phase

of Atlantic Multi-decadal Oscillation (AMO) is known to be associated with decreased flow conditions over most of the United States [*Enfield et al.,* 2001; *Tootle et al.,* 2005; *Timilsena et al.,* 2009]. AMO is also known to modulate the decadal to multi-decadal variability of flow in the upper Colorado River Basin [*McCabe and Dettinger,* 1999, 2007; *Hidalgo,* 2004; *Nowak et al.,* 2012]. While ENSO, AMO and PDO drive western United States hydroclimatology as evidenced by many researchers, AMO and PDO are the dominant drivers of flows in the Upper Colorado River Basin at inter-annual and decadal time scales as recently demonstrated by *Nowak et al.* [2012] and *Bracken et al.* [2014]. Lower Colorado Basin flows are also modulated by these climate forcings [*Thomas*, 2007].

There is a rich history of traditional time series simulation techniques [*Salas,* 1980; *Wei,* 2006] that fit linear models to the flow series. These models have done well with data where the hydrologic data did not exhibit long memory or nonlinear dependence, or quasi-oscillatory dynamics, or was not easily transformed to a Gaussian marginal distribution using the commonly used transforms. Nonparametric approaches were proposed to improve upon these methods to better reproduce nonlinear and non-Gaussian features in a Markovian context [*Lall,* 1995; *Lall and Sharma,* 1996*; Sharma et al.,* 1997]. A second approach that was introduced at about the same time was the use of a moving block bootstrap (*Vogel and Shallcross,* 1996) to address non-Markovian dependence. Subject to the choice of a block length, this method allows time series simulation that incorporates some long memory characteristics. However, it does not lend itself to conditioning on climate indices or other predictors of the time series of interest. Subsequently, wavelet based auto-regressive moving average methods were introduced to address the modeling quasi-oscillatory dynamics by *Kwon et al.* [2007]. Their approach was to decompose the time series into a small set of quasi-periodic components [*Torrence and Compo*, 1998] and a residual

time series. A traditional autoregressive moving average model is then fit to each of them components, including the residual process. The components are simulated and summed to obtain simulations of the original series. This method performed very well in capturing the global spectral properties, but not the nonstationarity of the spectrum. *Nowak et al.* [2011] enhanced this approach by scaling the components with their scale averaged wavelet power, a time varying estimate of the variance over selected scales, before fitting the autoregressive models, and then rescaling the simulated components with the same. This approach captured the nonstationarity in the spectrum very well. Recently, *Bracken et al.* [2014] showed that regime-like behavior of the Colorado River flows are forced by AMO and PDO, and used a non-homogeneous hidden Markov model to simulate the flow properties using these two climate forcings.

Given this background, we present a novel algorithm, WKNN that stands for wavelet-K-nearest neighbor which integrates over some of the features developed more recently. As in [*Kwon et al.*, *2007*] a wavelet projection is used to decompose each climate index into a small set of components, each of which explains a statistically significant fraction of the variance of the time series and is limited to a specific frequency band. Each component time series is then modeled using a k-nearest neighbor, block bootstrap method that is introduced. The goal of the method is to conditionally draw a block from the historical component time series given a current state vector. The k-nearest neighbors of the current state vector are used to provide samples of the conditioning distribution, distribution and a block of time series values that succeeds one of these k-nearest neighbors is then drawn at random, thus providing a conditional block bootstrap. A repeated application of this procedures allows one to develop a full time series with the appropriate time-frequency variability for the component time series. The

component time series are then summed to provide a simulation of the climate index of interest. Once the climate index time series are available, annual flows for each year are simulated using the [*Lall and Sharma, 1996*] k-nearest neighbor approach, conditional on the state space defined by that year's simulated climate indices. Following this procedure we are able to maintain the time frequency structure of the climate indices, and of the conditional distribution of annual flows given the climate indices.

The K-NN bootstrap approach was proposed by *Lall and Sharma* [1996] and applied to monthly streamflow simulation (i.e., lag-1 model). This method has been applied to multivariate stochastic weather generation [*Rajagopalan and Lall,* 1999; *Yates et al.,* 2003*; Caraway et al.,* 2014], paleo streamflow reconstruction [*Gangopadhyay et al.,* 2009], water quality modeling [*Towler et al.,* 2009] and others. The idea of resampling blocks of *B* capitalizes on the fact that there is significant dependence in the climate signals at least of lag *B* that needs to be captured. Typical literature on block bootstrapping described in this book [*Efron and Tibishirani,* 1993] is unconditional or without the feature vector and the neighbor selected as described above. Here we incorporated the feature vector to better able to capture non-stationarity. The modification with block resampling combined with wavelet components is unique and the novel aspect of this research.

The chapter is organized as follows. The data used in this research is presented first followed by the methodology and its components. Model validation is described and then the results. The summary of the results and discussion conclude the paper.

2.2 Data

The observed and paleo data of annual Colorado River streamflow and annual, climate indicators used are described below.

2.2.1 Colorado River flow at Lees Ferry, AZ

The Lees Ferry flow gauge, through which 90% of the flow in the basin passes, divides the Colorado River Basin into the upper and lower operational basins. Naturalized water year flow (sum of flows during Oct-Sep) at this gauge for the period 1906-2012 is used in this study. Monthly naturalized flow is computed by removing anthropogenic effects such as regulation and diversions. It is updated regularly by the United States Bureau of Reclamation [*Prairie and Callejo,* 2005] (http://www.usbr.gov/lc/region/g4000/NaturalFlow/current.html). The data has been used for planning studies in the basin and in other research [*Regonda et al.*, 2011; *Nowak,* 2011; *Miller et al.,* 2012]. In addition, tree ring reconstructed flows for the pre-1906 period covering 1490 to 1905 from *Woodhouse et al.* [2006] are also used in this study. The reconstructed data is available here: http://treeflow.info/upco/coloradoleeswoodhouse.txt.

2.2.2 Climate Indices, AMO and PDO

The AMO index [*Enfield et al.,*2001] is computed as a monthly area weighted average of North Atlantic (0 to 70^{o} N) sea surface temperatures (SST), which is subsequently de-trended, based on 5^{o} x 5^{o} resolution Kaplan SST [*Kaplan et al.,*1998]. Values were obtained from the NOAA Physical Sciences data website (http://www.esrl.noaa.gov/psd/data/timeseries/AMO/) for the period 1856 to present. The paleo reconstruction of annual AMO for the period (1650 – 1990) is based on reconstructions of annual sea surface temperature anomalies (SSTA) for the North Atlantic Ocean (0 to 70^{o} N) from tree rings [*Gray et al.,* 2004] and was obtained from the

NOAA website (ftp://ftp.ncdc.noaa.gov/pub/data/paleo/treering/reconstructions/amo-gray2004.txt).

Monthly PDO anomalies from 1900 to present are available from the University of Washington (http://jisao.washington.edu/pdo/PDO.latest). The annual data were taken as the average of the monthly (averaged over Oct-Sep, to be consistent with the flow) values in this analysis. The PDO is calculated as the first principal component of the Northern Pacific SST [*Zhanget al.,* 1997; *Mantua et al.,* 1997]. Annual PDO values for the period 993 – 1996, based on tree rings from *Pinus flexilis* in California and Alberta, Canada, were generated by *MacDonald and Case* [2005] and are available from the NOAA website (ftp://ftp.ncdc.noaa.gov/pub/data/paleo/treering/reconstructions/pdo-macdonald2005.txt).

In summary, we use historical and paleo-reconstructed records that cover a common period from 1906 - 2012, for the Colorado River flow at Lee's Ferry, the AMO and the PDO.

2.3 Proposed Methodology

The methodology we propose has three broad steps: (i) Decompose the large scale climate indices to obtain dominant signals in specific frequency bands that explain a statistically significant fraction of the signal's variance [*Torrence and Compo,* 1998; *Kwon et al.,* 2007]. (ii) Simulate these dominant signals independently using a new block K-nearest neighbor (K-NN) bootstrap approach. We refer to these two steps as wavelet KNN (WKNN); and (iii) Simulate the streamflow using K-NN bootstrap conditioned on the simulated climate forcings [*Lall and Sharma*, 1996] from the previous step. These steps are described below.

2.3.1 WKNN - Wavelet Decomposition

The first step is to decompose the climate indices using wavelets into orthogonal quasi-periodic components. For a detailed expose on wavelet analysis for geophysical applications we refer to *Kumar and Foufoula-Georgiou,* [1997] and *Foufoula-Georgiou and Kumar* [1994]. Here we follow the implementation procedures described in [*Torrence and Compo,* 1998; *Kwon et al.,* 2007; *Nowak et al.,* 2011]. A brief description is provided here.

The continuous wavelet transform of a discrete time series for a period *a* and time *n,* is given by:

$$W_n(a) = \sum_{j=0}^{N-1} \hat{x}_j \hat{\psi}^*(a\omega_j) e^{i\omega_j n\delta_t} \quad ---------(1)$$

where $\hat{x}_j$ is the discrete Fourier transform of the original time series; $\hat{\psi}^*(a\omega_j)$ is the Fourier transform of the wavelet function, ψ; *N* is the number of data points in the original data; δ_t is the time factor or time step (for annual data it is equal to 1) and ω is the angular frequency.

The Morlet is the preferred wavelet function for its boundary properties [*Torrence and Compo,* 1998] and its simplicity for time series applications. It is given by:

$$\psi_0(\eta) = \pi^{-1/4} e^{i\omega_0\eta} e^{-\eta^2/2} \quad ---------(2)$$

where ω_0 and η are the non- dimensional frequency and time parameters respectively [*Torrence and Compo,* 1998] . Since we use the Morlet wavelet, ω_0 = 5 is chosen [*Kumar and Foufoula-Georgiou,* 1997].

The wavelet spectrum represents the power at a period *a* and time *t*. In the wavelet literature the period *a* referred as scale. We refer to this as a period in the context of the quasi-

oscillatory modes of the time series used in this research. Averaging this across time provides the global wavelet spectrum. Tests of the statistical significance of the power at a given scale are typically based on a null hypothesis of a white or red noise process [*Torrence and Compo,* 1998]. Here, we used white noise for the null hypothesis. The global and nonstationary spectra of AMO and PDO are shown in Figures 2.1 and 2.2, respectively. Figures 2.1 (a) and 2.1(b) show the wavelet spectra of AMO for the observational and paleo periods, respectively. The white noise based confidence levels are shown for the global spectrum. Significant power can be seen in the 32 – 128 year period and longer for the paleo record. For the PDO (Figure 2.2), the multi-decadal band of 8 – 32 year period is dominant in recent decades in the observational period and sustained throughout the paleo period. The variation of PDO over a broad range of timescales is consistent with *Steinman et al*., [2015]. For the longer periods, the data is limited and thus, as indicated by the cone of influence, claims of significance of the power are not supported.

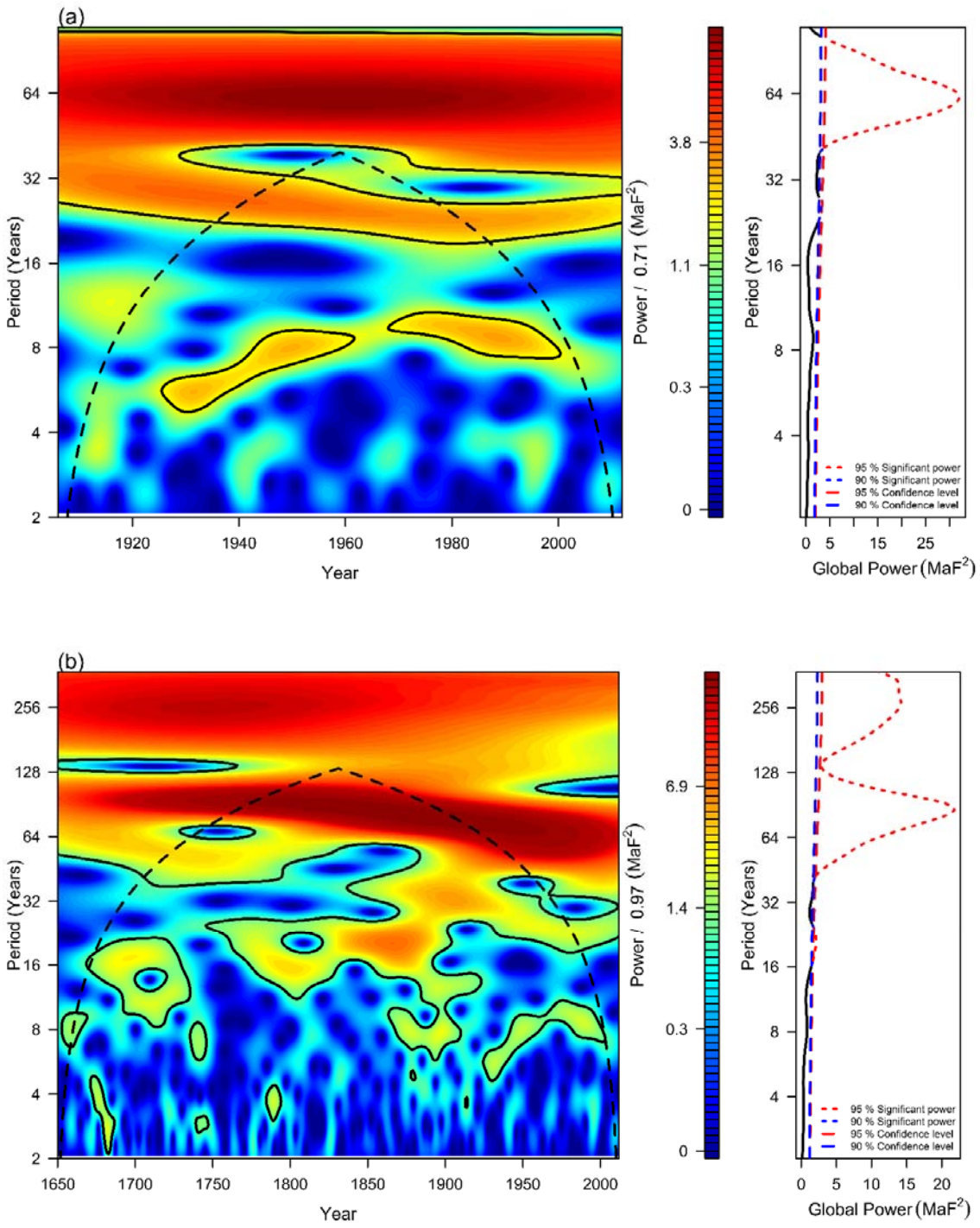

Figure 2.1: (a) Wavelet spectra of historic AMO and (b) Wavelet spectra of the historic and paleo AMO. Local power spectrum is on the left; the blue color demonstrates the lower power spectra and the red color the higher, and the dotted line is the cone of influence. The right hand side plot is the global power spectrum with 90% and 95% confidence level from white noise.

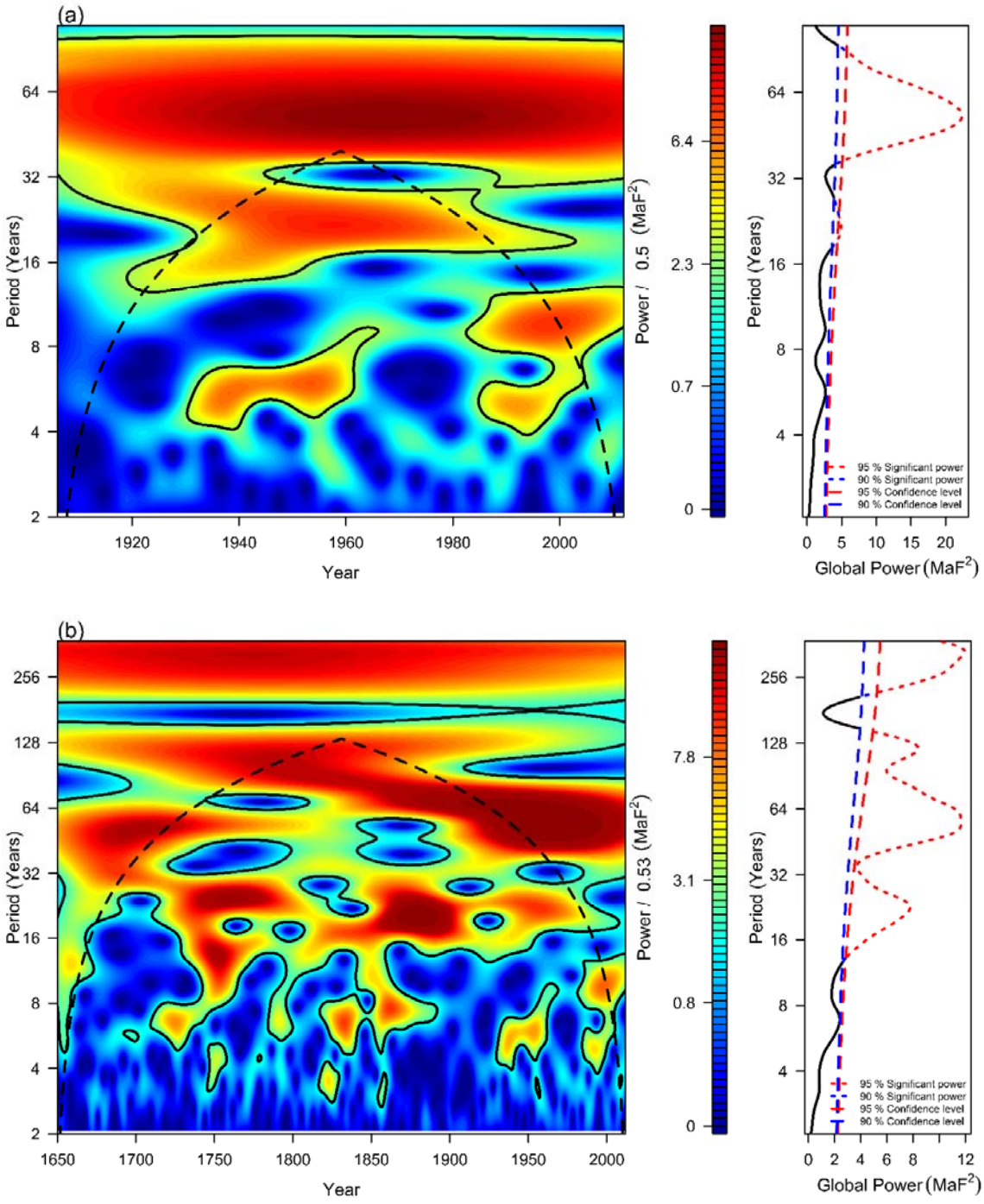

Figure 2.2 (a) Wavelet spectra of historic PDO and (b) Wavelet spectra of the historic and paleo PDO. Local power spectrum is on the left; the blue color demonstrates the lower power spectra and the red color the higher, and the dotted line is the cone of influence. The right hand side plot is the global power spectrum with 90% and 95% confidence level from white noise.

A component signal representing a frequency band where statistically significant power is identified, is obtained as:

$$x'_n = \frac{\delta_j \delta_t{}^{1/2}}{C_\delta \psi_0(0)} \sum_{j=j_1}^{j_2} \frac{R\{W_n(a_j)\}}{a_j{}^{1/2}} \quad \text{---------- (3)}$$

where C_δ and δ_j are reconstruction and scale factors respectively. $\psi_0(0) = \pi^{-1/4}$ is the factor that removes the energy scaling for Morlet wavelet function; *R* denotes the real part of the wave; and s_j is the scale. The j_1 and j_2 are the lower and upper limits of the frequency range over which the average is computed. For example, in the case of PDO this would correspond to the 8 and 32 year periods, for j_1 andj_2.

2.3.2 WKNN - Simulating the Climate Signal using Block Bootstrap

The steps are described below for simulating a sequence of a component signal of a climate index:

(i) For each reconstructed component signal, the characteristic period, $\bar{P}$, is identified, as: $\bar{P} = \frac{j_1 + j_2}{2}$ where j_1 *and* j_2 are upper and lower periods of the reconstructed signal. Then a block size, *B,* is computed which is half of $\bar{P}$.

(ii) For a given time *t,* a 'feature vector' of length *B* is created $[x_t, x_{t-1}, \ldots x_{t-B}$; *where* x_t *is the climate signal*] and *K* nearest neighbors of this feature vector based on Euclidean distance, are identified in the full record of the reconstructed component time series.

(iii) One of the k-nearest neighbors is randomly selected using a probability metric described by [*Lall and Sharma, 1996*], that is based on a likelihood function that is

based on the Euclidean distance of each neighbor from the current vector. The resulting probability of choosing the i[th] neighbor is given as:

$$W_i = \frac{\frac{1}{i}}{\sum \frac{1}{i}} \; ; \; i \; = 1,2,..,K \; - - - - - - - - (5)$$

(iv) Suppose the neighbor *j* is selected which corresponds to a calendar time *T*. A sequence of time series values for a block of length *B* that follows –i.e., $x_{T+1}, x_{T+2}, \ldots, x_{T+B}$ then constitutes the simulated values for the succeding *B* time steps *T*+1, *T*+2,..., *T*+*B*.

(v) The simulated block becomes the new feature vector and steps (ii) through (iv) are repeated to simulate the signal for time steps *t*+*B*+1, *t*+*B*+2, .., *t*+2*B*

The above steps are repeated to generate a sequence of any desired length *B* time steps at a time. *Lall and Sharma* [1996] proposed a heuristic choice for *K* as, $K = \sqrt{N}$ where *N* is the number of data points.

The initial block is selected randomly from the nearest neighbors of the first block of the climate signals. The above steps are applied to simulate sequences of all the reconstructed component signals. These simulated sequences of component signals are added to obtain the sequence of total signal. This is done for each climate index separately – i.e., AMO and PDO thus resulting in a sequence of simulated climate signal vector for each time, $Y_t = [AMO_t, PDO_t,]$.

2.3.3 Streamflow Simulation - Conditioned on Climate Signals

For each year conditioned on the simulated vector of signal of the climate indices, the streamflow needs to be simulated. This can be viewed as simulation from the conditional probability density function: $f(flow_t \mid Y_t)$ where the vector $Y_t = [AMO_t, PDO_t,]$ is the vector of signals of climate indices at time t, as described in the previous section. The K-nearest neighbors of Y_t are found from the historical data and one of neighbors (i.e., a historical year) is selected using the k-nn probability metric in equation 5. The streamflow of the selected year becomes the simulated flow for time t. This is repeated for each year with the simulated climate index vector to generate an ensemble of streamflow sequences.

2.3.4 WKNN Projection of the Climate Signals and conditional streamflow projection

The simulation algorithm presented in section 2.3.2 can be used in a streamflow projection application. Climate signals are projected and flow is resampled as follows.

(i) Current block of size B of the climate signals are used as a reference to identify the nearest neighbors from the past.

(ii) Sequences of climate signals of the desired projection window are resamples following the identified nearest neighbors from the past. The resamples sequences are projections.

(iii) Streamflow that corresponds to the projected climate signals is the streamflow projection.

2.4 Model Validation

We applied the methods of the previous section to simulate Lees Ferry streamflow using the two climate indices, AMO and PDO. We tested the model in two modes: (i) ability to simulate the primary statistics of the series and, (ii) the ability to simulate multi-decadal projections.

Since the climate indices are simulated based on low frequency components, the block bootstrap has relatively fewer blocks to select from when simulating for the historic period (1906-2012) using historic data. To demonstrate that this is not an issue, we simulated one of the climate indices, PDO, using WKNN with the entire record (paleo and historic) for the period longer historic period 1650 – 2012 and computed a suite of distributional and spectral statistics for comparison.

Then we applied it to the observed streamflow 1906 – 2012 (107 years), wherein WKNN was applied to generate 500 ensembles of the two climate signals, each of length 107 years. For each simulated climate signal vector, using K-NN resampling, streamflow values are generated. This validation approach is typical of any stochastic time series models – wherein the models are fitted to the data and simulations are made from them. A suite of distributional statistics of the simulated flow sequences is computed from the simulations – mean, variance, lag-1 autocorrelation, probability density functions (PDFs) and wavelet spectrum – and compared with those of the historical observational record. Wavelet spectrum is computed for the median flow of the simulations (i.e. median of ensemble of simulations at each time step) for comparison with the wavelet spectrum of the historic data. This demonstrates the ability of the method to capture the statistics and nonstationarity in the variability of the time series. To demonstrate the practical utility we compute deficit and excess statistics and compare them with the observations. We

point out that these aspects of performance of the flow simulations are solely dependent on the model's capabilities as they are not incorporated in the model.

To demonstrate the utility of the method in multi-decadal projections we apply the methodology and simulate streamflow sequences for 20 years at a time. This time horizon is chosen for its importance in near term planning and management decisions [*United States Department of the interior*, 2001].

This is done as follows: suppose we wish to simulate flow sequences for 20 years starting in 1906. We use pre-1906 data to fit the WKNN model and starting with 1905, simulate 500 ensembles of climate signals for the 20-year period 1906-1925. Conditioned on the simulated vector of climate signals, the streamflow is generated via K-NN bootstrap, also using pre-1906 data – therefore, making the projections truly blind. This is repeated for all the years in 1906-2012 thus, from each year a 20-year projection is made. We show the boxplot of ensembles of projected 20-year mean along with the 20-year mean flow of the natural flow. As mentioned earlier, skillful multi-decadal projections are potentially useful for water resources planning on the river system.

2.5 Results

We applied the WKNN approach directly to the Lees Ferry flows and generated simulations for the observational period. In this the component signals of the flows were generated using block bootstrap and subsequently the noise component was added to obtain the complete flow variance. As expected, the simulations could not capture the nonstationarity in the spectrum and poorly on other statistics (figures not shown). This is mainly due to the fact we have to add the noise in order to get the full flow variance. Simulating streamflow from signals

of large scale climate forcings seems to perform skillfully. Furthermore, this model can be combined with simulations of climate forcings from global climate models to exploit the teleconnections. Below we describe results from our proposed model.

2.5.1 Climate Index Simulation

The component signals of AMO are based on the period ranges of 23 - 27 years and 40-90 years [Figure 2.1]; while those of PDO are based on 20 – 27 years and 40-90 years [Figure 2.2]. The higher period ranges are outside the cone of influence, more so during the observational period, but they are within for most part during the paleo period. Furthermore, the relationship between these indices and Lees Ferry flow in these general period bands has been shown by others [*Nowak et al.,* 2011; *Switanek and Troch,* 2011]. The spectral power of the climate indices shows temporal variability (Figures 2.1 and 2.2) as mentioned above, indicative of nonstationarity which also induces quasi-periodicity. The nonstationarity in the flows will be described later. Our objective here is to simulate the flow conditioned on these signals and to the extent they are significant we exploit their quasi-periodic behavior and links to flow.

As mentioned, in order to test the performance of the WKNN model in simulating the climate indices, we first demonstrated on the simulations of the climate index, PDO, for the longer historic period 1650 – 2012 using both the paleo and observed data. Simulating the longer period (1650 – 2012) allows for a rich variety of blocks to be resampled. The component signals are simulated using the block bootstrap approach described in the methodology section and the residuals are simulated using a lag-1 K-NN bootstrap [*Lall and Sharma,* 1996], for consistency. However, a standard lag-1 auto regressive model (AR1) was also be used and the results were quite similar. Thus simulated PDO sequences were used to compute a suite of statistics and compared with that from the longer period. We show results from simulations of PDO as the

performance of simulations from AMO is similar. Figure 2.3 shows the boxplots of basic distributional statistics – mean, variance, skew and lag-1 autocorrelation of simulated PDO with the historic values shown as red dots. It can be seen that the simulations capture the observed statistics within the inter-quartile range, except for variance and lag-1 autocorrelation which are under simulated. However, the actual difference between the historic value and the median of the simulations are quite small ~0.2 for variance and ~0.09 for lag-1 autocorrelation.

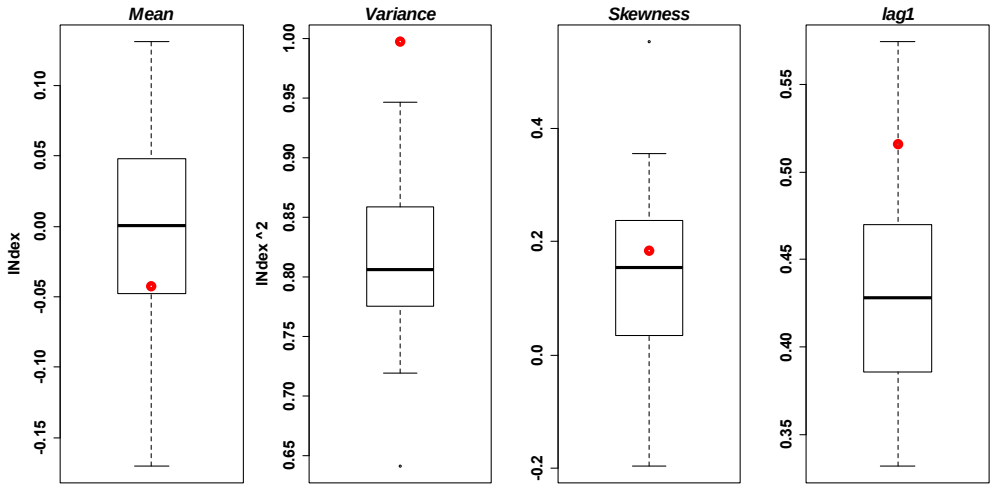

Figure 2.3 Boxplots of basic distributional statistics from the PDO simulations, red dot is the corresponding value of the longer historical period (1650 – 2012).

Figure 2.4 shows the simulated and historical PDF, which also is seen to be captured quite well, with the simulated PDF being more symmetric.

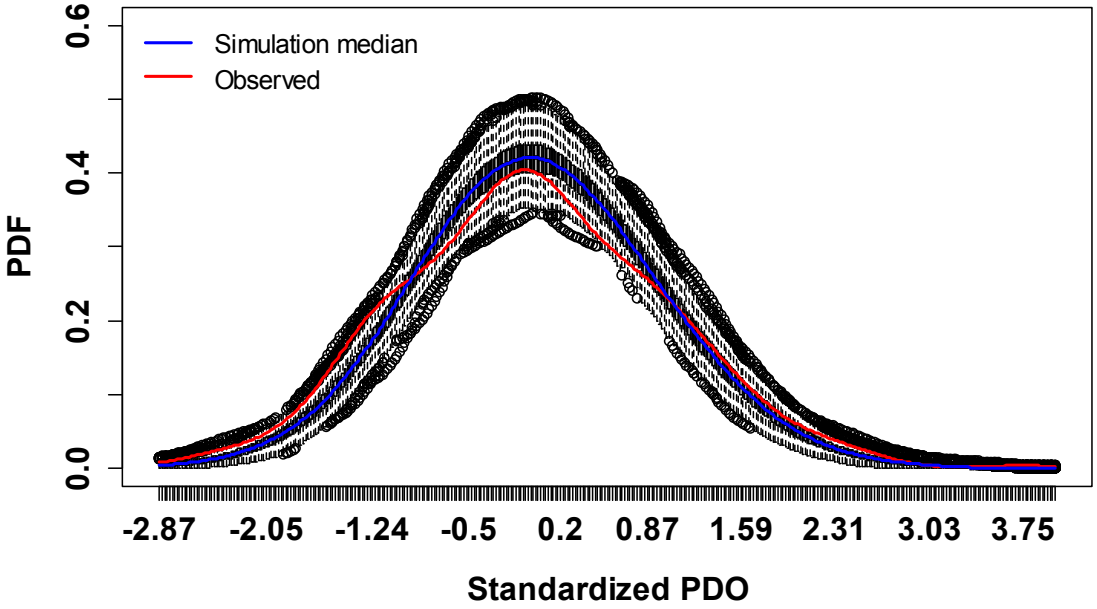

Figure 2.4 Probability Density Functions of simulated PDO simulation shown as boxplots, the blue line is the median PDF and the red is from the historical data.

The wavelet spectrum of the historical data and the median spectrum from the simulations are shown in Figures 2.5 a and b, the global spectra are on the side of these panels.

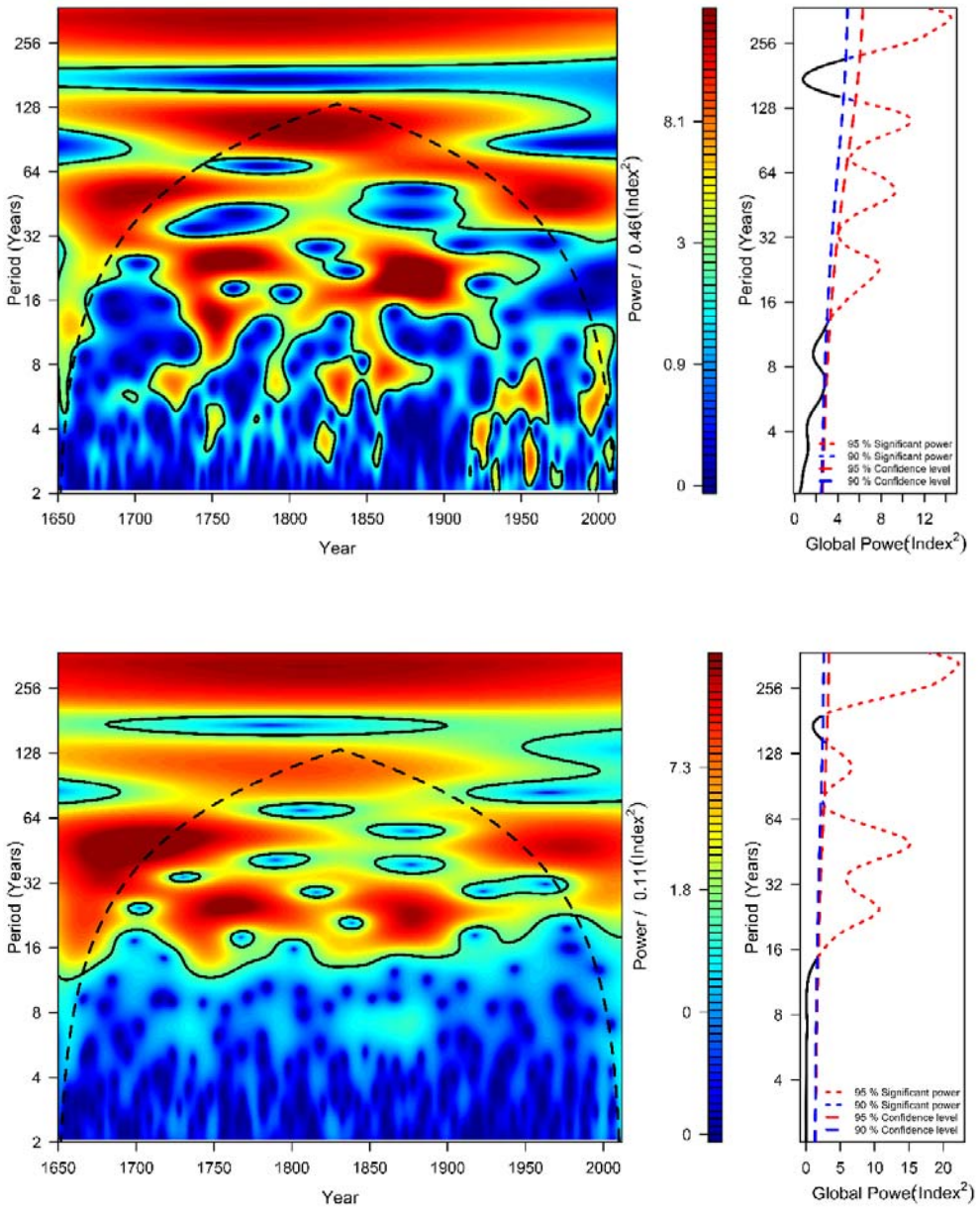

Figure 2.5 (a) Power spectrum of longer historic PDO anomaly (1650 -2012) – local spectrum on the left and global on the right, (b) Same as (a) but median spectrum of PDO from the WKNN simulations

It can be seen that the local and global spectra are very well simulated. All four spectral peaks in the historic period (Figure 2.5a) are captured well in the simulations (Figure 2.5b). Furthermore, the nonstationarity in the spectrum – the 32-64 year band being active during 1650-1750 and then during 1950-present (Figure 2.5a) is well captured in the simulations (Figure

2.5b). Similarly the 16-32 year band which is active during 1750-1900 and weaker in recent decades is also well captured by the simulations. These results demonstrate the capability of WKNN in simulating distribution and nonstationary features of the signal of climate indices – which are important to generate sustained wet/dry sequences of the flows.

2.5.2 Lees Ferry Streamflow Simulations

We used the WKNN to simulate PDO and AMO for the historical period (1906-2012) and conditionally simulate the streamflow. Figure 2.6 shows the boxplots of distributional statistics from flow simulations along with the historical values. It can be seen that the simulations reproduce very well the basic statistics - mean, variance skew and lag-1 autocorrelation. We note that the lag-1 correlation in the streamflow is entirely simulated from the climate indices – considering this, the simulations are quite good.

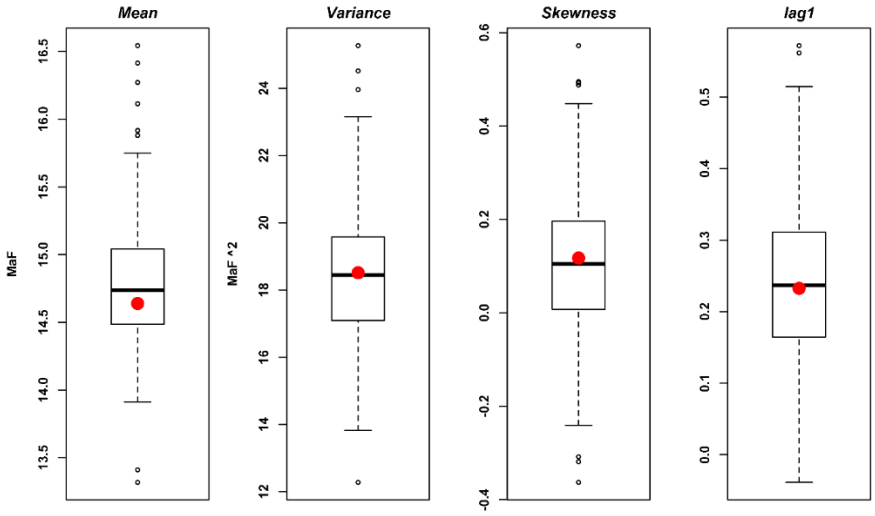

Figure 2.6 Boxplots of basic distributional statistics from the Lees Ferry flow simulations, red dot is the corresponding value of the historical data (19066 – 2012).

The boxplots of the PDF (Figure 2.7) from the simulations also capture the historical PDF very well indicating that the shape of the distribution and consequently the cumulative distribution function is also reproduced.

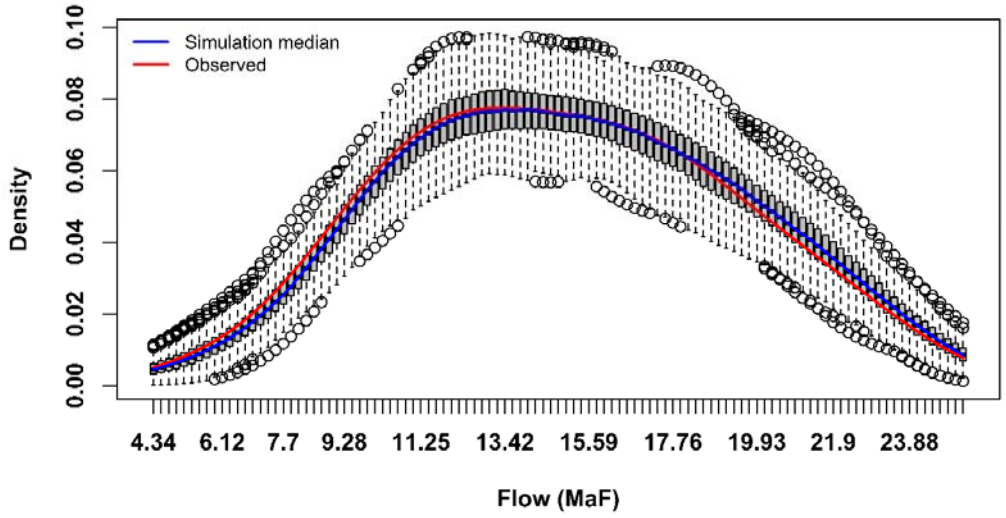

Figure 2.7 Probability Density Functions of simulated Lees Ferry flow shown as boxplots, the blue line is the median PDF and the red is from the historical data.

We calculated the excess and deficit statistics based on the median annual flow of the historical period (1906-2012), 14.52 Million Acre Feet (MAF). Excess is defined as the magnitude of flow in excess of the median and deficit the magnitude less than the median. We computed the total, maximum and minimum magnitude of the excess and deficit sequences to assess the ability of the simulation in capturing these spell quantities. The boxplots of these statistics from the simulations are shown in Figure 2.8 along with the corresponding values from the historical sequence as red dots. It can be seen that the deficit and excess statistics are asymmetric with lower values for the deficit and higher for the excess indicative of how well they are reproduced by the simulations.

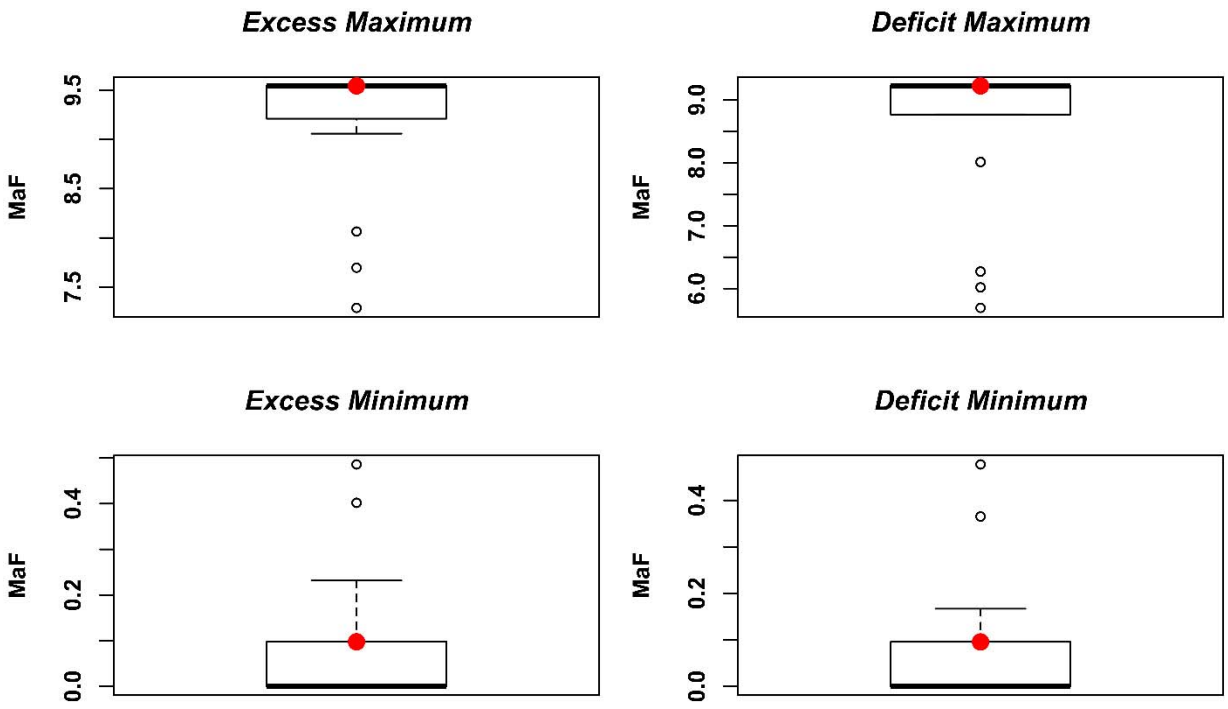

Figure 2.8 Boxplots of Deficit and excess statistics from the simulations along with the corresponding values based on historical series shown as red dots.

To further assess the performance of the simulations in capturing wet and dry sequences which are crucial for water resources management, we computed storage statistics using the sequent peak algorithm [*Loucks and Van Beek,* 2005]. In this, for a given flow sequence and a selected demand (or yield) to be met the required reservoir storage is computed. Thus, storage-yield curve is obtained for several demand scenarios. The effect of critical droughts is captured in this approach. Figure 2.9 shows the boxplots of storage for different demand levels from the simulations along with that from the historical flow sequence. It can be seen that the storage from the historical flow sequence (red dots) is very well captured within the boxes, indicating that the simulations are able to reproduce the stretches of wet and dry sequences that are important in the storage calculations and, in facilitating robust long term planning.

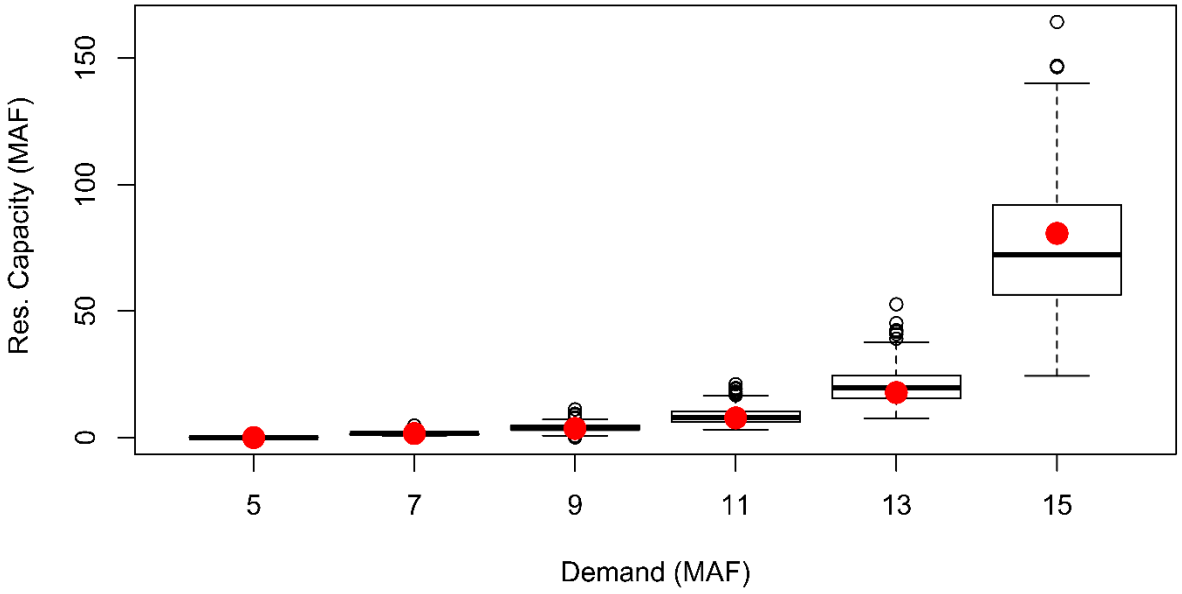

Figure 2.9 Boxplots of storage for several demand values based on the simulations overlaid by the storage from the historical flows shown as red dots

The spectrum of the median flows from the simulations and that of the historic flows are shown in Figure 2.10. The nonstationarity in the spectrum – especially the power in the 8-16 year period in recent decades is very well captured by the simulations. The global spectrum (figures on the right in both the panels) too is simulated well although the amplitude of the median peaks is smaller. The fact that the nonstationarity in the flow spectrum is captured purely from the climate indices is remarkable. We point out that the simulation methodology is not designed to reproduce the spectrum or distributional properties of the flows as the flows are simulated as a consequence from the climate indicators. The median of all the spectra for each time and period was found to be similar to the spectrum of the median flows from the simulations described in Figure 2.10.

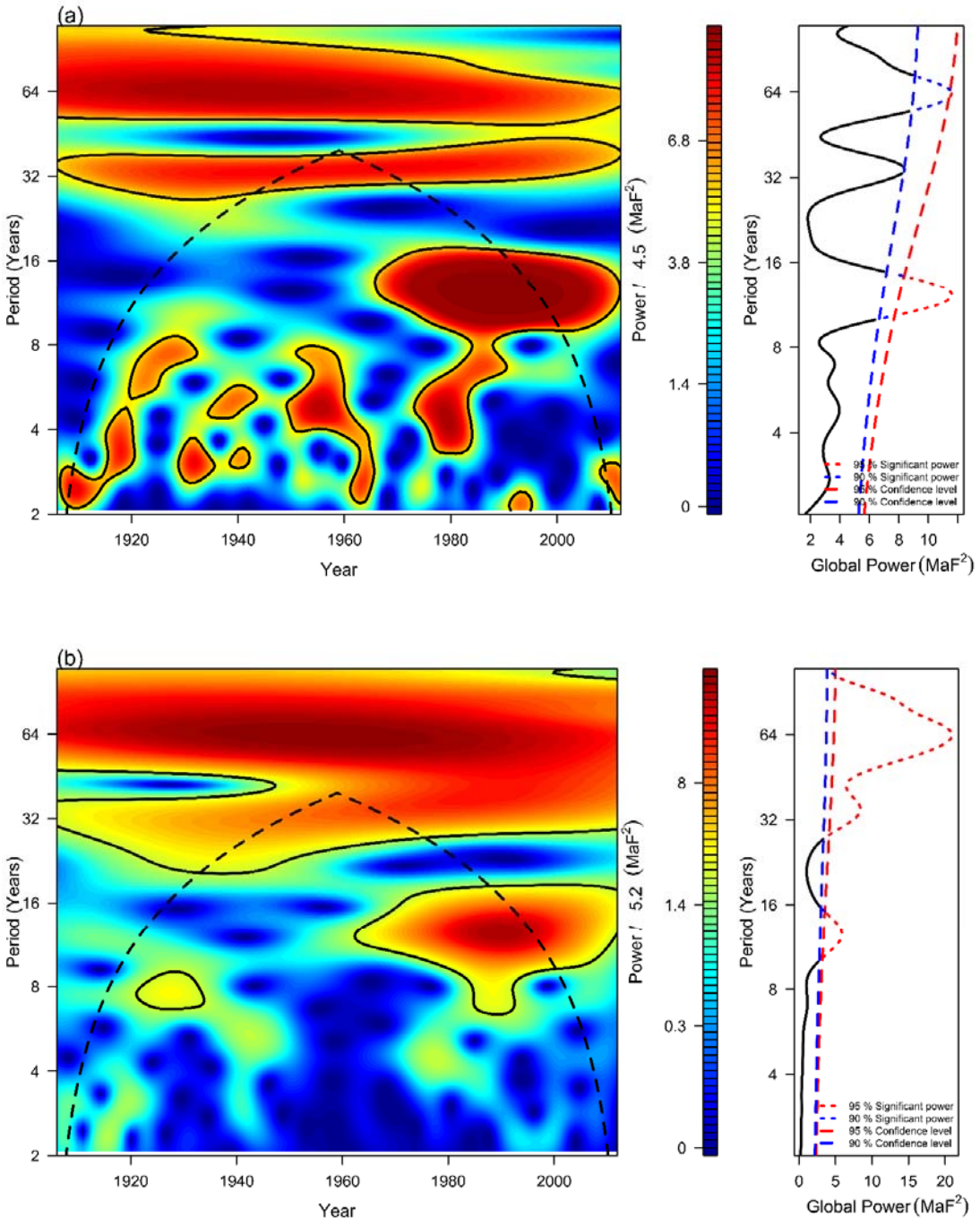

Figure 2.10 Power spectra of the Lees Ferry flow (a) from the median of the simulations (b) historic flow - local spectrum on the left and global on the right.

The decadal (8-16 year period) variability, however, is not significant in the climate indices (Figure 2.1(a) and Figure 2.2(a)), but it is clear in recent decades in the spectrum of PDO (Figure 2.2a).

The coherence of Lees Ferry flow with AMO and PDO (Figure 2.11a and b) clearly show the multi-decadal (32-100 year) association with AMO and PDO (Figure 2.11a and b) and association at the 8-16 year period in recent decades with PDO (Figure 2.11b). The significant coherence of Lees Ferry flow with PDO in the 8-16 year period as shown in Figure 2.11(b) in recent years suggest the modulating effect of PDO on the Colorado River flow at decadal time scales.

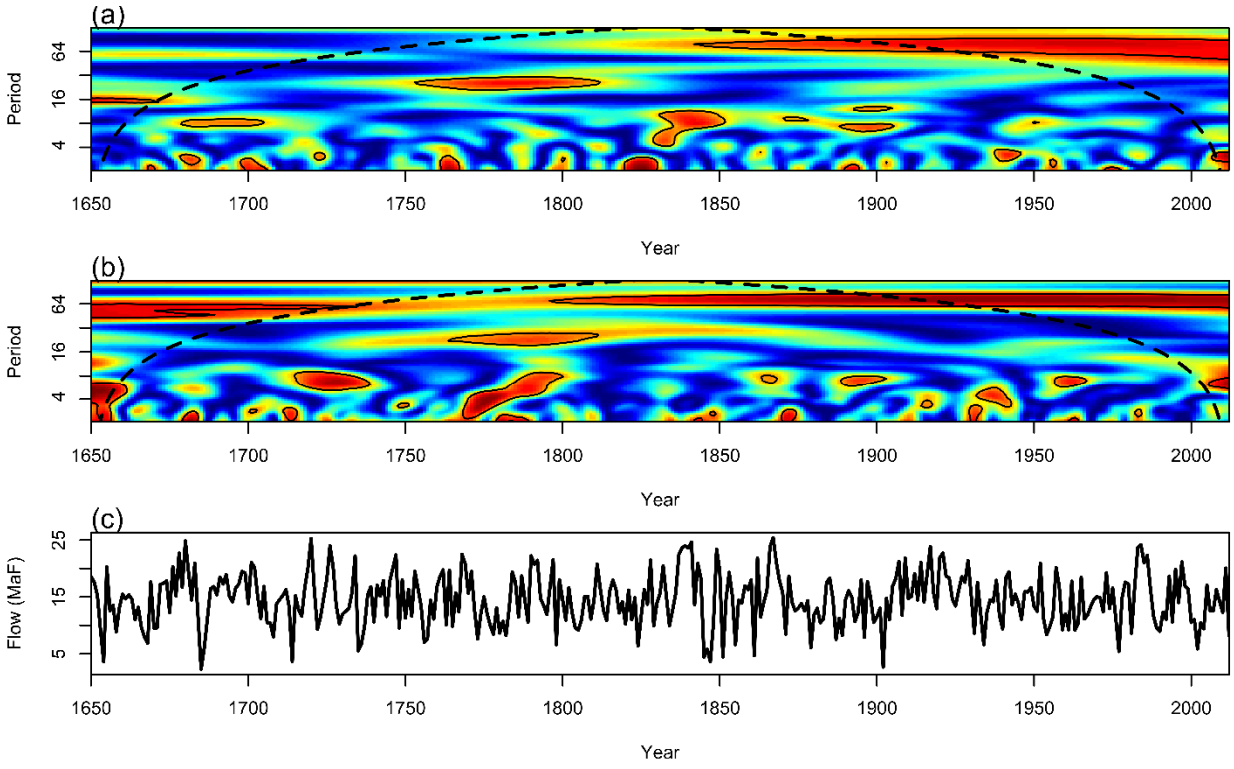

Figure 2.11 (a) Coherence plots of the Lees Ferry flow with AMO; (b) is same as (a) but the coherence of the Lees Ferry flow with PDO; (c) timeseries plot of the Lees Ferry flow.

Simulations were made for the full length of paleo data (1560 – 1905) and the statistics were compared with that of the paleo data. The performance was similar to that from the historic data described above.

We generated ensembles of 20 year projections for each year starting from 1890 using the methodology as described above. The ensembles of projected 20-year mean flows are shown as boxplots and the 20-year mean flow from history is shown as solid line (Figure 2.12).

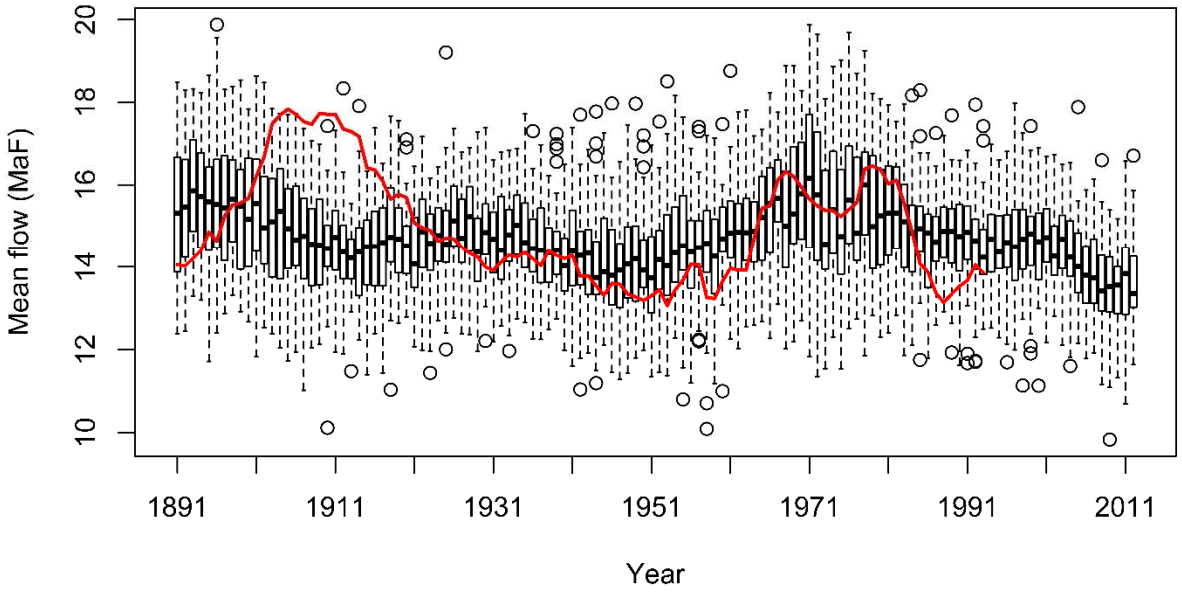

Figure 2.12 Timeseries plots of the Projections. The box plots are the 20 year mean projections and red line is the 20 year mean observed flow at Lees Ferry. The 20 year mean observed flow (red) stops in 1991 (the 1991-2010 mean flow) and the 20 year mean projections continue until the end of 2010.

It can be seen that the ensembles reproduce the observed temporal characteristic of the 20-year mean flows very well. However, the high flows during the early part of the record (1906 – 1920) are under simulated. This is due to the fact that the flow simulation is based on bootstrapping past flows and for this period, the flows are large relative to pre-1906 flows which do not have sustained period of high flows. Another reason is that the high flow periods in the past should coincide with the climate forcings, else the neighbors selected based on climate variables will not correspond well with high flows for resampling. The sustained wet period of

1906-1920 has good coherence with the AMO and PDO anomalies in the 64 year period band (Figure 2.11). The 20 year projections of climate indices for the 1906 -1920 epoch are resampled mostly from ~1840 (64 years back from 1906) which is the nearest neighbor to the climate indices at the start of 1906. Thus, the flows are also simulated largely from this period, which is relatively lower. We note that methodology is able to capture well the high flow period of 1980s as simulation during this period is able to resample high flow values from the 1906-1920 period. The projections perform very well from 1920-1960, where we don't have extreme wet periods sustained periods. The 1980s wet period is captured by the projections as well. This wet period is not sustained for longer period as in the early 1900s and resampling was possible from the past paleo data as well as from the early 1900s wet period.

2.6 Summary and discussion

As the anthropogenic climate change discussion has become mainstream, the climate sensitivity of hydrologic time series has evinced considerable interest. By and large, the dynamic range of hydroclimatic variation over the last millennium in places such as Colorado, appears to be much larger than the relatively modest, yet uncertain projections from a chain a coupled models of the ocean-atmosphere and hydrology. Specifically, the physics based models do not adequately reproduce the inter-annual, decadal and multi-decadal variations that are in evidence from tree rings, and the associated reconstructions of hydrology of the region. As a result, water managers seek methods by which storage needed to meet demand and correspondingly the potential reliability and resilience of existing projects relative to these climate variations, can be assessed. This is the context for the methods developed and exemplified in this paper.

The causal framework for low frequency variations in regional streamflow suggests that these variations are derived from like variations in large scale climate phenomena, such as the AMO and the PDO. Consequently, the need to develop long term, stochastic simulations of those indices emerged as a first step in developing an approach for low frequency simulations of the streamflow, and led to the strategy presented here. The WKNN method developed was applied in this manner, and also directly to the 106 years of Colorado River flows at Lees Ferry (figures not shown). The direct application led to performance considerably poorer than the application following the climate causal framework, suggesting that using the paleo-proxies for the climate indices and then conditioning the streamflow on the simulated indices is superior to a direct attempt to model low frequency variability in the streamflow series. This is very interesting since the AMO, PDO, ENSO and NAO have seen significant efforts at paleo-reconstruction and collectively influence hydrology over much of N America and parts of Europe and Asia. Developing a library of the simulations of these indices may then allow local investigators the ability to use the appropriate indices to conditionally simulate streamflow with the proper low frequency character.

In future work, we plan to explore the application to other settings, and to extend our prior work on multivariate simulation [*Lall et al.,* 2015] to this setting as well.

3 A Comparison of Wavelet and Hidden Markov Based Stochastic Simulation and Projection Methods on the Colorado River Streamflow

A version of this chapter has been submitted for publication as a journal paper.

Abstract

Linear timeseries models have been the mainstay for stochastic streamflow simulation. Recently, wavelet and Hidden Markov based modeling approaches were developed to better capture nonstationarity and non-gaussian characteristics present in the streamflow, which the linear models cannot. This paper presents a comparison of three recently developed timeseries models: Wavelet-based Auto Regressive (WARM), Hidden Markov Model (HMM) and Wavelet-based Time Series Bootstrap Model (WKNN). The first method is applied directly on the streamflow, while the other two methods incorporate large scale climate forcings – Atlantic Multidecadal Oscillation (AMO) and Pacific Decadal Oscillation (PDO). The use of climate forcings with HMM for streamflow simulation is a new methodological contribution. The comparisons are made on the performance skill in a simulation and projection modes using the Lees Ferry flow timeseries in the Colorado River Basin (CRB). The three methods are generally very good in capturing all the distributional statistics and non-stationary features present in the historic data in a simulation mode. For short term projections (1 ~ 3 years) the HMM seems to perform slightly better than the other two methods, which will be immense use in short term (1-2 years) operations and planning of water resources systems on the River. For longer term projections (~20years) WKNN performs much better, which can be very useful in water resources planning.

3.1 Introduction

Water resources management in any river basin aims to plan for potential long term supply-demand imbalances through investment in infrastructure and implementation of policies that govern the use of the water and the operations of the human controlled system. Resilient plans can address periodic imbalances due to hydrologic variability through temporary measures such as M&I conservation or fallowing agricultural land and are especially effective when the need for these measures can be anticipated in advance [*Grantz et al.,* 2007; *Regonda et al.,* 2011]. Additionally, sustainable water resources systems must be able to adapt to uncertain future changing demands and supplies due to, e.g., demographics and climate change. Thus, effective management requires an understanding of projected hydrologic variability at timescales that range from seasonal to multi-decadal. Stochastic streamflow simulation has been useful as a planning tool by providing ensembles of future hydrologic sequences that can be input to stochastic simulation models to evaluate the performance and reliability of system designs, policies and operational decisions [*Loucks and Vanbeek,* 2005, chp 7].

Typically, time series models are fitted to the historic streamflow data and then used to simulate ensembles of flow sequences which have the same statistical properties as the historic. Linear time domain models [*Wei,* 2006], also called parametric models, have been the staple of stochastic streamflow simulation [*Salas,* 1980]. These models assume stationarity of autocorrelation in the time series, data to be normally distributed, and a linear relationship of the autocorrelation – which tend to be restrictive as these assumptions are hard to satisfy in streamflow data. Non-parametric [*Lall,* 1995] timeseries simulation models have been proposed to improve upon these drawbacks mainly based on kernel density estimators [*Lall and Sharma*, 1996; *Rajagopalan and Lall*, 1998; *Sharma et al.,* 1997]. None of these time domain methods

can capture the spectral properties present in the observation series, especially nonstationarity in the spectra. These features are important for capturing the wet and dry sequences that are crucial for water resources management and planning at short and long time scales [*United States Department of the Interior,* 2001].

Wavelet based timeseries simulation models, an attractive alternative for modeling the spectral characteristics, have been gaining popularity since the first Wavelet Auto Regressive Model (WARM) was introduced by *Kwon et al.* [2007] and later enhanced by *Nowak et al.* [2011]. The WARM approach fits autoregressive (AR) models to the wavelet filtered signal components of the timeseries with the residual or noise modeled as white noise, i.e., normal distribution. For details of wavelet analysis, the reader is referred to [*Torrence and Compo,* 1998; *Kwon et al.,* 2007; *Nowak et al.,* 2011].The fitted AR models can be used to make short and long term projections (1 ~ 20 years). However, for simulation of historic series the stationarity assumption of AR models limits their ability to capture nonstationarity in the spectra. To improve the simulation, *Nowak et al.* [2011] enhanced the WARM model by normalizing the signal components by their respective Scaled Average Wavelet Power (SAWP) [*Torrence and Compo,* 1998] prior to fitting an AR model, thereby making them stationary. The enhanced WARM model was applied to the CRB at Lees Ferry and shown to faithfully reproduce the non-stationary spectral characteristics of the streamflow [*Nowak et al.,* 2011].

The hydroclimatology of Western United States is increasingly known to be modulated by Atlantic Multi-decadal Oscillation (AMO), Pacific Decadal Oscillation (PDO) and El Nino Southern Oscillation (ENSO) [*Tootle et al.,* 2005, *Timilsena et al.,* 2009; *Enfield et al.,* 2001; *McCabe et al.,* 1999; *McCabe et al.,* 2007; *Hidalgo,* 2004; *Nowak et al.,* 2012] at multi-decadal time scales. Recent research [*Nowak et al.,* 2012; *Bracken et al.,* 2014; *Switanek and Troch*,

2011] indicates the upper CRB specifically has teleconnections strongly with AMO and PDO and weakly with ENSO. Incorporating this understanding in a WARM framework, the authors recently developed a wavelet based K-Nearest Neighbor (WKNN) conditional streamflow simulation model [*Erkyihun et al.,* 2015]. In this, the wavelet derived signal components of the climate forcings are generated with a block-K-NN (BKNN) resampling approach replacing the AR part of WARM (Figure 2). The BKNN has the ability to capture nonlinearity and non-Normal features thereby alleviating these drawbacks of AR models. Then the stream flow is conditionally resampled based on the nearest neighbors of the thus generated climate forcings. This method was also applied to the CRB flows and was shown to capture the historic features of the flow very well and also provide good projections especially at longer time scales.

Hidden Markov Models (HMM) [*Zuccuni & MacDonald* , 2009] have also been proposed recently for time series simulation. The observed time series is modeled as a realization from hidden states, with each state characterized by a probability density function (PDF). The number of hidden states, their transition probabilities from one state to another (i.e., the Markov part) and the parameters of the state PDFs are obtained using objective criteria [*Zuccuni & MacDonald* , 2009]. Simulation proceeds by first simulating the state from the transition probability and then sampling a value from the respective state PDF. Recently, *Bracken et al.* [2014] developed an HMM streamflow simulation model with a slight modification to modeling the state transition probabilities using large scale climate indices of AMO and PDO. Applying this to the CRB flows, the model showed very good performance in capturing the characteristics of the streamflow including non-stationary spectral features. In this research the authors modified the HMM streamflow simulation method [*Bracken et al.,* 2014] by applying the HMM to the climate indices AMO and PDO to simulate them separately, and simulating the streamflow conditionally

via K-NN resampling, similar to WKNN. The modification is made in such a way that the performance of the HMM model can be compared with the WKNN model under the same conditions.

The objective of this research is to formally compare the three recently developed methods (WARM, WKNN and HMM) which have demonstrated skill for stochastic streamflow simulation. The projection skills of the three models for different projection windows is analyzed to identify appropriate model for water resources planning and management. This is motivated by the need for robust stochastic simulation and projection of streamflow at short and long time scales for effective water resources planning and management [*Vera et al.,* 2010; *United States Department of the interior,* 2001].

This paper is organized as follows. First the data used for comparison followed by brief descriptions of the models simulation and projection approaches. Comparisons of the models results are then presented to demonstrate the performance of the simulation and also to identify suitable model based on their projection skill at different projection windows at short and longer time scales. Summary of the results and discussion section concludes the paper.

3.2 Data

The observed and paleo data of Colorado River streamflow and large scale climate indicators used in this research are described below.

3.2.1 Colorado River flow at Lees Ferry, AZ

The Lees Ferry flow gauge divides the CRB into the upper and lower operational basins, through which 90% of the Colorado River flows. The United States Bureau of Reclamation (Reclamation) regularly updates the monthly neutralized flow of this gauge by removing

anthropogenic effects such as regulation and diversions [*Prairie and Callejo,* 2005]. The naturalized monthly data from 1906 to 2012 can be obtained from the Reclamation website: http://www.usbr.gov/lc/region/g4000/NaturalFlow/current.html

The annual naturalized flow of the Lees Ferry flow, derived from the monthly data from 1906 to 2012, is used in this study. In addition, tree ring reconstructed flows for the pre-1906 period covering 1490 to 1905 from *Woodhouse et al.* [2006] are used in this study (http://treeflow.info/upco/coloradoleeswoodhouse.txt).

3.2.2 Climate Indices AMO and PDO

The AMO index[*Enfield et al.,*2001] is computed as a monthly area weighted average of North Atlantic (0 to 70^{o} N) sea surface temperatures (SST), which is subsequently de-trended, based on 5^{o} x 5^{o} resolution Kaplan SST [*Kaplan et al.,*1998]. It is updated regularly by the national Oceanic & Atmospheric Administration (NOAA) at monthly time scale. The monthly data from 1856 to present is available at NOAA website: http://www.esrl.noaa.gov/psd/data/timeseries/AMO/. The paleo reconstruction of annual AMO[*Gray et al.,* 2004] for the period (1650 – 1990) is based on reconstructions of annual sea surface temperature anomalies (SSTA) for the North Atlantic Ocean (0 to 70^{o} N) from tree rings and was obtained from the NOAA website: ftp://ftp.ncdc.noaa.gov/pub/data/paleo/treering/reconstructions/amo-gray2004.txt.

Monthly PDO anomalies from 1900 to present are available from the University of Washington: http://jisao.washington.edu/pdo/PDO.latest. It is calculated as the first principal component of the Northern Pacific SST [*Zhang et al.,* 1997; *Mantua et al.,* 1997]. The annual data were taken as the average of the monthly values in this analysis. The paleo annual PDO values for the period 993 – 1996, are based on tree rings from Pinus flexilis in California and

Alberta, Canada [*MacDonald and Case*, 2005] and are available from the NOAA website: ftp://ftp.ncdc.noaa.gov/pub/data/paleo/treering/reconstructions/pdo-macdonald2005.txt.

3.3 Model description

Below a brief description of the three models along with the steps for simulation and projection modes. In a simulation mode, the aim is to generate ensemble of sequences, each ensemble the same length as the historic data and compare a suite of statistical characteristics – distributional, correlation and spectral to understand the performance. In a projection mode, the aim is to generate an ensemble of sequences of desired length from a specified point in time.

3.3.1 Hidden Markov model

The basic principle behind the HMM model is to represent the observed time series as a realization from non-observable (hidden) Markov process, S_t (t=1,2,3,…,T) with a transition probability matrix and appropriate state specific PDFs [*Zuccuni & MacDonald*, 2009, *Ibe*, 2009; *Bracken et al.*, 2014]. The general form of HM model (from *Zuccuni & MacDonald* , 2009; *Bracken et al.*, 2014) shown in the schematic in Figure 3.1 and can be represented as:

$$\Pr\left(S_t \middle| \boldsymbol{S}^{(t-1)}\right) = \Pr(S_t|S_{t-1}), t = 2,3, \dots, T \quad ----- \quad (1)$$

$$\Pr\left(X_t \middle| \boldsymbol{X}^{(t-1)}, \boldsymbol{S}^t\right) = \Pr(X_t|S_t), t \in \mathbb{N} \quad ------- \quad (2)$$

Where: X_t is the observed sequence; S is the hidden state and S_t is the hidden state sequence

$$\gamma_{jk} = \Pr(S_{i+1} = k \mid S_i = j)$$

$$\Gamma = \begin{bmatrix} \gamma_{11} & \cdots & \gamma_{1m} \\ \vdots & \ddots & \vdots \\ \gamma_{m1} & \cdots & \gamma_{mm} \end{bmatrix}$$

Where: Γ is the transition probability matrix of the hidden state sequence.

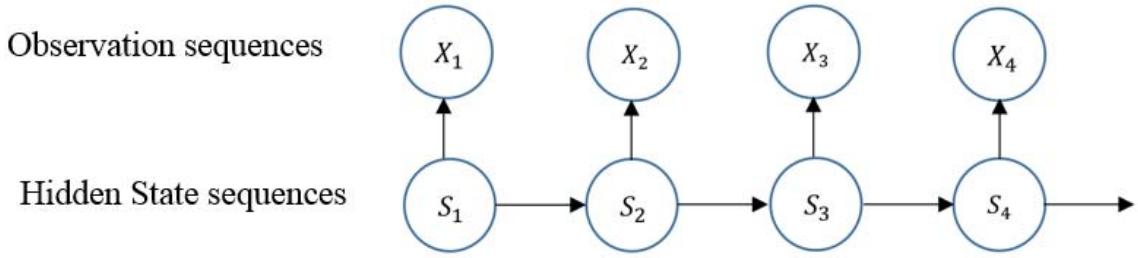

Figure 3.1 Basic HMM model adopted from Zuccuni and MacDonald, 2009.

The HMM approach seeks to recover the hidden states sequences from the observation sequences through optimal number of hidden states (m), state transition probabilities (Γ) and probability distribution parameters($\mu_k, \sigma_k;\ k = 1,2, \dots, m$); where μ_k & σ_k are the mean and standard deviation of probability distribution of state k The optimal model parameters are determined through iterative process called the Baum-Welch algorithm, a special case of Expectation Maximization (EM) procedure [see *Ibe,* 2009; *Zuccuni & MacDonald*, 2009].

The authors modified the application of HMM from *Bracken et al.* [2014] in that the HMM was applied to the climate indices, AMO and PDO, which is used to simulate them and conditionally generate the streamflows via K-nearest neighbor bootstrap. The optimal states, transition probabilities and the state PDF parameters are listed in Table 3-1

Table 3-1 Hidden Markov model parameters

	m	μ	σ	δ	Γ
Lees Ferry flow	2	$[17.9, 13.22]$	[3.75,3.79]	[1,0]	$\begin{bmatrix}0.92 & 0.08\\0.02 & 0.98\end{bmatrix}$
AMO	2	$[-0.82,0.76]$	[0.62,0.61]	[1,0]	$\begin{bmatrix}0.96 & 0.04\\0.02 & 0.98\end{bmatrix}$
PDO	3	$[0.92, -0.87,0.23$	[0.89,0.65,0.29	[0,0,1]	$\begin{bmatrix}0.77 & 0.00 & 0.23\\0.00 & 0.89 & 0.11\\0.21 & 0.17 & 0.62\end{bmatrix}$

Simulation

The simulation steps are as follows:

(i) The fitted HMM of PDO, as mentioned above, provides a best estimated sequence of states for each year of the historical data. Using this state sequence, a value is generated from the corresponding state PDF, thus generating a sequence of PDO for the same length as the historic data. This is repeated to generate an ensemble of 107 sequences each of the same length as the historic data.

(ii) Repeat step (i) for AMO to generate an ensemble of 107 sequences each of the same length as the historic data

(iii) For each simulated AMO, PDO pair, x_t at time *t,* K nearest neighbors are identified from the historical pairs using Euclidian distance. The nearest neighbor is given the highest weight and the farthest the least using a weight function that decays as 1/*i, i* = 1,2,..,K. A neighbor is selected (i.e., bootstrapped) using this weight function and the corresponding streamflow is the simulated for time *t.* This is repeated for all times. The heuristic choice of number of neighbors $K = \sqrt{n}$ was proposed by *Lall and Sharma* [1996]. This K-NN bootstrap method has been used widely for streamflow simulation [*Prairie et al.,* 2006; *Grantz et al.,* 2005], weather generators [*Rajagopalan and Lall,* 1999; *Yates et al.,* 2003*; Caraway et al.,* 2014] and recently with wavelets, WKNN method [*Erkyihun et al.,* 2015] compared here.

Projection

The projection steps starting from time *t* are as follows:

(i) Based on the states of PDO at current and past times along with the transition probability matrix, a state of PDO is generated for time *t+1.* From the generated PDO state, a value is sampled from the corresponding state PDF at time *t+1.* This is repeated for the desired projection length: *t+2, t+3,... , t+n.*

(ii) Step (i) is repeated for AMO

(iii) For each simulated AMO, PDO pair, using K-NN bootstrap method described in the simulation section above, streamflow projection is generated.

(iv) The above steps are repeated several times to generate an ensemble of streamflow sequence, each of the desired projection length.

3.3.2 Wavelet Auto Regressive Model (WARM)

The WARM [*Kwon et.al,* 2007] dwells on the signal component of the time series so that classical Auto Regressive (AR) model fit can be applied skillfully. The signal component of the timeseries is identified by the 90 % - 95% significant test using the white noise as a null hypothesis. The identified significant component between periods j_1 and j_2 is extracted from the original timeseries using the wavelet timeseries reconstruction function (Equation 3). This reconstructed component is also known as the signal component of the timeseries. Depending on the nonstationarity characteristics of the timeseries at different frequencies, there can exist more than one signal component in the timeseries. With this, more signal reconstructions are performed. The residual has no structure or lag auto correlation, thus is regarded as the "noise" component of the timeseries. The reconstructed signal components are relatively "smooth" and "periodic" when compared with the original timeseries (see Figure 3.2). Adding the signal and noise components altogether, by design, forms the original timeseries. Details of wavelet technique can be found in *Torrence and Compo* [1998]; *Kwon et al.,* [2007]; *Nowak et al.* [2011].

Reconstruction of the original time series, shown in the Figure 3.2 schematic, over a set of periods j_1 and j_2 can be obtained as:

$$x'_n = \frac{\delta_j \delta_t{}^{1/2}}{C_\delta \psi_0(0)} \sum_{j=j_1}^{j_2} \frac{R\{W_n(a_j)\}}{a_j{}^{1/2}} \quad \text{---------- (3)}$$

Where C_δ is reconstruction factor, $\delta_j \delta_t$ are scale and time factors respectively. $\psi_0(0) = \pi^{-1/4}$ Is the factor that removes the energy scaling for Morlet wavelet function, R denotes the real part of the wave and a_j is the scale. j_1 and j_2 are the lower and upper periods that brackets the desired periods.

This method has the ability to reproduce the distributional statistics, but fails to reproduce the non-stationary characteristics of the timeseries, as the AR model is stationary by design. Figure 3.2 represents the logical representation of the WARM method. For details the reader is referred to *Kwon, et al.* [2007] and *Nowak et al.,* [2011].

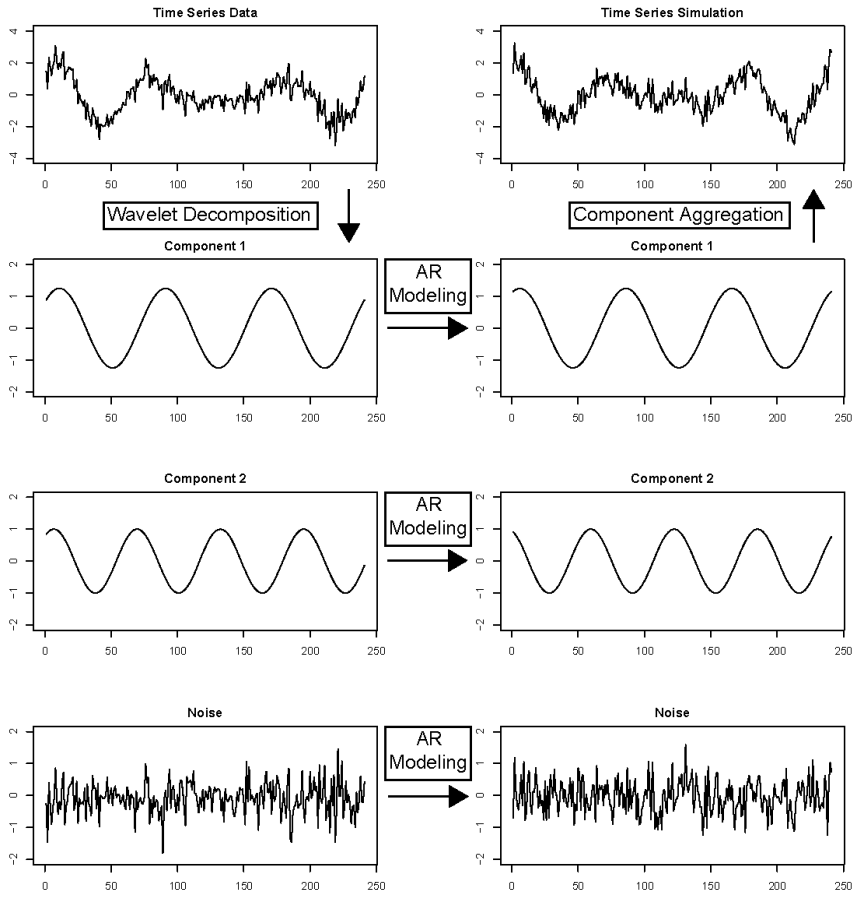

Figure 3.2 The WARM model adapted from *Kwon et al.* [2007].

To capture the nonstationarity in the timeseries better, *Nowak et al.* [2011] introduced an enhancement for WARM. The enhancement is mainly improving the skill of the AR model on the signals. In this modification, the variance of each of the signals was first calculated as Scaled Averaged Wavelet Power (SAWP) (Equation 4). The SAWP, i.e., the variance of the time series within the selected periods, is given by:

$$\bar{W}_n^{\,2} = \frac{\delta_j \delta_t}{C_\delta} \sum_{j=j_1}^{j_2} \frac{\left|W_n(a_j)\right|^2}{a_j} \quad ----------(4)$$

Where C_δ is reconstruction factor and $\delta_j \delta_t$ are scale and time factors respectively.

The signal component are then normalized by the SAWP to create "stationary" signal so that AR model fit is even more skillful. This is accomplished by dividing the reconstructed component (Equation 3) by SAWP (Equation 4). The normalized components are then subjected to the AR model to generate realizations in simulation mode. The realizations of each of the components are then back standardized by the respective SAWP to bring back the nonstationarity in each component.

Simulation

The WARM is applied directly on the Lees Ferry streamflow time series. The simulation follows the schematic presented in Figure 3.2 and the steps are described as follows

(i) Wavelet timeseries reconstruction is performed to obtain the signal component(s).

(ii) For each of the reconstructed signal components, AR model fit is performed.

(iii) Based on the fitted AR model in (ii) stochastic realization is generated for each component.

(iv) The residual component is represented by generating values from normal distribution using the mean and variance of the residual "noise" component of the timeseries.

(v) The generated realizations of the signals and noise components are summed to get the realization of the original timeseries.

(vi)The above steps are repeated several times as desired to get the simulation ensemble.

The WARM method as demonstrated by previous studies [*Nowak et al.*, 2011] fails to capture the spectral and non-gaussian characteristics of the Lees Ferry streamflow. For this, the

authors also applied the WARM model on the climate indices for conditional simulation of the Lees ferry flow following the steps presented in the HMM description above.

Projection

The WARM projection proceeds as follows:

(i) Wavelet timeseries reconstruction and AR model fit of the signal component is performed for the timeseries up to the current time, t.

(ii) Based on the AR model parameters in (i), the signal component is projected for to generate values at time steps $t+1, t=2, \ldots, t+n$.

(iii) Step (ii) is repeated for all the signal components.

(iv) The residual component is generated from normal distribution as described in the simulation section for times $t+1, t=2, \ldots, t+n$.

(v) The projected values of the signal and noise components are aggregated to get the projection of the timeseries.

(vi) Steps i-v are repeated as many times as desired to get projection ensembles.

3.3.3 Wavelet Based K-NN (WKNN) model

The WKNN model as described in Chapter 2 has a similar structure as the conditional WARM. What makes the WKNN different is that the signals of the timeseries components are modelled using the block bootstrap method rather than the AR model [Erkyihun et al., 2015]. For details of the block bootstrap method, refer [*Efron and Tibishirani*, 1993]. The WKNN is applied to the climate indices AMO and PDO simulating them separately. The streamflow is conditionally resampled based on the simulated AMO and PDO – using K-NN bootstrap

described in simulation step (iii) in the HMM section above. Brief description of the method is presented here.

Simulation

The timeseries is first decomposed into dominant signal and noise components [*Torrence and Compo*, 1998; *Kwon et al.*, 2007]. The dominant signals are then simulated using a block K-nearest neighbor (K-NN) bootstrap approach [*Efron and Tibishirani*, 1993; *Lall and Sharma*, 1996] described as follows

(vi) For each reconstructed component signal (Equation 4), the characteristic period, $\bar{P}$, is identified, which is the mean of periods included in the reconstruction: $\bar{P} = \frac{j_1 + j_2}{2}$ where j_1 *and* j_2 are upper and lower periods of the reconstructed signal. Then a block size, *B*, is computed which is half of $\bar{P}$.

(vii) For a given time *t*, a 'feature vector' of length *B* is created $[x_t, x_{t-1}, \ldots x_{t-B+1}\ ; where\ x_t\ is\ the\ climate\ signal]$ and *K* nearest neighbors of this feature vector are identified based on Euclidean distance, from the reconstructed signal.

(viii) One of the neighbors is selected using a weight function which weights the nearest neighbor the most and the farthest the least. The weight function is given as:

$$W_i = \frac{\frac{1}{i}}{\sum \frac{1}{i}}\ ;\ \mathrm{i}\ = 1,2,..,K \quad ------- \quad (5)$$

(ix) Suppose the neighbor *j* is selected which corresponds to time *T*. A block *B* of successive reconstructed signal values –ie., $x_{T+1}, x_{T+2}, \ldots, x_{T+B}$ forms the simulated values for *B* time steps *t*+1, *t*+2, .., *t*+*B*.

(x) The simulated block becomes the feature vector and following steps (ii) through (iv) will simulate the signal for time steps $t+B+1$, $t+B+2$, .., $t+2B$.

The above steps are repeated to generate a sequence of any desired length B time steps at a time. *Lall and Sharma* [1996] proposed a heuristic approach for K as $K = \sqrt{n}$, where n is the number of data points.

The above steps are applied to simulate sequences of all the reconstructed component signals. Thus simulated sequences of component signals are added to obtain the sequence of a timeseries.

Projection

The projection algorithm is the same as the simulation. Unlike the simulation mode, the projections are generated considering data only from the past. The WKNN projection is performed following the steps presented below.

1. Wavelet decomposition to identify the signal and noise components of the climate indices.
2. Fit a block KNN model and then predict the climate signals for the desired lead time.
3. The projected climate signals form a feature vector using which nearest neighbors are identified from the past data in the climate signals space and one of the nearest neighbors are selected.
4. The flow that corresponds to the selected neighbor is resampled. The resampled flow is the projected flow that correspond to the time with climate signals feature vector.

3.4 Model Comparisons

The models are compared in the simulation and projection modes. For the simulation mode, from each model 500 ensembles of streamflow are generated, each of length 107 years (same as the historic data). A suite of statistics – mean, variance, skewness and lag-1 autocorrelation – are computed for each ensemble and displayed as boxplots along with the corresponding value from the historic flows. This is done for all of the three models. The historic value falling within the box (i.e., interquartile range) indicates the ability of the model to capture the statistics. PDFs from the simulations are also plotted as boxplots along with the PDF of the historic data. To demonstrate the ability of the methods to capture nonstationary spectral features and, consequently, the wet and dry epochs, which are important for water resources systems management, median wavelet spectrum of the ensembles from each model is shown with the spectrum of historic data. Wavelet spectrum is computed for each ensemble member and the median value of the spectrum for each period and time is computed, thus providing the median spectrum from the ensembles.

For projection mode, blind projections of flows are made for a 20-year period starting from each and average flow for several lead times are computed and compared with that of the historic values. For example, starting in year 1906, the HMM model is fitted on data pre-1906 and the projection method described earlier is applied to make 1, 3, 5, 10, 15 and 20-year projections. This is repeated for all the years in the period 1891-2012 and for all the models. The ensembles are displayed and the skills are determined using correlation coefficient.

3.5 Results

3.5.1 Simulation

Streamflow simulations were generated using HMM, WARM, *conditional WARM* and WKNN models as described in the previous section. As a complement to WARM, just for simulation mode, the authors included *conditional* WARM which is same as WKNN except the block bootstrap approach for simulating the climate forcings AMO and PDO is replaced with AR models. The suite of distributional statistics is computed and compared with that of the historic. The boxplots of distributional statistics – mean, variance, skew and lag 1 auto correlation – from the simulations and that of the historic flows as dots are shown in Figure 3.3. The observed values are within the interquartile ranges of the boxplots indicating that all the three models exhibit good performance in capturing the distributional statistics in the simulations. The only exception is the under simulation of lag 1 autocorrelation by the HMM and to a slight extent by WARM simulations. The HMM does not explicitly model the autocorrelation in the time series unlike the wavelet based models, most of the autocorrelation is captured by the transition probabilities of the Markov chain – also observed by *Bracken et al.* [2014].

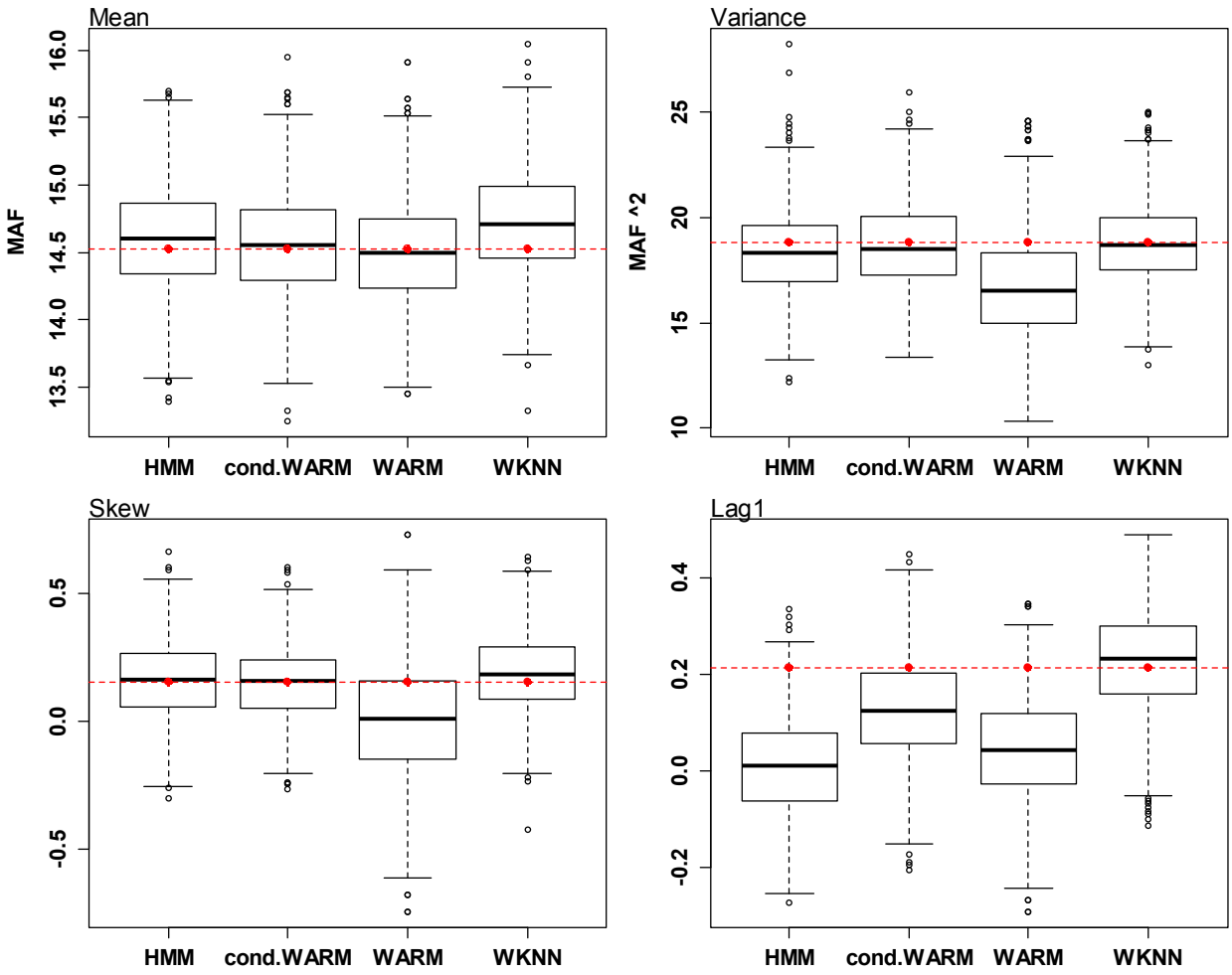

Figure 3.3 : Boxplots of distributional statistics – mean, variance, skew and lag-1 autocorrelation from the three models, with the corresponding historical values shown as red dots and red dashed line. A conditional WAREM simulation model is also applied to see the relative performance of the model

The PDFs of the simulations and the observed flow are compared by generating boxplots of the PDFs from the simulations overlain by the PDF of the observed data shown in Figure 3.4. The median PDF of the simulations (blue) captures very well the PDF of the historic flow (red) from all the three models except the WARM model The WARM simulates from AR models which assumes Normal distribution, as mentioned in the previous section – hence, it has difficulty capturing the historic flow PDF which is non-Normal with positive skew Figures 3 and

4 show that all the three models are very good in simulating the PDF and distributional statistics in a simulation mode.

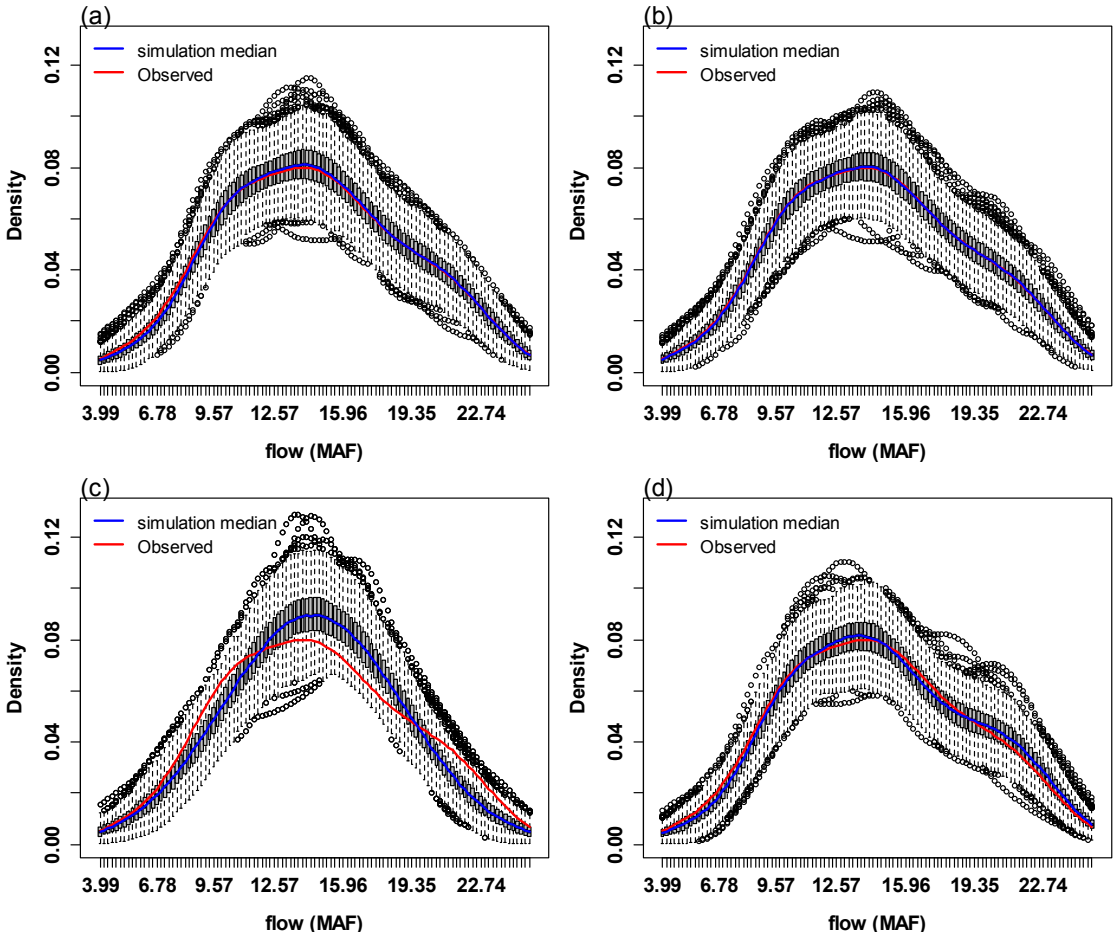

Figure 3.4: PDFs of simulations from (a) HMM, (b) conditional WARM, (c) WARM and (d) WKNN models. The median of the PDF from the simulations is in blue and that of the historic is in red.

In order to investigate the capability of the models to capture spectral features, wavelet spectra were computed for the median of the simulations of each method and the wavelet spectra of the historic flows are shown in Figure 3.5. The models reproduce the wavelet spectra very well including the decadal (8 -16 year) variability in the recent decades. The conditional wavelet based methods (Figures 5b and d) perform better than HMM in reproducing the recent decadal spectral features. As expected the WARM approach (Figure 3.5c) smooths the power in the

decadal band making it more stationary. The WARM approach generates the streamflow component signals using stationary AR model – hence the nonstationarity in the decadal band is not reproduced. As mentioned, the *conditional WARM* simulates the climate forcings using AR models and then conditionally the streamflow, which is quite similar to WKNN, shows similar performance. As indicated before, the HMM captures nonstationarity purely from the Markov transition of the states of the climate forcings and that the spectral features are not directly modeled, unlike the wavelet based methods. Considering this the HMM performance is remarkable.

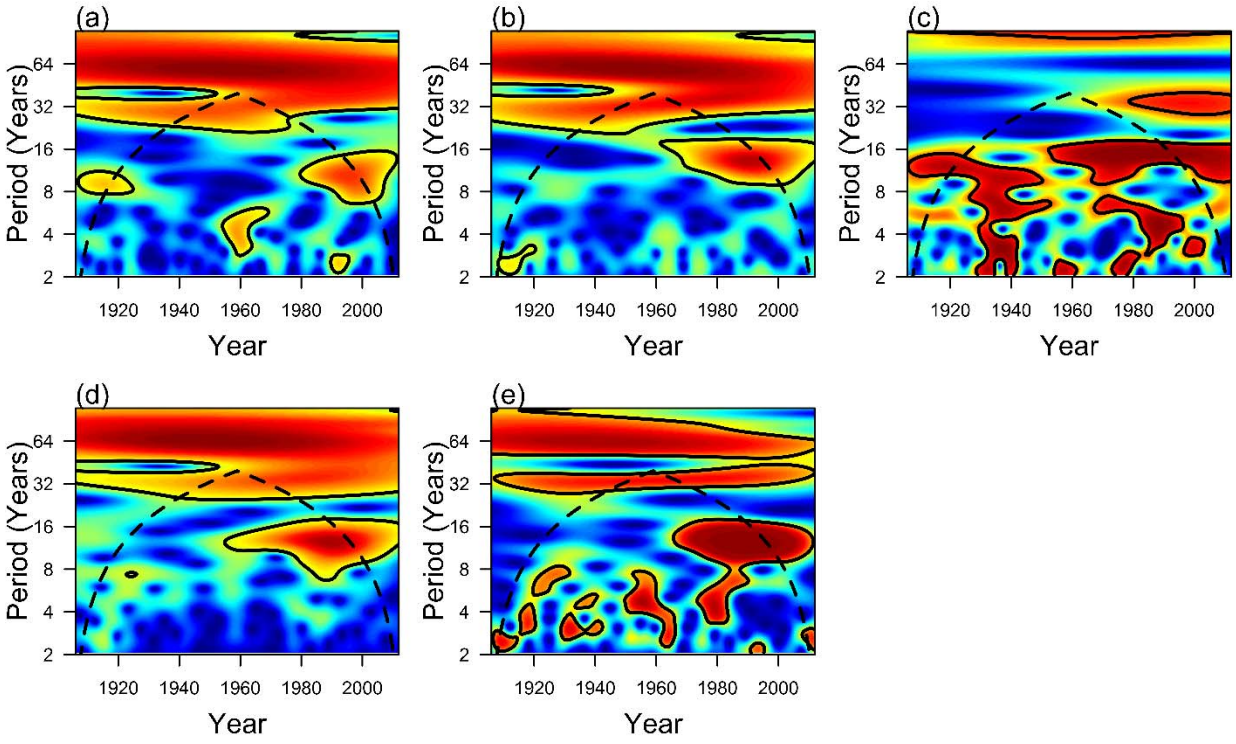

Figure 3.5: Wavelet power spectra from the median of the simulations of (a) HMM, (b) Conditional WARM, (c) WARM and (d) WKNN models. The dashed line is the cone of influence indicating the region beyond which the inference is limited by data. The wavelet spectrum of the historic flow is in panel (e).

From the above results it is clear that all the three conditional stochastic streamflow simulation models are very good at capturing the distributional and nonstationary spectral features in a simulation mode. The methods together offer a robust alternative to traditional linear time series methods. \

3.5.2 Projection

Following the projection algorithms described in the model description section, the HMM, WARM and WKNN models are used to generate projections of Lees Ferry streamflow for the period 1891 – 2012. The projections are made for a 20-year period starting from each year and the mean of the projections at several lead times (1, 3, 5, 8, 10, 15 and 20 years) are computed and compared against the corresponding mean values from the historic flows. The standard R^2 is computed for each lead time and each model. Boxplots of the projections along with the corresponding historic values are also shown for selected lead times for visual comparison.

Figure 3.6 shows the boxplots of projections of 20-year mean flow from the three methods for the 1891-2012 period. It can be seen that the projections from HMM and WARM (Figures 3.6 a and b) do not capture the historical 20-year mean (shown in red). The simulations from WKNN (Figure 3.6 c) track that historical series very well, compared to HMM and WARM, especially from ~1925. Interestingly, all the methods perform poorly in the 1891 – 1925 period. The authors have two explanations for this – (i) this is one of the sustained wet epochs of Lees Ferry streamflow in the entire paleo and observed period and, (ii) this period is the interface of the paleo and historic period. For WKNN and HMM there are no analogs to this wet period hence the projected ensembles are lower than the historic (Figure 3.6c). Similarly for WARM which fits an AR model to the paleo data during this period for projections and hence cannot generate high flows.

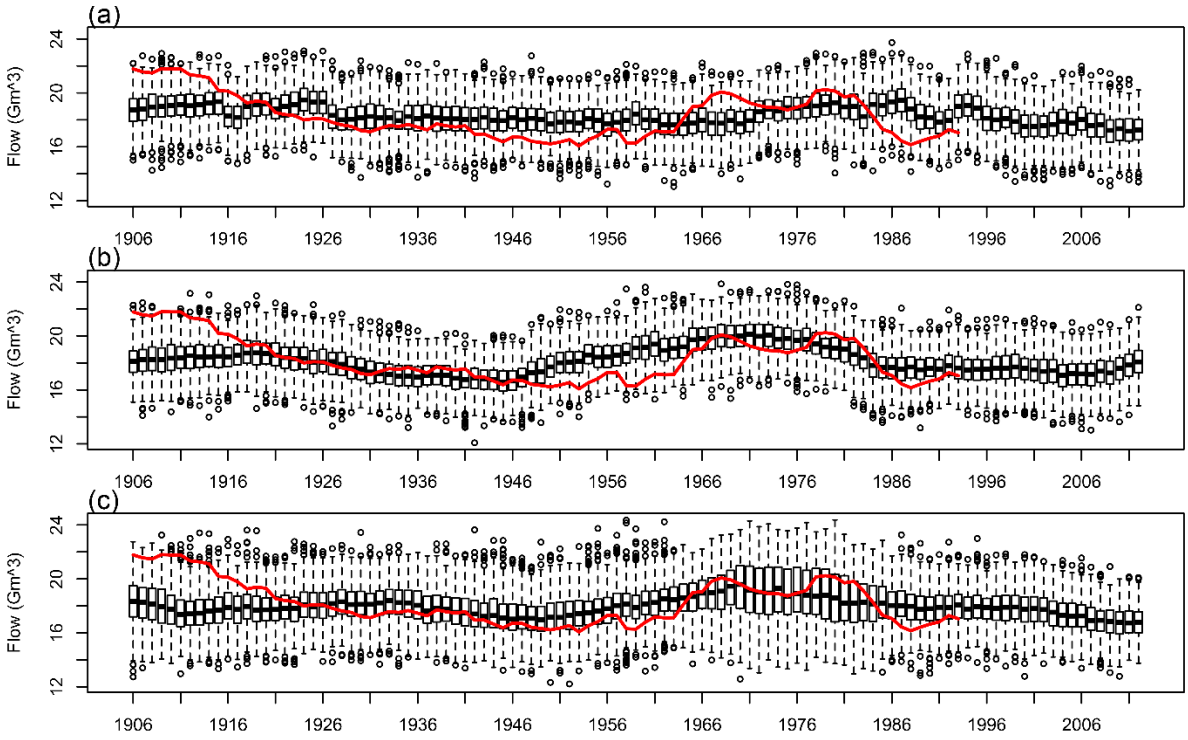

Figure 3.6 Boxplots of the 20 year mean projections of Lees Ferry flow from (a) HMM, (b) WARM and (c) WKNN. The 20 year mean of the historic flows are shown as red line.

Figures 7 and 8 show the boxplot of projections of two lead times 10-year and 5-year mean flow, from the three methods for the 1981-2012 period, respectively. It can be seen that projections from HMM better capture the historic mean for both these lead times (Figures 7a and 8a) compared to WARM and WKNN (Figures 7b,c and 8b,c). The projections from HMM and WARM capture the wet epoch of early 20th century better at this shorter time scale and they also perform better at 1 and 3-years (Figures not shown). It seems to suggest that WKNN has a better performance at longer lead time, while HMM is better at shorter lead times and WARM is in between. This is corroborated by the skill measure R^2 in Figure 3.9. The authors can see that WKNN has the highest skill at long lead time ~20-year while HMM has higher skill ~5-10 years.

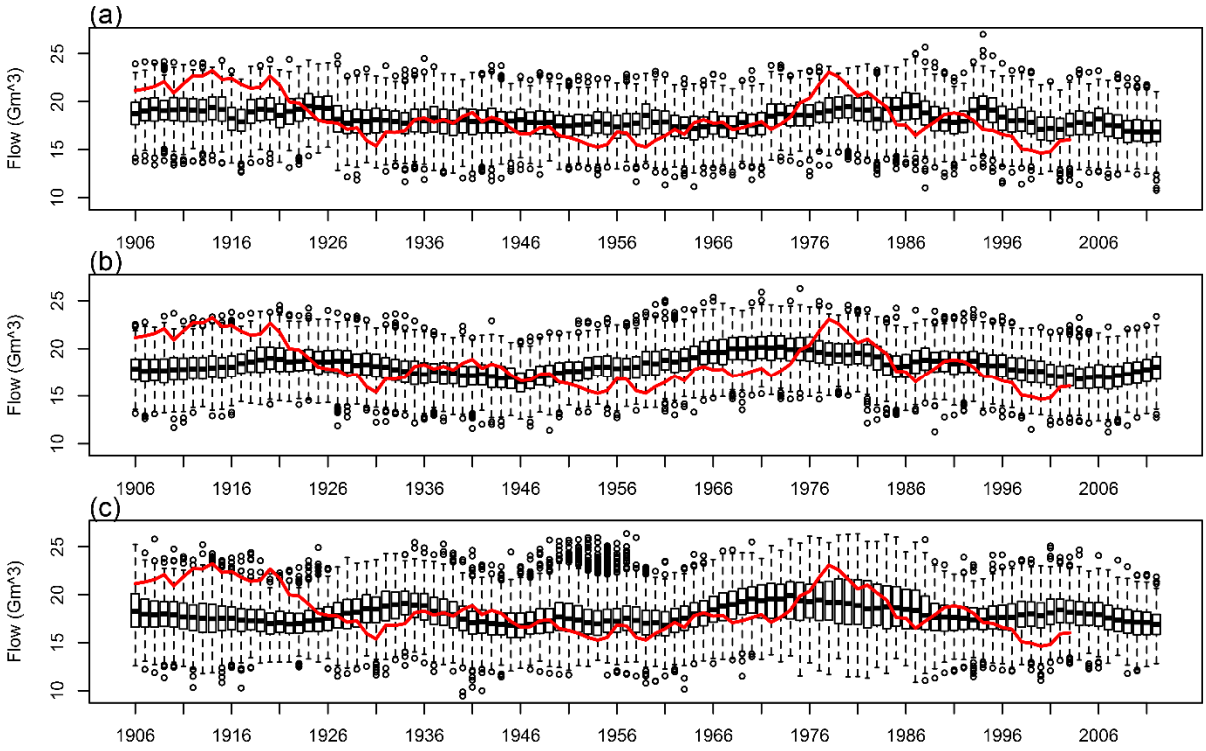

Figure 3.7 Same as Figure 3.6 but for 10-year mean projections

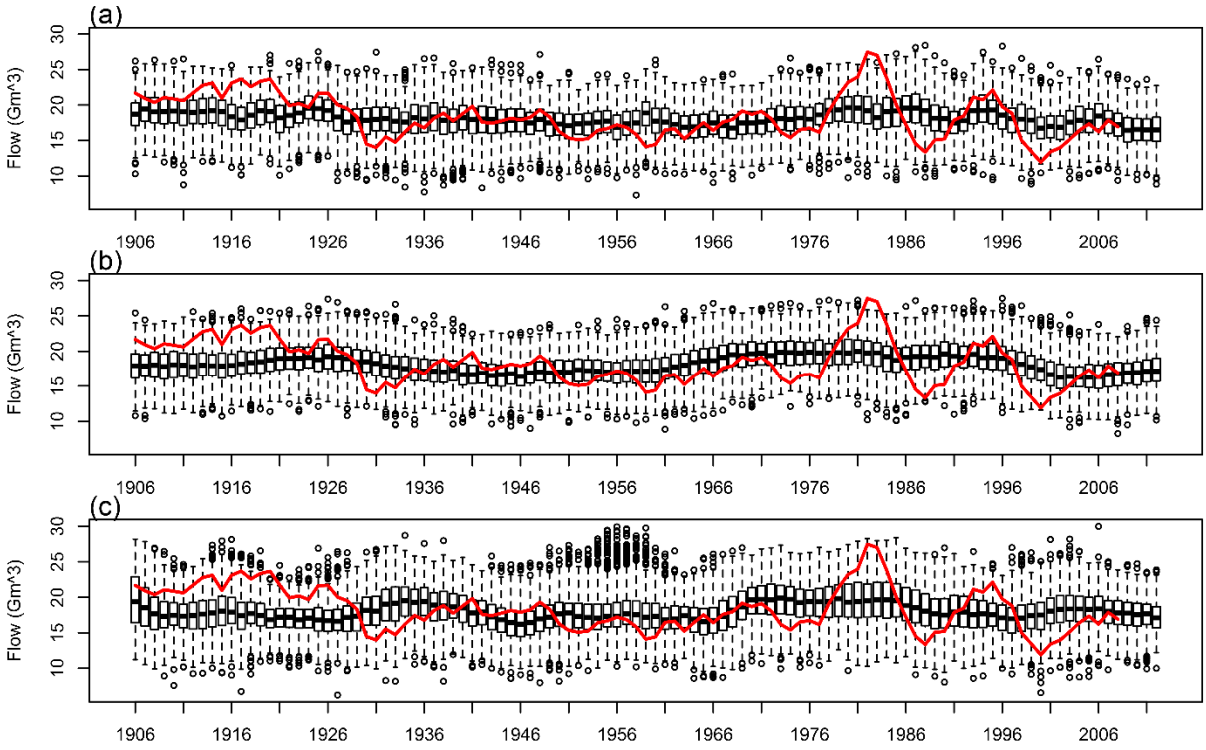

Figure 3.8 Same as Figure 3. 6 but for 5-year mean projections

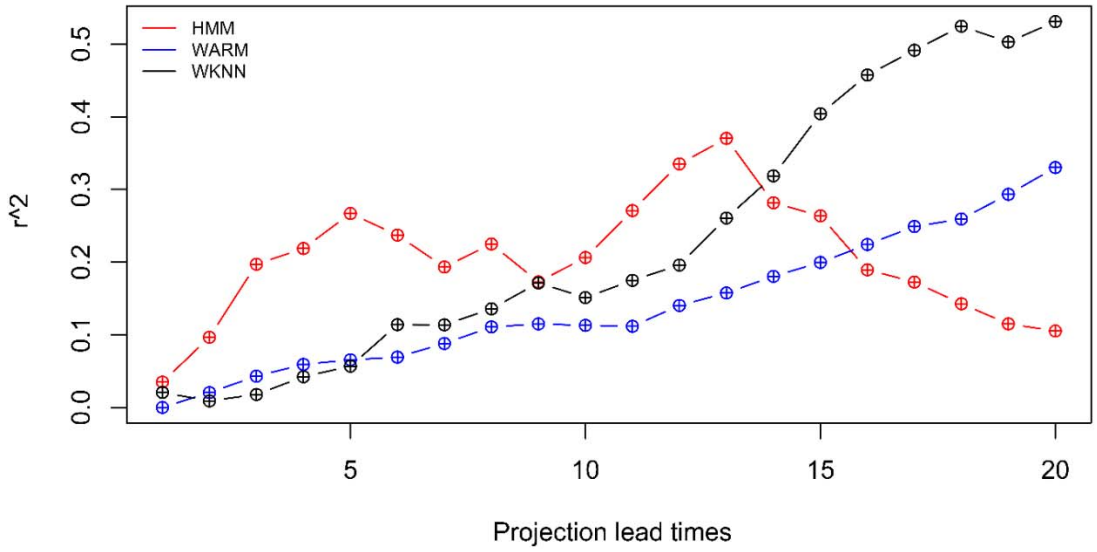

Figure 3.9 R^2 values, a skill measure, of mean flow projections at various lead times (in years) from the three methods

The R^2 values at 1-year lead time are low for all the models, but they increase for HMM with high ~5-year lead time, and longer for WKNN. The authors offer plausible reasoning for this counter intuitive behavior. The low skill at 1-year is mainly due to boundary issues with WARM and WKNN. These two methods use the wavelet component values of the climate forcings at the boundary, the estimates of which in the boundary are known to have high variability [*Torrence and Compo,* 1998], to then project the future 20-year period using AR or block bootstrap influencing the projections at shorter time. This high variability leads to reduced R^2 in 1-2 year lead time. However, at longer lead times, since the wavelet components simulate the quasi-periodic behavior well, at longer lead times this translates into skillful projection of climate forcings and consequently, projections of streamflow – thus, the higher skill at longer lead time. At 1-3 year time scales a higher R^2 is achieved only with simulating the historic flow

accurately. But at longer time scales the skills are based on the mean flow (5-year mean, 10-year mean, 20-year mean etc.) and this averaging reduces the variability and increases the R^2.

3.6 Summary and Discussion

The authors compared three recently developed timeseries simulation models: HMM, WARM and WKNN on the flow time series at Lees Ferry gauge on the Colorado River. All three models perform well in capturing the distributional statistics and PDF and the nonstationary spectral features were better captured by HMM and WKNN. The nonstationary spectral features were better captured by WKNN and HMM compared to WARM. The authors implemented the HMM in a new approach than what was applied in *Bracken et al.,* [2014]. In that, here, the HMM was applied to the climate indices and the flow is generated conditionally. While *Bracken et al.,* [2014] applied the HMM on the streamflow directly.

The models were applied to blind projection and the skill estimated on the average flow at several lead times from 1 to 20 years. The authors found that WKNN showed good skill at longer lead times (~15-20 years) and HMM at shorter (~1-5years) and WARM was in between. WKNN, with its ability to simulate quasi-periodicities in the climate forcings by the wavelets, combined with the ability to capture nonlinearities by the block bootstrap, enables long lead projection skill. None of the models, were capable of reproducing the wet epoch in the early 1900s. This is largely due to the fact that the conditional resampling approach for streamflow in these methods does not have analog prolonged wet periods in the paleo record to draw from. The HMM and WARM models show a better performance of capturing the early 1900s at shorter lead times that will be useful in short term planning.

Colorado River streamflow exhibits significant multidecadal variability [*Nowak et al.,* 2012] that enable skillful projections. The combination of paleo and historic data provides for a

rich variety of scenarios. The WKNN has been used in conjunction with a decision model on the Colorado River and demonstrated to provide improved decision making guidance (*Erkyihun et al,* 2015). The model comparison effort in this paper, provides insights into the stochastic methods available for short and long time scale simulation. The authors hope this will spawn efforts to enhance these methods.

The performance of the projections are determined by using data from the past as there is no future reference streamflow to compare the projections with. The nonlinear dynamical based ensemble simulation technique (Chapter 4) provides ways to recover the dynamics and time varying predictability of streamflow to identify the credibility of the projections to be used for water resources planning and management.

4 A Nonlinear Dynamical Systems based Modeling Approach for Stochastic Simulation of Stream flow and Understanding Predictability

A version of this chapter has been submitted as a journal paper

Abstract

We propose a time series modeling approach based on nonlinear dynamical systems to recover the underlying dynamics and predictability of streamflow and to produce projections with identifiable skill. First a wavelet spectral analysis is performed on the time series to identify the dominant quasi-periodic bands. The time series is then reconstructed across these bands and summed to obtain a signal time series. This signal is embedded in a *D*-dimensional space with an appropriate lag τ to reconstruct the phase space in which the dynamics unfolds. Time varying predictability is assessed by quantifying the divergence of trajectories in the phase space with time, using Local Lyapunov Exponents (LLE). Ensembles of projections from a current time are generated by block resampling trajectories of desired projection length, from the K-nearest neighbors of the current vector in the phase space. This modeling approach was applied to the naturalized historical and paleo reconstructed streamflow at Lees Ferry gauge on the Colorado River which offered three interesting insights: (i) The flows exhibited significant epochal variations in predictability. (ii) The predictability of the flow quantified by LLE is strongly related to the variance of the flow signal and large scale climate. (iii) Blind projections of flows during high predictable epochs showed good skill in capturing the distributional and threshold exceedance statistics and poor performance during low predictability epochs. These results suggest the possibility of the use of this predictability metric as part of an adaptive and flexible water management approach.

4.1 Introduction

With increasing demand for water, such as in the Colorado River Basin (CRB), available water resources have to be managed wisely to address possible supply-demand imbalances. Understanding the variability and predictability of the river flow and the ability to generate realistic flow scenarios is vital in planning and decision making in any river basin.

Linear models or parametric time series modeling techniques have been the traditional staple of modeling and simulating time series, especially streamflow (e.g., *Salas,* 1980). Parametric modeling techniques such as Auto Regressive Moving Average (ARMA) model the time series as a sum of mean and random components, with the mean component modelled as a linear function of past values. Furthermore, they assume data to be normally distributed. Simulations from these models capture the distributional statistics such as mean, standard deviation and lag correlations – but do not capture non-Gaussian and non-stationary features. Non parametric time series models such as the K- Nearest Neighborhood (K-NN) bootstrap [*Lall, 1995*; *Lall and Sharma,* 1996; *Rajagopalan and Lall*, 1998] and kernel density based [*Sharma et al.,* 1997] techniques with their local modeling feature resolve non-Gaussian features well but may not adequately model low frequency variability. For a review of parametric and nonparametric methods for hydrologic time series modeling we refer the reader to *Rajagopalan et al.* [2010]. Simulation from wavelet spectra has been proposed as a way to model the dominant periodicities [*Kwon et al., 2007*] and subsequently modified to capture nonstationarity [*Nowak et al., 2011*]. While there is a suite of time series modelling methods briefly mentioned above, none of them, however, models the underlying dynamics nor takes advantage of predictable regimes to provide skillful simulations.

A nonlinear dynamical systems based time series modelling approach aims to reconstruct the underlying dynamics and, consequently, exploit it for prediction and simulation. The phase space, or multidimensional space, within which the dynamics is purported to evolve, is reconstructed from the observed time series [*Packard et al.,* 1980]. This invokes the mathematical result that a reconstructed phase space with appropriate dimension and time delay (thought of as de-correlation time scale) is a good proxy for the true space within which the unknown dynamics of the system unfolds [*Takens,* 1981]. The state of the system at any time point can be mapped on to the phase space, and using local maps [*Farmer and Sidorowich,* 1987] short term forecasts are made. Thus, the skill is related to the predictability of the current state of the system in the phase space unveiled through local Lyapunov exponents [*Abarbanel et al.,* 1992; *Guégan and Leroux, et al.,* 2009; *Kantz,* 1994; *Nese* 1989; *Wolf et al.,* 1985]. Forecasts from this approach have been shown to outperform those from traditional time series approaches [e.g., *Casdagli et al.,* 1990; *Grassberger et al.,* 1991; *Tsonis,* 1992; *Elsner and Tsonis, 1992*; *Sangayomi et al.,* 1996; *Regonda et al.,* 2005]. These methods require long time series data and thus have been applied widely in financial and medical applications [e.g., *Kantz and Schreiber,* 1997, 1998] but limited in geophysical applications.

One of the early applications to geophysical time series was to model and predict the rise and fall of the Great Salt Lake water levels [*Sangayomi et al.,* 1996; *Lall et al.*, 1996; *Lall et al.,* 2006], forecasting an index of El Nino Southern Oscillation [*Regonda et al.,* 2005] and recent hydrologic applications [*Kirchner,* 2009; *Peterson et al.,* 2014]. These applications, especially of Great Salt Lake water levels, were made possible due to low noise and long time series sequences – which are ideal for nonlinear dynamical based time series modeling. For short and

noisy time series, smoothing is done to reduce the noise [*Schreiber and Grassberger*, 1991; *Porporato and Ridolfi*, 1996, 1997] and enable reconstruction of the dynamics.

For noise reduction, wavelet analysis [*Torrence and Compo,* 1998] is a robust option. We used this to smooth the Colorado River flow to obtain the signal present in the flow series, which is then used in dynamics recovery. Our approach in this paper is a blend of K-NN simulation from the embedding of the system recovered from the wavelet reconstructed signal component of the time series. The embedding requires a determination of the delay time, τ, and embedding dimension, D, through the methods of Average Mutual Information (AMI) [*Moon et al.*, 1995] and False Nearest Neighborhood (FNN) [*Kennel et al., 1992; Abarbanel and Lall, 1996*], respectively. The K-NN simulation technique is then applied on the feature vector in the embedding space for the simulation. Details of the embedding and simulation algorithms are presented in the methodology section.

In addition to ensemble forecasts using K-NN, we also identify time series epochs where we can characterize predictability as a function of time through Local Lyapunov Exponents (LLE) [*Abarbanel et al.,* 1992; *Bailey et al.,* 1995; *Guégan and Leroux, et al.,* 2011]. This is similar to the approach [*Lall et al.,* 2006; *Moon et al.*, 2008] where local prediction error criteria such as local generalized cross validation and local generalized cross validation with leverage were introduced and validated as a measure of potential predictability accounting for the predictive error and predictive error accounting for asymmetry of the neighbors, respectively. The LLE's assess how the separation of two initial points in the embedded space diverges or converges exponentially over a finite future time interval. Predictability is high when the initial condition is locally stable (LLE<0, or small positive), and low otherwise. The LLE thus informs

the use of the forecast in management. We provide an application to the Lees Ferry flow data in the CRB and illustrate performance for both predictable and non-predictable time epochs.

The paper is organized as follows: It starts with a description of the data we used to demonstrate the application of the proposed method; this is followed by the proposed methodology. Then, the results are presented followed by a discussion and summary.

4.2 Study Datasets

Historic and Paleo data used in the study are listed in Table 1 along with links to their sources and are described below.

Table 4.1: Historic and Paleo data used in the study and links to their sources.

Data	Historic	Paleo Reconstructed
AMO (Climate index)	http://www.esrl.noaa.gov/psd/data/timeseries/AMO/	ftp://ftp.ncdc.noaa.gov/pub/data/paleo/treering/reconstructions/amo-gray2004.txt
PDO (Climate index)	http://jisao.washington.edu/pdo/PDO.latest	ftp://ftp.ncdc.noaa.gov/pub/data/paleo/treering/reconstructions/pdo-macdonald2005.txt
Lees Ferry (Streamflow)	http://www.usbr.gov/lc/region/g4000/NaturalFlow/current.html	http://treeflow.info/upco/coloradolees woodhouse.txt

The primary data set is the streamflow at the Lees Ferry gauge on the CRB. This is an important gauge on the river through which 85-90% of the flow in the basin passes. Naturalized flow developed by removing anthropogenic reservoir effects (regulation and consumptive use) is maintained by U.S. Bureau of Reclamation [*Prairie and Callejo,* 2005] and is available for the historic period 1906 to 2012. Paleo reconstructed flow [*Woodhouse et al.*, 2006] is available for years 1490 to 1997.

The Atlantic Multidecadal Oscillation (AMO) and the Pacific Decadal Oscillation (PDO) have been shown to influence the low frequency variability of the Colorado River flow [e.g., *Nowak et al.*, 2012; *Bracken et al.*, 2014]. We use these two climate indices to understand the predictability of the Lee's Ferry flow. The AMO index [*Enfiel et.al.,* 2001] is computed as a monthly area weighted average of North Atlantic (0 to 70^o N) sea surface temperatures (SST), which is subsequently de-trended based on 5^o x 5^o resolution Kaplan SST [*Kaplan et.al.,*1998]. Values were accessed from the NOAA Physical Sciences data website for the period 1856 to present. The paleo reconstruction of annual AMO for the period 1650 to 1990, based on reconstructions of annual sea surface temperature anomalies for the North Atlantic Ocean (0 to 70^o N) from tree rings [*Gray et al.,* 2004], was obtained from the NOAA website. Monthly PDO anomalies from 1900 to present are available from University of Washington. The annual data were taken as the average of the monthly values in this analysis. The PDO is calculated as the first principal component of the Northern Pacific SST [*Zhang et al.,* 1997; *Mantua et al.,* 1997]. Annual PDO values for the period 993 to 1996, based on tree rings from *Pinus flexilis* in California and Alberta, Canada, were generated by *MacDonald and Case* [2005] and are available from the NOAA website.

4.3 Modeling Approach

Unlike traditional stochastic methods that consider the observed process to be a combination of a mean (i.e., signal) and a random component, the nonlinear dynamical approach considers the observed time series as realizations of a dynamical system. Since the dynamical system is unknown, its recovery from the time series involves reconstructing the phase space from observations. Theoretical results [e.g., *Takens,* 1981; *Packard et al.,* 1980] suggest a geometrical correspondence between appropriately reconstructed phase space from the

observations and the true space in which the unknown dynamics unfolds. The geometry of the reconstructed space can provide insights into predictability, and local maps in the embedded space can be developed for skillful prediction and simulation.

4.3.1 Embedding

A D dimensional embedding can be developed from the observed time series $x(\mathrm{t}), \mathrm{t} = 1, 2, .., \mathrm{N}$ using a time delay of τ. The *D*-dimensional vector of the time series can be written as:

$$\boldsymbol{y}(\boldsymbol{t}) = x(t), x(t+\tau), \ldots, x(t+(D-1)\tau); \qquad t = 1, .., N - (D-1)\tau \quad ----- \quad (4\text{-}1)$$

The two parameters *D* and τ, are estimated from the observed data using the procedure described in the forthcoming paragraphs. Real data sets are noisy (with dynamical and measurement errors). Therefore, estimates of the parameters can be unreliable [*Schreiber and Kantz*, 1996] leading to phase space which has poor skill in forecast and simulation. Smoothing can reduce the noise [*Schreiber and Grassberger*, 1991; *Porporato and Ridolfi*, 1996, 1997], but if not done properly it can alter the underlying dynamics [*Sivakumar et al.,* 1999b]. Here we propose to first smooth the streamflow data using wavelets to obtain the signal present in the flow series and estimate *D* and τ for the signal.

Wavelet methods are widely used to decompose time series into signal and noise. An accessible description of these methods is provided by *Torrence and Compo* [1998]. Past application of wavelets to Lees Ferry streamflow can be found in *Nowak et al.* [2011]. The signal extraction from the time series involves four steps: (i) compute the wavelet spectrum of the time series,$x(t)$; (ii) identify spectral bands where the global variation meets a statistical significance test of being different from the background noise; (iii) reconstruct or project the time series on to each of the bands that is significant; and (iv) sum each of the reconstructed series to recover the signal. The Morlet is the preferred wavelet function for its boundary properties and its simplicity for discrete time series applications. We used this wavelet to decompose the streamflow timeseries and for signal extraction. This approach has been applied to

modeling and simulating the Colorado River flow series [*Nowak et al.,* 2011] and for rainfall and temperature in Florida [*Kwon et al.,* 2007]. We refer the reader to these papers and the review paper by *Torrence and Compo* [1998] for details on wavelet analysis. The main steps in obtaining the reconstructed signal is described below. Suppose the frequency band of interest is defined as the interval $\{j_1, j_2\}$, then the reconstructed time series within this band is obtained as:

$$X'_t = \frac{\delta_j \delta_t{}^{1/2}}{C_\delta \psi_0(0)} \sum_{j=j_1}^{j_2} \frac{R\{W_t(S_j)\}}{S_j{}^{1/2}} \quad (4\text{-}2)$$

where C_δ is a reconstruction factor, and δ_j and δ_t are the scale averaging coefficient and time factors respectively. $\psi_0(0) = \pi^{-1/4}$ is the factor that removes the energy scaling, both specific to the Morlet wavelet function. $R\{.\}$ denotes the real part of *W,* the wavelet transform of the data , and S_j is the scale; j_1 and j_2 are the lower and upper scales, respectively. The temporal variance of the reconstructed band is quantified by the Scaled Averaged Wavelet Power (SAWP) and is given by:

$$\bar{W}_t{}^2 = \frac{\delta_j \delta_t}{C_\delta} \sum_{j=j_1}^{j_2} \frac{|W_t(S_j)|^2}{S_j} \quad (4\text{-}3)$$

Reconstruction is done for all the significant bands using the above procedure and they are summed to obtain the signal of the original time series. Similarly, the temporal variances are summed to obtain the SAWP of the signal.

The delay time τ represents the average length of the memory in the system, also be considered as the de-correlation time scale. This can be estimated from mutual information (MI) at various lags using two dimensional histograms [*Fraser and Swinney,* 1986] or kernel density estimators [*Moon et al.,* 1995]. This is tantamount to computing the nonlinear autocorrelation of a time series at various lags. The AMI at a lag *m,* is estimated as:

$$I_m = \sum_{k=1}^{N-m} P(x(k), x(k+m) log_2 \left[\frac{P(x(k), x(k+m))}{P\big(x(k)\big)P(x(k+m))} \right] - - - - - - - - \text{(4-4)}$$

Where: P$(x(k), x(k+m))$ is the joint probability density function and $P\big(x(k)\big), P(x(k+m)$ are the marginal probability density functions, estimated using kernel density estimators, and N is the number of observations. If τ is too small, components in a delay vector are nearly identical, such that adding new components does not provide new information. On the other hand, if τ is too large, successive components are totally unrelated. Popular choices for τ include the first zero crossing of the autocorrelation function and the first minimum of mutual information function [*Fraser and Swinney*, 1986]. The average MI is computed for various lags, and the time delay τ is chosen as the lag of the first minimum of the AMI [*Abarbanel and Lall,* 1996]. Typically, the effectiveness of a model is not highly sensitive to the choice of τ [Kantz and Schreiber, 1997] within the range of minimum AMI or zero crossing of autocorrelation.

Two popular methods for estimating the embedding dimension, *D,* are: the Grassberger-Procaccia [*Grassberger and Procaccia*, 1983a,b] approach (GPA), which estimates the dimension mostly as "fractal" or "non-integer," and the False Nearest Neighbor (FNN) method [*Kennel et al.,* 1992], which computes an integer dimension suitable for embedding. Here, we apply the FNN technique. In this approach the time series $x(t), t = 1, .., N$ is successively embedded in a D_0 dimensional space. For each vector at a current level of embedding, k-nearest neighbors are identified. Then a check is done as to how many of these nearest neighbors are still nearest neighbors as the embedding dimension is increased. Those that fail to be neighbors are called false neighbors. For each D_0, the fraction of false neighbors is computed:

$$r = \frac{\left|\boldsymbol{y}_{i+1} - \boldsymbol{y}_{j+1}\right|}{\left\|\boldsymbol{y}_i - \boldsymbol{y}_j\right\|} ; r \leq r_t \quad ---------- \quad (4\text{-}5)$$

Where $\boldsymbol{y}_i$ and $\boldsymbol{y}_j$ are vectors in dimension D_0 and $\boldsymbol{y}_{i+1}$ and $\boldsymbol{y}_{j+1}$ are the corresponding vectors in dimension D_{0+1}. If the ratio $r > r_t$, where r_t is a threshold [*Kennel et al.,* 1992; *Kantz and Schreiber,* 1997], then D_0 is increased and the computation is repeated until the ratio condition is met or D_0 exceeds a reasonable value, in which case the conclusion is that the time series may not correspond to a low dimensional dynamical system.

4.3.2 Predictability - Local Lyapunov Exponents

Predictability of the signal is quantified using Lyapunov exponents(λ). A Lyapunov exponent measures the rate at which the initial separation of two points in the phase space ($\delta \boldsymbol{y}_0$) grows or shrinks after *n* time steps. A Local Lyapunov Exponent (LLE) may be computed over a finite time starting from any point in the time series, which corresponds to a vector in the embedded space. LLE considers the evolution forward from nearby points in the embedded space to estimate the divergence or convergence of trajectories in the embedded space corresponding to that initial condition. The LLE, $\lambda_d(\boldsymbol{y}, L)$, can be computed for each point $\boldsymbol{y}$ in the phase space and for any corresponding time step, for a finite evolution period, *L,* and for each dimension *d* (*d* = 1,..*D*). Thus, LLE can be obtained for each *L* and *d.* For details on the calculations we refer the readers to [*Abarbanel et al.,* 1992, 1993*; Bailey et al*., 1995; *Abarbanel and Lall;* 1996; *Oseledec,* 1968 and *Wolf, et al.*, 1985]. Negative values of the exponents indicate convergence of the trajectories towards a locally stable point and thus good predictability, while positive values indicate divergence of trajectories and less predictability. The maximum value of the exponents among all dimensions will provide the predictability limit.

4.3.3 Ensemble Simulation

The simulation involves identifying nearest neighbors in the phase space of the signal and resampling a flow trajectory. The implementation at any time *t* proceeds as follows:

(i) Construct the phase space of the flow signal using the embedding dimension and delay obtained from the methods described above.

(ii) For the time *t,* the *feature vector,* $\boldsymbol{y}(t)$, that represents the current state of the system in the embedded phase space is selected.

(iii) K-nearest neighbors (K-NN) of the feature vector in the embedded phase space are selected. Weights are assigned to the neighbors using a weight function that gives highest weight to the nearest K neighbors and least to the farthest [*Lall and Sharma,* 1996]. A heuristic value of $K = \sqrt{N}$ is shown to work well.

(iv) One of the nearest neighbors is selected using the weights. Suppose the selected neighbor in the phase space corresponds to a point in time, *j.*

(v) The sequence or trajectory of the actual flow from time *j* to *j+M,* where M is the desired length of simulation, is selected to be the simulated flow sequence. This can then be thought of as a conditional block bootstrap [*Efron and Tibishirani*, 1993].

(vi) This process is repeated 500 times to produce ensembles of trajectories (i.e., projections) of length M. Note that this is a blind simulation technique in that only data prior to time *t* are used in the simulation.

Steps v and vi differ from the traditional procedure where a local map (e.g., local polynomial), fitted between the K-NN of the phase space vectors and their one step ahead successors, is used to provide a one-step forecast of the time series [e.g., *Farmer and Sidorowich,* 1987; *Casdagli et al.,* 1990; *Grassberger et al.,* 1991; *Tsonis,* 1992; *Sangayomi and Lall,* 1996; *Lall et al.*, 1996, 2006; *Salas.,* 1980; *Wei,* 2006 and *Regonda et al.,* 2005; *Asefa et al.,* 2005]. They allow a multi-step forecast while preserving

the trajectory continuity as well as accounting for the spread across trajectories. This overcomes the problem associated with numerical diffusion that is often associated with iterated one step ahead forecasts.

4.4 Results

The nonlinear dynamics system identification, predictability and simulation are demonstrated on the flow at Lees Ferry in the CRB. Wavelet analysis of the long paleo reconstructed Lees Ferry flow was performed and time varying and global spectra are shown in Figure 4.1.

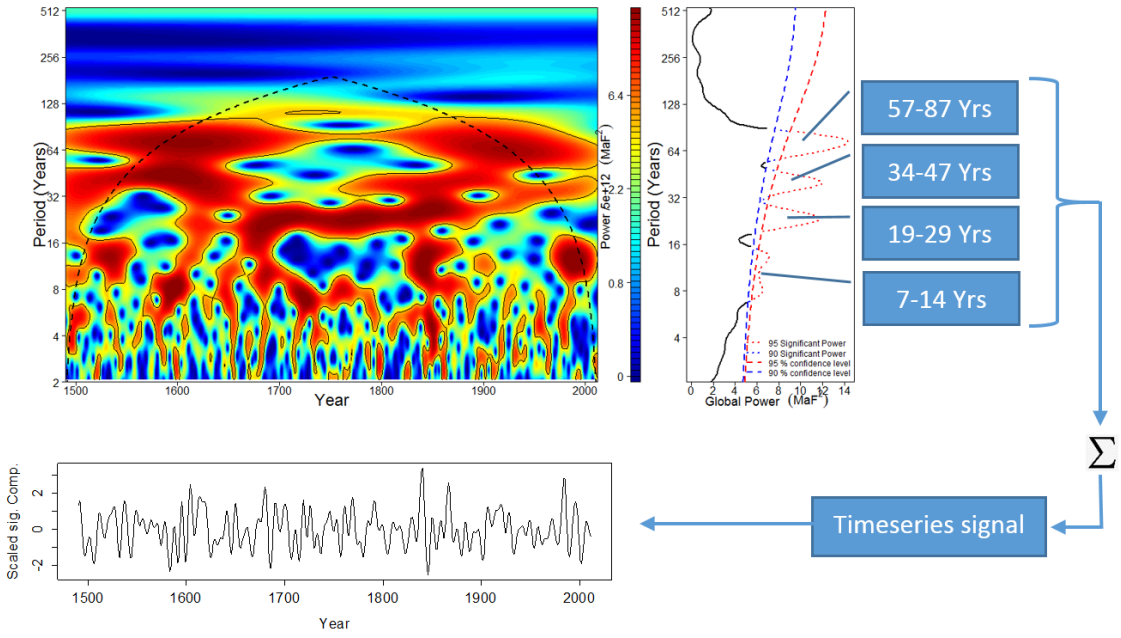

Figure 4.1: Wavelet spectra of paleo reconstructed and observed Lees Ferry flow. The time varying spectrum is in the top left and the global spectrum in top right. Periods that are significant at 90-95% confidence level are indicated. Signal time series obtained as the summation of band filtered components is shown in the bottom.

Four spectral bands are found to have variation that is significantly different from background noise at the 95% confidence level: 57 ~ 87 years; 34 ~ 47 years, 19 ~ 29 years and 7 ~ 14 years. Furthermore, these spectral bands exhibit interesting temporal modulation, for

example, the 57 ~ 87 years and 34 ~ 47 years bands are dominant during 1500 to 1650 and post 1850; the 19 ~ 29 years band is present mainly during 1650 to 1850; and the decadal band of 7 ~ 14 years waxes and wanes throughout the length of the record with a strong presence in recent decades. By summing the information in these bands together, we are recovering the joint variation across different organized sources of information that have a low frequency character, and drop the higher frequency phenomena. The question, then, is whether this low frequency kernel modeled using nonlinear dynamics is able to provide insights into the low frequency evolution of the system into the future, i.e., given that we used signals with periods from 7 to 87 years, does the modeling approach presented here inform the evolution of the mean flow and/or its variance over the next decade or two? This is what we explore in this section.

The AMI computed at various lags using the kernel density based estimators [*Moon et al., 1995*] is shown in Figure 4.2a. The first minimum is at lag 3 but we found a lag of 2 to be good at reconstructing the phase space (discussed later) – thus, we selected a time delay τ of 2 years (Figure 4.2a). As mentioned earlier the model is generally insensitive to the choice of τ within this range of low AMI [*Fraser and Swinney,* 1986]. To identify the best embedding dimension, *D*, the percentages of false nearest neighbors were computed for various embedding dimensions and the selected *D* is shown in Figure 4.2b. The FNN is almost zero for dimension of 3 and zero for 4. We tried both and found no significant difference in the simulation skill and Lyapunov exponents, so we chose *D* of 3 to be parsimonious.

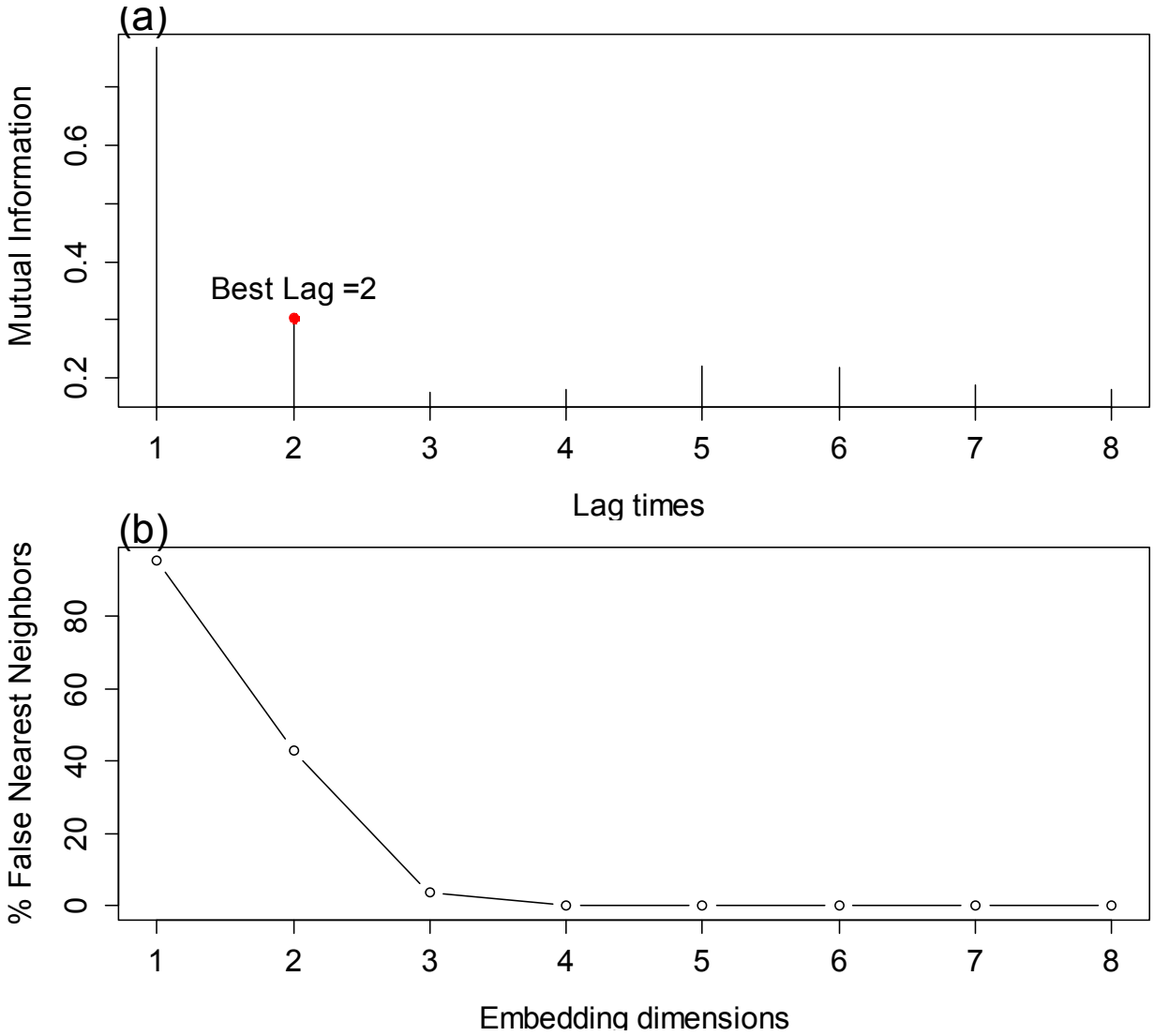

Figure 4.2: (a) Average Mutual Information of the signal time series of Lees Ferry flow, corresponding to various lag time (in years). (b) Percentage of False Nearest Neighbors corresponding to various embedding dimensions of the signal time series of Lees Ferry flow.

Local Lyapunov exponents of the Lees Ferry flow signal for various time steps or scales (referred as *L*) are shown in Figure 4.3. Note that the exponents remain constant after *L* of 16 years. The average exponents corresponding to a large *L*, say 64 years, are the global Lyapunov exponents – which are 0.27, -0.03 and -0.53, respectively, in the three dimensions. Here $\lambda_1 > 0$, which is an indicator of chaos and the first dimension (or direction), inhibits predictability;

λ_2 close to 0 tells us that this system can be modeled by a set of differential equations; and, $\lambda_3 <$ 0 suggests the third dimension provides predictability.

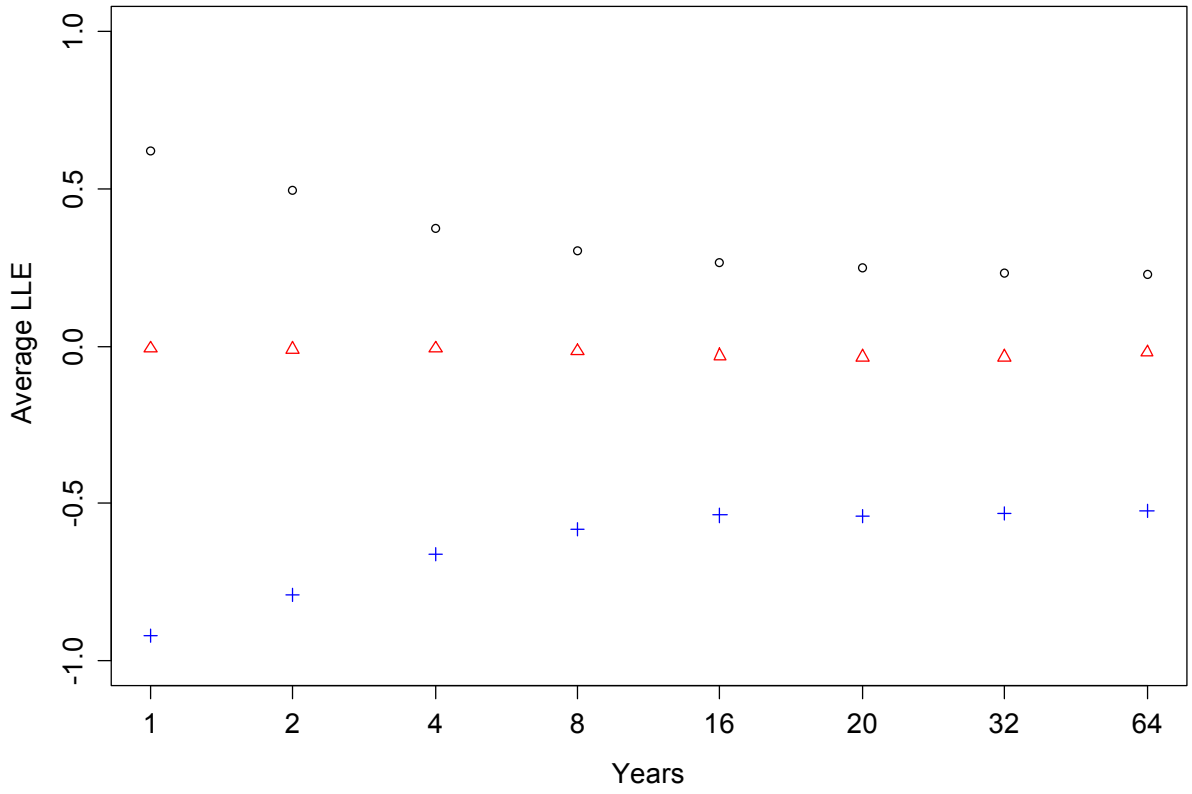

Figure 4.3: Average Local Lyapunov exponents of the Lees Ferry flow signal for the three dimensions evaluated at various time steps or scale (also referred to as L).

The predictability is dictated by the highest Lyapunov exponent, as that leads to divergence of trajectories and, consequently, reduced predictability [*Abarbanel and Lall,* 1996]. The average global Lyapunov exponent over the three dimensions for the entire phase space is -0.1, indicating that the system is conservative. The value of the largest exponent $\lambda_1 = 0.27 =$ 1/3.7 in units of $year^{-1}$ suggests that on an average the errors along the orbit or initial conditions grow as *exp[t/3.7]*, so that after around 4 years or so, the predictability drops rapidly [*Abarbanel*

and Lall, 1996]. However, this predictability varies substantially over time or over parts of the phase space. To understand this, the time varying LLE for a 20-year period (each value plotted is the average of a following 20-year period) for the three dimensions are shown in Figure 4.4a and their average is shown in Figure 4.4b. During epochs when the LLE of the first dimension – which is generally positive and inhibits long lead predictability – is lower, the overall predictability of the system is enhanced. For example, consider the period 1820-1839 when the average LLE is most negative – during this period λ_1 varies in the range of 0.05, which indicates a predictability of ~20 years. At other epochs the predictability varies from 1 to 20 years. For ease of demonstration we use the time varying average LLE (Figure 4.4b) in selecting high and low predictability epochs for simulation. The selected 20-year high predictable epochs are 1731-1750 and 1820-1839, and a couple of low predictability epochs selected are 1681-1700 and 1841-1860.

The temporal variability of predictability is seen from the time varying average LLE (Figure 4.4b) – along with the temporal variability of the signal variance, SAWP, of the Lees Ferry flow signal. There are distinct epochs where the average exponent is close to zero, indicative of reduced predictability, and where the average exponent is highly negative suggesting good predictability. Furthermore, the LLEs track the signal SAWP very well – indicating that reduced predictability epochs coincide with increased signal variance and that good predictability epochs are consistent with reduced signal variance, which are quite intuitive. That the predictability of the Lees Ferry flow system waxes and wanes over time and is consistent with the variability of the signal is very interesting and has significant implications for water resources management.

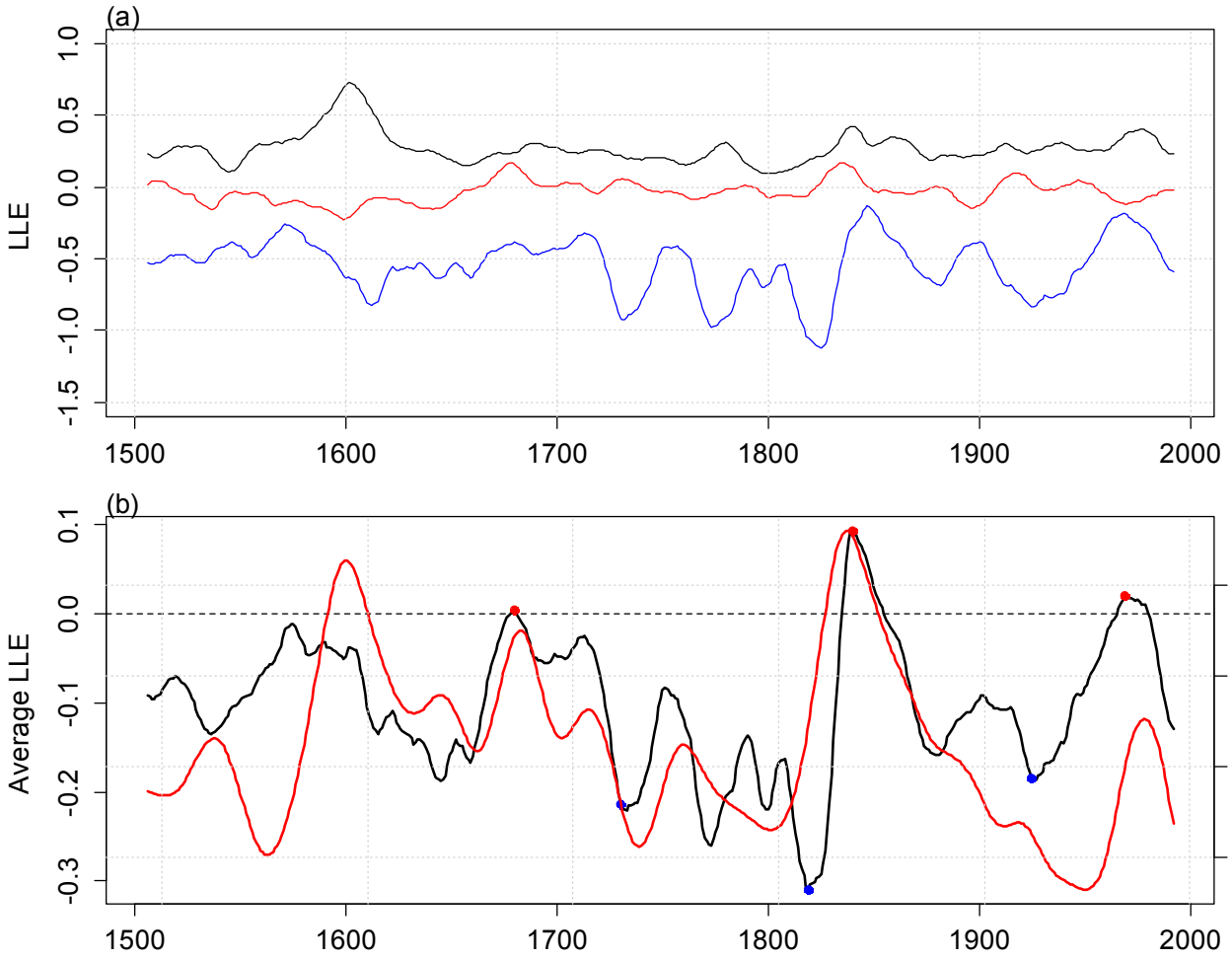

Figure 4.4: Average Local Lyapunov exponents at each year with a time step of 20 years (a) for the three dimensions and (b) for the Lees Ferry flow signal (black) and the 20-year SAWP of the flow signal (red). The value of the exponent at each year corresponds to the average of following 20-year period - similarly for the SAWP. The selected epochs of high predictability 1731- 1750, 1820-1839 and 1926-1945 are shown as blue dots and the low predictability epochs 1681-1700, 1841-1860 and 1970-1989 as red dots.

The embedding in the three dimensions is displayed in Figure 4.5. The attractor is in the form of a scroll with the trajectories at the center representing the low frequencies, and the outer strands are period excursions at even lower frequencies. This is similar to that seen in *Abarbanel and Lall*, [1996] for the dynamics of the Great Salt Lake levels. To understand the evolution of these epochs in the phase space, the trajectories of these epochs are plotted on the attractor and are shown in Figure 4.5.

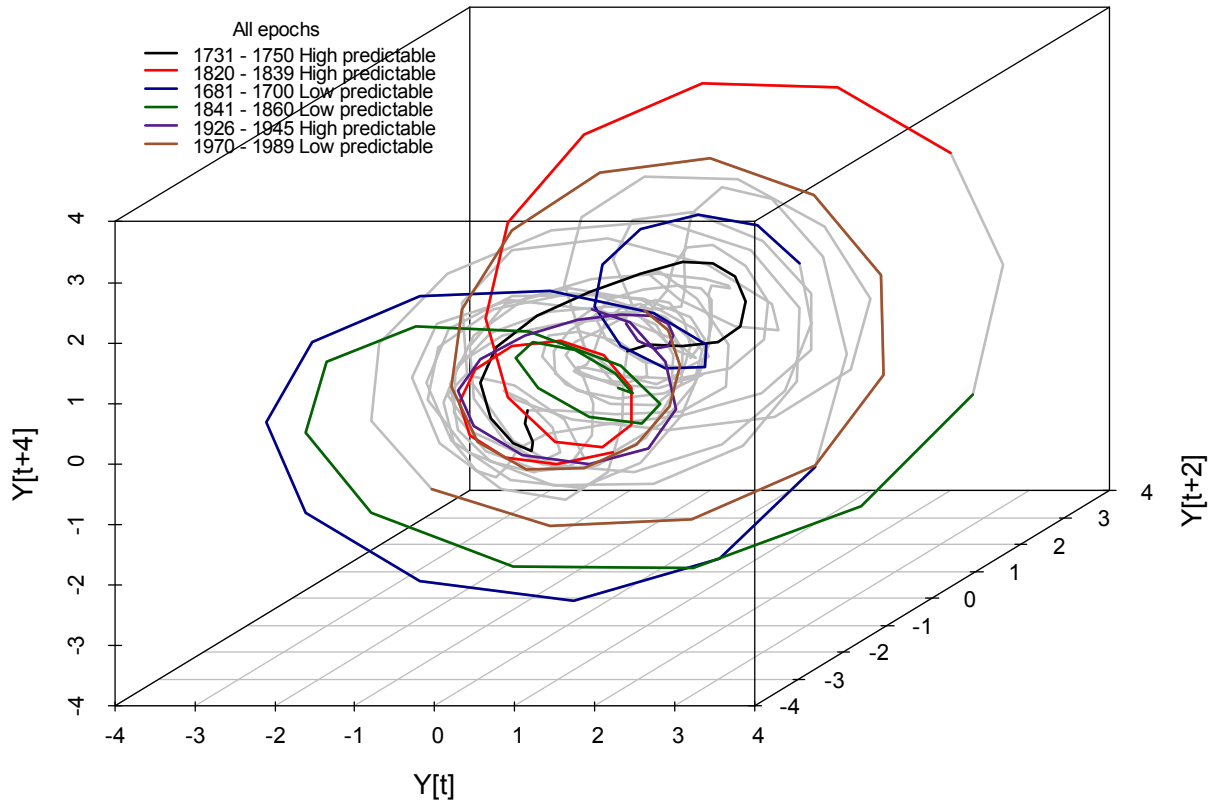

Figure 4.5: Trajectories of epochs shown in the phase space - high predictable epochs 1788-1807 (red) and (b) 1820-1839 (green); low predictable epochs 1681-1700 (blue) and 1841-1860 (cyan) and, 20th century epochs 1926-1945 (magenta) and 1970-1989 (yellow).

An interesting observation emerges in that the low predictable epochs (1681-1700; 1841-1860 and 1970-1989) have their trajectories excursing to the outer parts of the attractor while, the trajectories of high predictable epochs (1788-1807; 1820-1839 and 1926-1945) tend to stay within the inner parts of the attractor. However, the trajectory of the high predictable epoch 1820 -1839 does an excursion to the outer reaches of the attractor. This is because the system transitions immediately to one of the lowest predictable epoch of 1841-1860, thus the later part of the 1820-1830 epoch is already in transition to being low predictable. These trajectories seem to suggest that the outer portions of the attractor are less predictable and thus unstable while the

inner parts provide higher predictability. This highlights the ability of the nonlinear dynamical systems based approach described and demonstrated above to capitalize on the regime dynamics for skillful projections, unlike traditional time series methods.

An interesting question is: what is the source of this predictability? Recent studies show the association between AMO and PDO in modulating the variability of Lees Ferry flow [e.g., *Nowak et al.,* 2012; *Bracken et al.,* 2014]. As an initial rudimentary effort to answering this question we relate the variability of the climate indices to Lees Ferry flow predictability. The SAWP of the signal of the climate indices, computed in the same manner as that of the flow, is shown along with the average LLEs (Figures 4.6 a,b,c). The variability of PDO and AMO seem to be out of phase with the predictability in that a higher variance of climate signal leads to high negative values and, consequently, higher predictability. This is clarified in Figure 4.6c which shows the average LLE along with the sum of the SAWP of signals of both of the climate drivers. The climate system is more predictable when the drivers have higher variability [e.g., *Kirtman and Schopf*, 1998] – which then imparts predictability to regional hydrology. We recognize that the linkage between variability in climate drivers and flow predictability is suggestive but not quantitatively sound. This would require detailed analysis of the predictability of the climate drivers and also the use of climate models to understand the mechanisms that translate predictability from large scale climate to the flow. However, this linkage between climate drivers and Colorado River flow signal is quite interesting; suggesting that the epochal natural of the predictability of Lees Ferry flow is orchestrated by the variability in large scale climate.

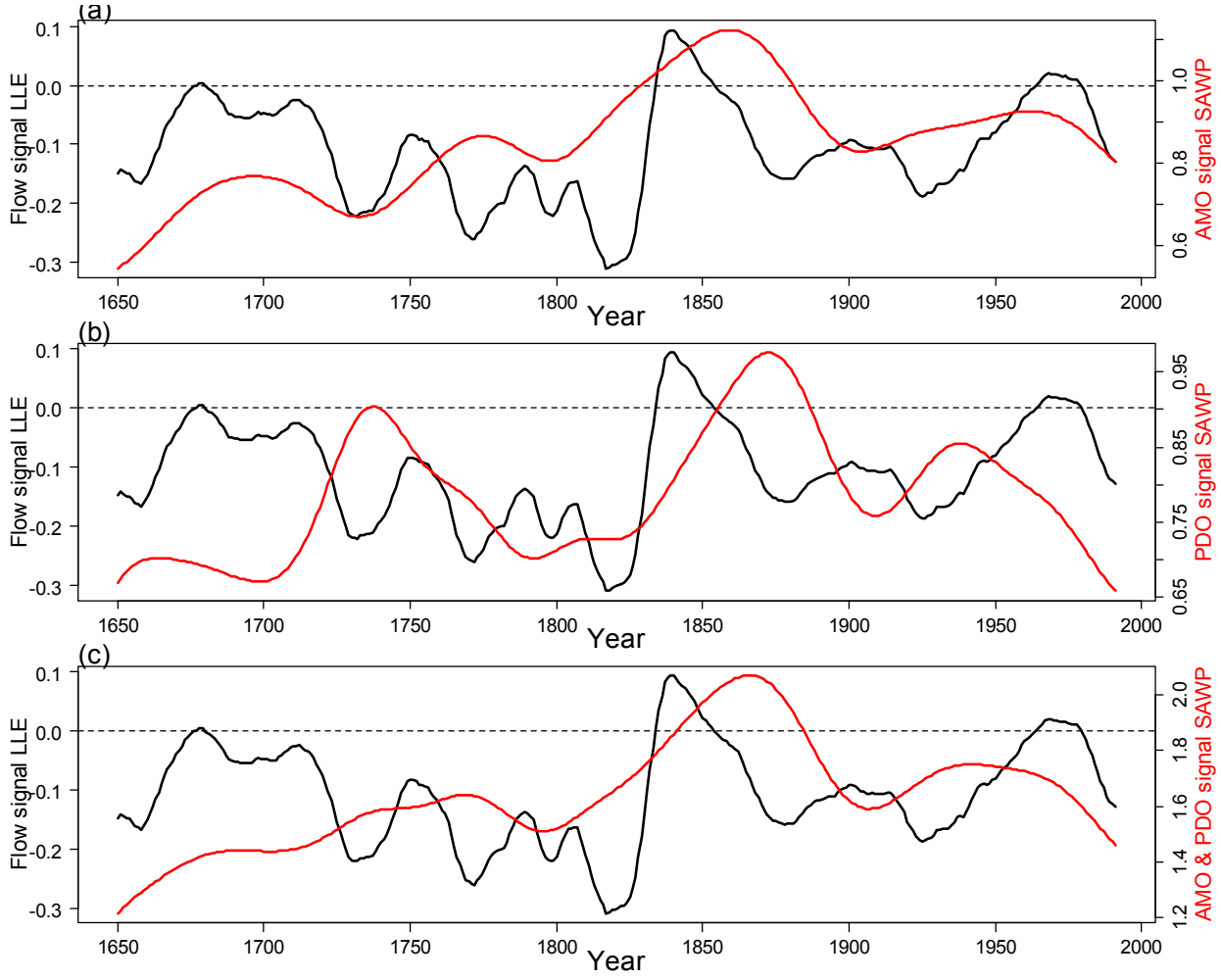

Figure 4.6: (a) Same as Figure 4.4 but with SAWP of the PDO signal (red). (b) Same as (a) but with SAWP of the AMO signal (red). (c) Same as (a) but with sum of SAWP of AMO and PDO signals (red).

We tested the epochal nature of the projection skills on four selected 20-year epochs mentioned above - high predictability epochs of –1731-1750 and 1820-1839 – and low predictability epochs of – 1681-1700 and 1841-1860. Blind projections were made for these 20-year periods using the block bootstrap method described in the previous section. The probability density functions (PDF) of the flow simulations are shown as grey along with their median PDF and that of the historic flows for the four epochs in Figure 4.7. The top panels (Figures 4.7a,b) show the PDFs of high predictability epochs and it can be seen that the projections capture the PDF of the historic very well. The PDFs of the projections from lower predictability epochs

(bottom panel, Figures 4.7c,d) misestimate the historic PDF. A Kolmogrov-Smirnov test suggested that the simulated and historical distributions of the high predictable epochs are indistinguishable and not the case for low predictable epochs.

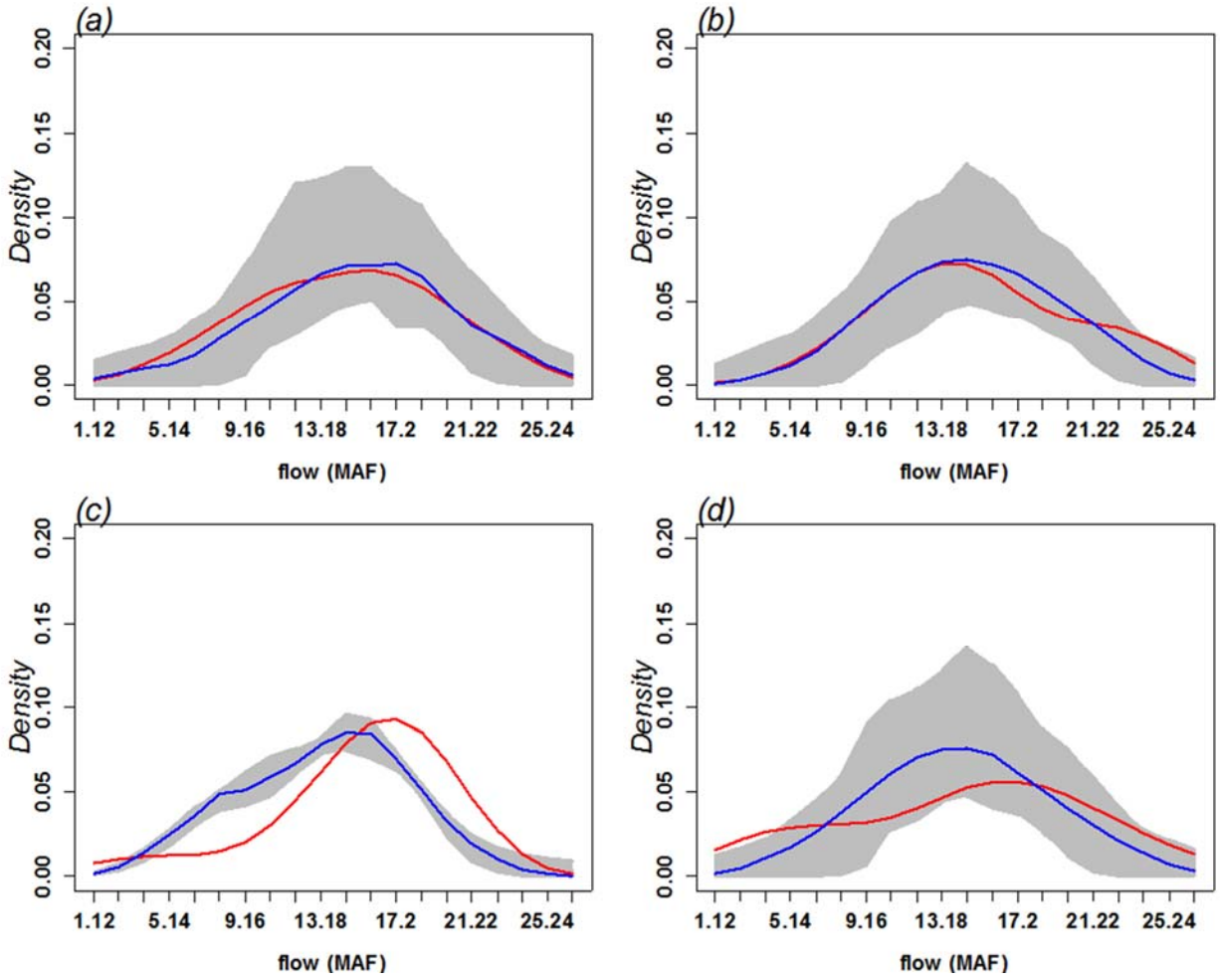

Figure 4.7: Probability Density Functions (PDFs) of flow projection ensembles (grey), their median (blue) and that of historic flows (red) for the high predictability epochs (a) 1731-1750 and (b) 1820-1839; and low predictability epochs (c) 1681-1700 and (d) 1841-1860.

The projection ensembles and the historic flows are shown in Figure 4.8 in which it can be seen that during the predictable epochs (top panels, Figures 4.8a,b) the median of the ensembles (horizontal line in the boxes) tracks the variability of the historic flows (red line) quite well, but not well during the epochs with lower predictability (bottom panels, Figures 4.8c,d).

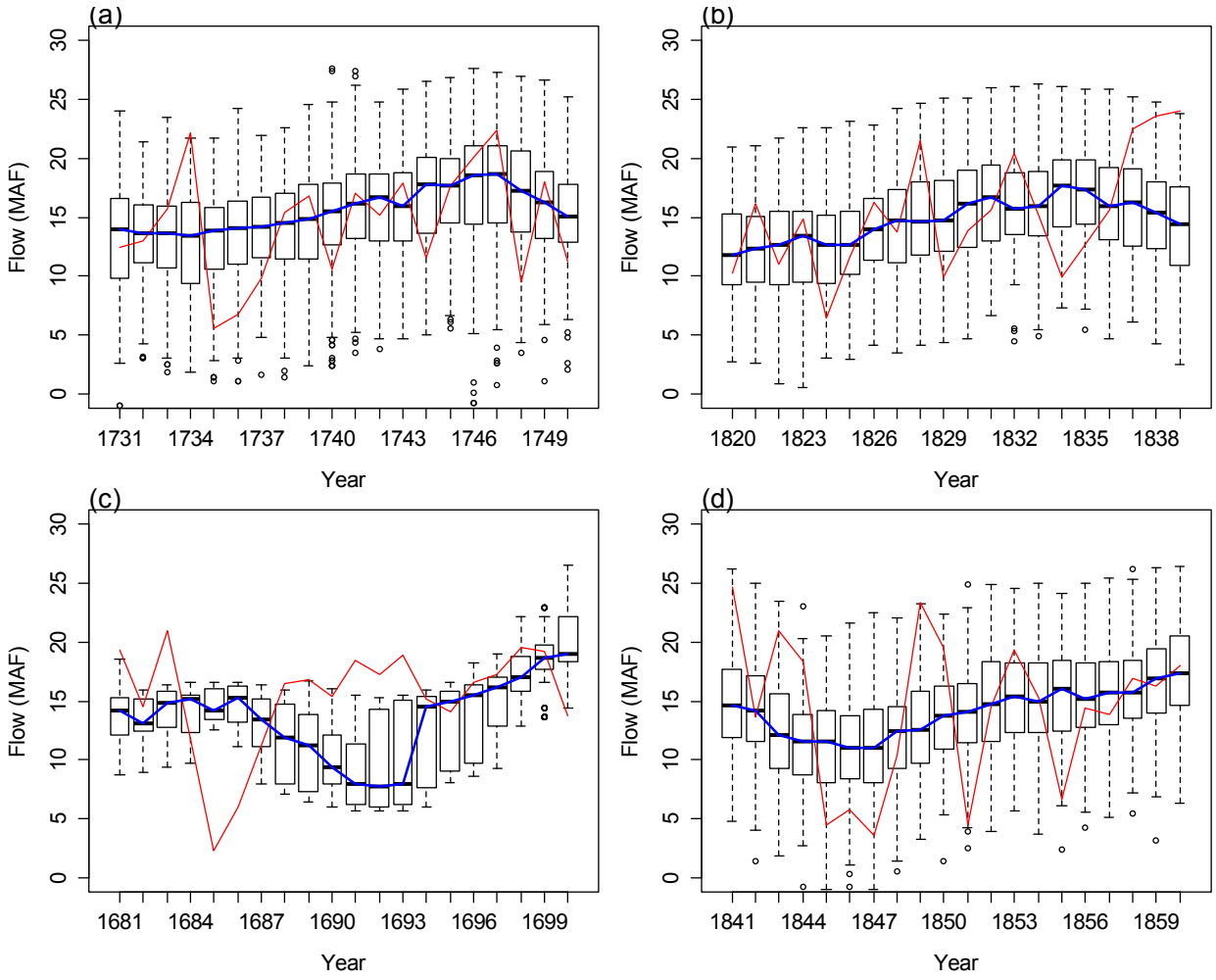

Figure 4.8: Projection ensembles (boxplot), median (blue) and the historic flows (red) for the high predictability epochs (a) 1731-1750 and (b) 1820-1839; and low predictability epochs (c) 1681-1700 and (d) 1841-1860.

An important utility of these projections is for use in multidecadal water resources planning and management. To this end, the ability to capture aspects of sustained wet and dry periods is crucial. Threshold crossing statistics of deficit and excess are computed for each ensemble based on the threshold of 15MAF (the long term average flow of the modern period) and are: total excess and deficit about this threshold, and maximum and minimum surplus and deficit over the 20-year horizon. These are shown as boxplots along with the corresponding values from the historic flows as red dots. Figure 4.9 shows the excess (top panels) and deficit (bottom panels) statistics for the high predictability epochs. The historic values (dots) of all

statistics are well captured by the simulations within the interquartile box of the simulations, and the excess and deficit minimum are over simulated. This indicates that excursions about the thresholds, which are higher order statistics, are also simulated very well, that could be of significant use in long term water resources planning.

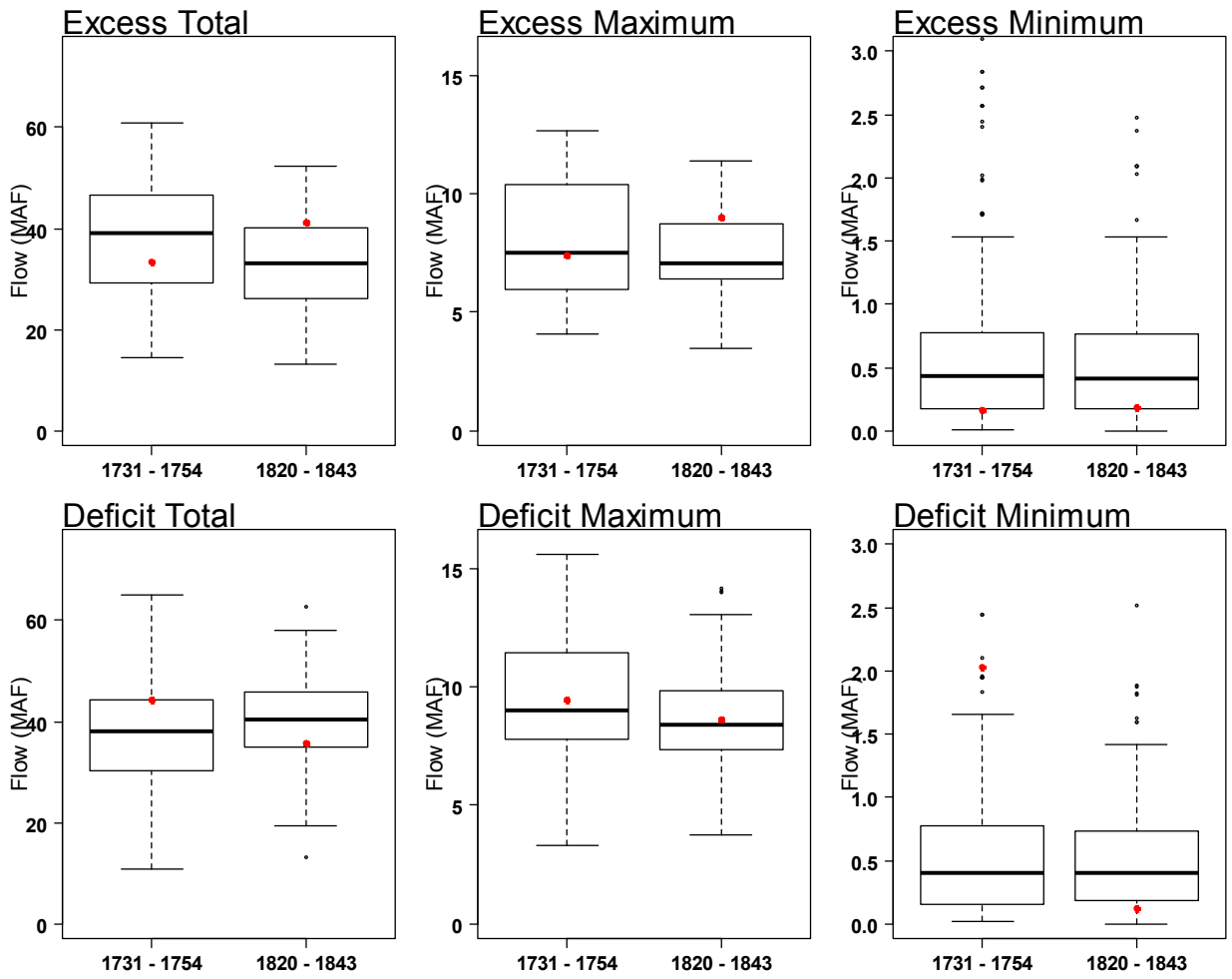

Figure 4.9: Boxplots of surplus and deficit statistics from flow projections for high predictability epochs 1731-1750 and 1820-1839 - (a) total surplus, (b) maximum and (c) minimum surplus from the projections. The values from the historic flows are show as red dots. Boxplots of deficit statistics - (d) total deficit, (e) maximum and (f) minimum deficit.

In comparison, the low predictability epochs show poor performance of the excess and deficit statistics (Figure 4.10), with most of the historic values outside the interquartile box of the

simulations. These results suggest that the predictability of the system dynamics permeates through all aspects of the system statistics.

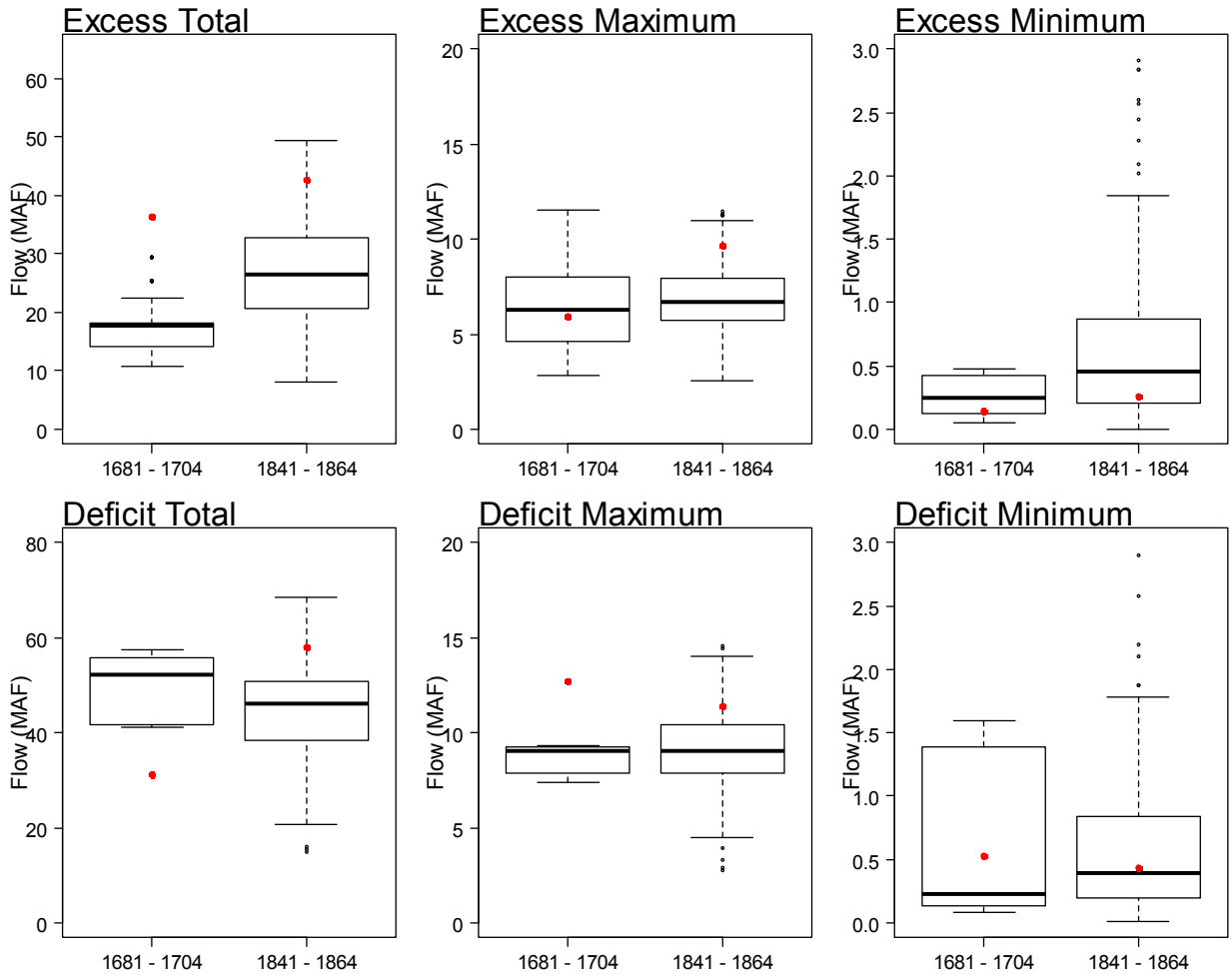

Figure 4.10: Same as Figure 4.9 but for low predictability epochs 1681-1700 and 1841-1860.

To further assess the performance of the simulations in capturing wet and dry sequences which are crucial for water resources management, we also computed storage statistics using the sequent peak algorithm [*Loucks and Van Beek,* 2005]. The results are consistent with the performance of deficit and excess statistics in that they are well captured in predictable epochs and poorly in low predictable epochs (figures not shown).

The basin has experienced several impactful events starting in the early 20th century - especially the water sharing agreements among Basin States in the early part of 20th century and the recent ongoing drought in the Western US and in the basin for over a decade. Interestingly, the Lyapunov exponents are quite negative during early 20th century indicative of high predictability and the recent decades of drought have low predictability (as the exponent values are closer to zero). To highlight these further, projections were made for two epochs from the last century (1926-1945 and 1970-1989) for which the PDFs are shown in Figure 4.11.

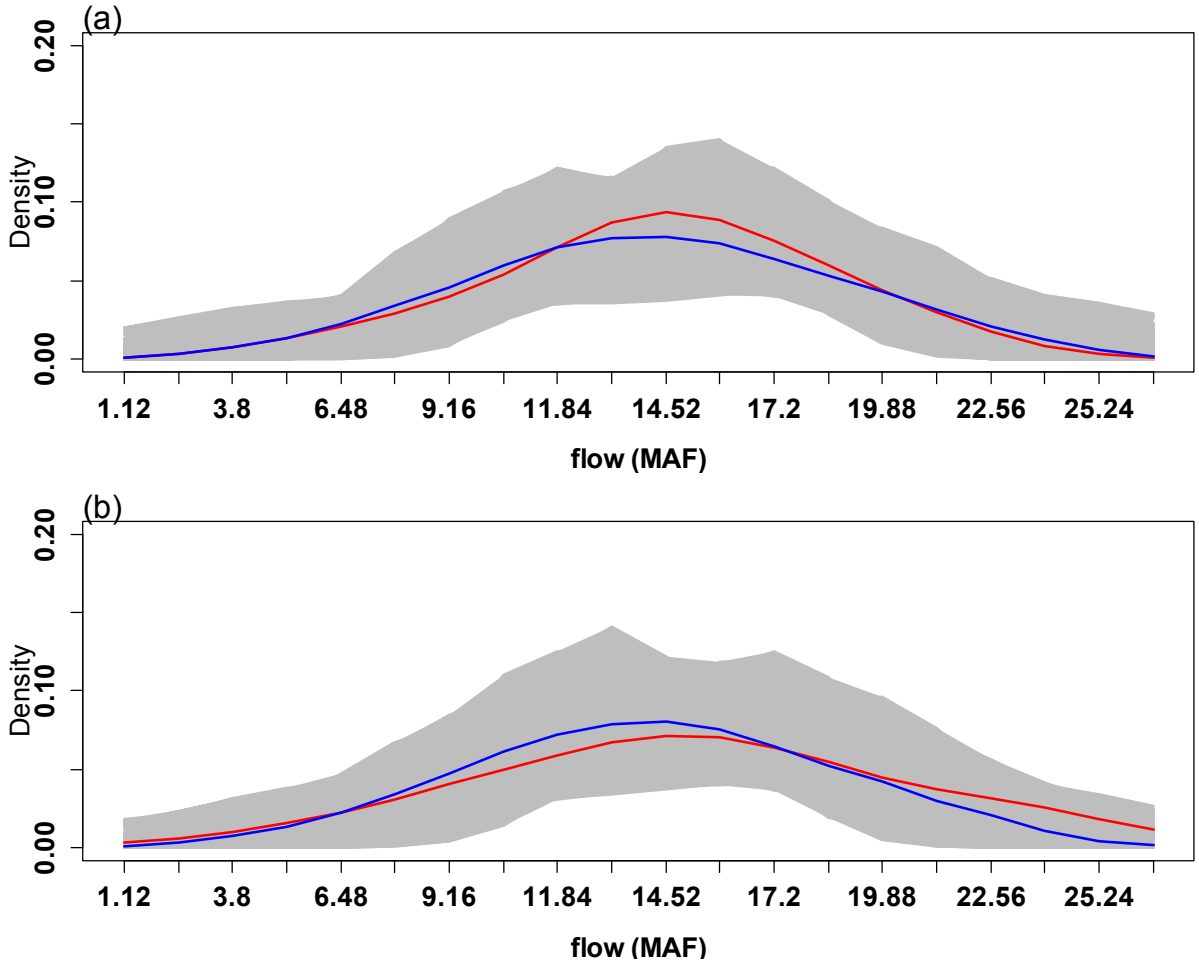

Figure 4.11: Probability Density Functions (PDFs) of flow projection ensembles (grey), their median (blue) and that of historic flows (red) for (a) early 20th century epoch 1926-1945 and (b) recent epoch 1970-1989.

Consistent with high predictability of the early part of 20th century, the projections capture the historic PDF very well. However, the PDFs of flow projections for the recent decades deviate significantly from the historic PDF, consistent with low predictability. The historic flow variability (red) falls within the interquartile range of the ensembles in most of the years, while in the later epoch (Figure 4.12b) the historic flow is outside the interquartile range for most of the years, conspicuously so during the high flow period of 1982-1986.

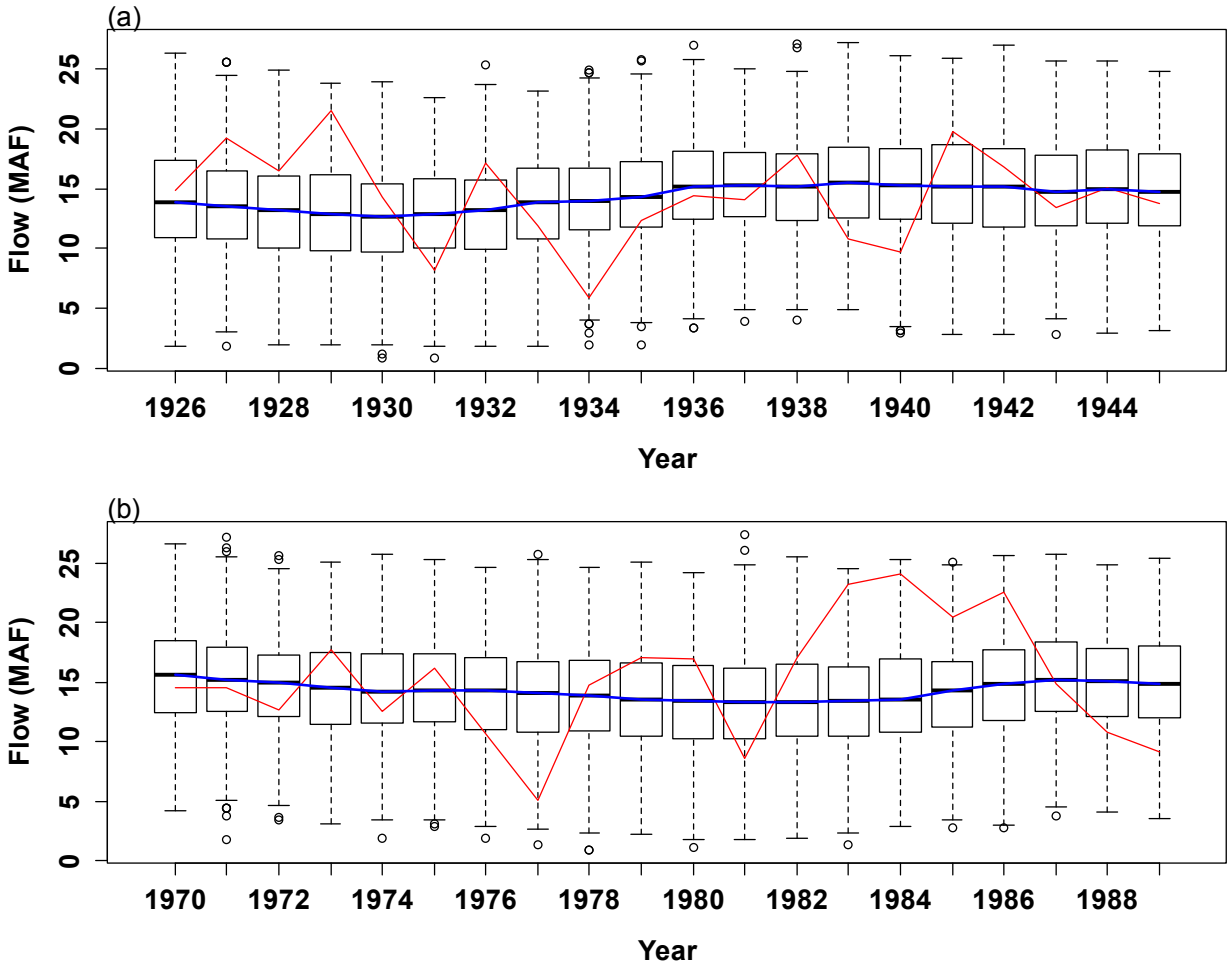

Figure 4.12: Projection ensembles (boxplot), median (blue) and the historic flows (red) for (a) early 20th century epoch 1926-1945 and (b) recent epoch 1970-1989.

4.5 Summary and Discussion

A novel approach to stochastic time series simulation is proposed, which is based on reconstructing the phase space in which the dynamics of the time series unfolds. The approach also provides insights into epochal variability of predictability of the time series. The phase space reconstruction requires embedding the time series in appropriately estimated *D* dimensions with a time delay of τ. Theory suggests that this maps to the true phase space in which the underlying dynamics unfolds enabling to take advantage of the system predictability to provide skillful projections and forecasts. Estimation of the two parameters *D* and τ from data with noise which includes geophysical time series are often unreliable and smoothing is suggested. We proposed obtaining the signal time series by wavelet filtering the original time series within significant frequency bands identified from wavelet spectral analysis. Thus the reconstructed phase space is that of the signal component of the time series. Lyapunov exponents measure the rate of divergence of trajectories in the reconstructed phase space providing an estimate of predictability – higher positive values indicating rapid divergence and thus lower predictability and vice-versa. The exponents can be computed locally in the phase space to provide temporal variability of predictability. Projections from a time point *t* involves (i) mapping the current state (or feature vector) of the system on to the reconstructed phase space, (ii) identifying K-nearest neighbors of the current feature vector and (iii) resampling one of them with a weight function – which corresponds a time *j,* and, (iv) a M-time step sequence (or trajectory) of original time series from the period *j* to *j+M* forms the simulated M-step projection. Identifying the neighbors in the phase space of the smoothed series and resampling the original time series is a new

approach to stochastic time series simulation. This is repeated to generate ensembles. Using data prior to time *t* enables blind projections, which is implemented here.

We applied this modeling approach to the long paleo reconstructed flow at Lees Ferry gauge, an important location on the Colorado River which represents 85-90% of its flow. Four dominant period bands in the 7 year to 57 year range were identified from the wavelet spectrum analysis; filtering the flow series in these bands provided the signal time series. The reconstructed phase space showed an inner and outer scroll indicative of lower and higher period variations. The global Lyapunov exponents were negative suggesting that the signal in the flow series is generally predictable. However, the local Lyapunov exponents showed significant epochal variations – with some epochs exhibiting high predictability (negative exponent values) and some low predictability (exponent values close to zero). The early part of 20th century when the Colorado River compact agreements were negotiated was a high predictable epoch and the recent decades with the prolonged and unprecedented drought in observed record has low predictability. The predictability coincides with the temporal variability of the signal variance – suggesting that periods of high signal variance impedes predictability and vice-versa. Furthermore, the temporal variability of the signal variance of large scale climate indices AMO and PDO also coincide with the temporal variability of the flow signal Lyapunov exponents – indicating that large scale climate features modulate flow predictability. Blind projections of stream flows during high predictable epochs show good skill and capture all the distributional, drought and surplus statistics, while the low predictability epochs had poor performance on these measures.

The time varying predictability of the streamflow offers interesting insight into the system. It suggests that low predictability epochs are an inherent part of the dynamics of the system and resistant to any improvements in modeling efforts – statistical or physical.

This also provokes the tantalizing idea that perhaps water resources management should adapt in a flexible manner to these predictability epochs. The local Lyapunov Exponents could be modeled as a time series and projections of low predictability epochs and high predictability epochs could trigger appropriate management and planning responses. This study opens new opportunities to perceive hydrologic predictability and consequently water management.

5 Application of Decadal Scale Projections Based on Large Scale Climate Indices to Decision Making in the Colorado River Basin

Abstract

Effective water resources planning and management requires skillful decisions on multi-year or decadal timeframes. In basins such as the Colorado River Basin (CRB), streamflow is not stationary but exhibits variability that reflects teleconnections with large scale climate indices such as Atlantic Multi-decadal Oscillation (AMO) and Pacific Decadal Oscillation (PDO). The Wavelet K-Nearest Neighbor (WKNN) model, a stochastic streamflow simulation and projection model developed as part of this research (see Chapter 2), identifies and reconstructs dominant quasi-periodic signals in the AMO and PDO using wavelet analysis, simulates each using block K-Nearest Neighbor (K-NN) bootstrap, then simulates the streamflow using a K-NN bootstrap conditioned on the simulated climate forcings, and has been demonstrated to produce skillful decadal scale projections of streamflow in the CRB. The Bureau of Reclamation's 2012 Colorado River Basin Supply and Demand Study (Basin Study) used scenarios to explore the use of options and strategies such as infrastructure development, conservation and efficiency improvements to address supply-demand imbalances. Each year in the simulated scenarios, decision criteria such as reservoir elevations and average flows over recent years were applied to determine system vulnerability and the need to implement options and strategies to mitigate future shortages. This chapter describes the addition of the WKNN generated decadal scale flow projections to the decision criteria. In addition, periods of poor predictability are identified by using a nonlinear dynamical system based approach to recover the underlying dynamics. Time varying predictability is assessed by quantifying the divergence of trajectories in the phase space

with time, using Local Lyapunov Exponents (LLE). Skillful decadal scale streamflow projections within the high predictable time epochs are used to indicate future flow conditions and improve decisions. An ensemble of projections is considered to be wet or dry based whether or not the mean exceeds some reference threshold and that information is used to constrain the decisions. Based on projections being wet, dry or unpredictable, improved decisions are shown to reduce cost or reduce shortage and are illustrated by tradeoff curves of risk of shortage vs. cost.

5.1 Introduction

Decisions in water resources planning and management are crucial to satisfy the multipurpose and conflicting uses of water in any river basin. The interaction of the available water with human activity and the environment is so complex that any particular action taken could have serious consequences in the interconnected system [*Gupta et al.,* 2011]. A good understanding and representation of the system in a decision model along with the rules and regulations provides a platform for the evaluation of alternatives [*Hashimoto et al.,* 1982; *Loucks and van Beek.,* 2005]. The use of stochastic timeseries models can provide a range of plausible flow scenarios that can be used to study and understand the system's response and to answer "what if" questions through scenario analysis [*Loucks and van Beek,* 2005] for the robustness of the decisions. Robust Decision Making is an approach to show the ability of the decision model to perform sufficiently well under the range of plausible futures [*Lempert* 2002a; *Lempert and Groves* 2010; *Means et al.,* 2010; *Groves et al.,* 2013; *Groves et al.,* 2015; *Lempert 2002a;Hall et al., 2012*]. This approach is a platform to evaluate and prioritize alternatives in terms of potential opportunities and risks under varying future flow conditions [*Wagener et al.,* 2006; *Reclamation,* 2012; *Groves et al.,* 2013]. In this, scenarios generated as a combination of future

plausible flows and demands provide the extent of future risks so that appropriate decisions can be made for mitigation. Decisions made to mitigate risks such as supply-demand imbalances at a given year are triggered by vulnerability indicators generated from the past state of the system [*Reclamation,* 2012; *Groves et al.,* 2013]. This approach ignores the future state of the flow.

Incorporating the future flow conditions in the decision framework [*Groves et al.,* 2008] conditions or modifies the level of risk (supply-demand imbalances) determined from the past state of the system. Streamflow magnitudes can sustain as low flows for multiple years or decades, for example, the recent drought in the south western US [*Barnett et al.,* 2008] and change over time to high sustained flows. Such sustained variability of the streamflow in this paper is referred as the nonstationarity characteristic of streamflow. The nonstationarity characteristics of the streamflow at the internal to decadal scale are, influenced by the natural climate variations such as SST [*Murphy et al.,* 2010].

Previous research [*Cook et al.,* 2004; *Meko et al.,* 2007] show that sustained droughts in the past can happen at the same magnitude and duration sometime in the future.

5.1.1 Streamflow simulation and projection

Long term (multi-decades to century scale) plans for the physical infrastructure and operating policies of a basin should be made with consideration of the long term variability of hydrology and demands such that risks and reliabilities can be quantified [*Hallegatte,* 2009; *Yohe et al.,* 2004]. For short term (seasonal) decision making, e.g., decisions about reservoir releases on daily or seasonal timescales, a wide range of forecasting techniques are in use that rely on information about current and forecasted weather/climate conditions and may also rely in part on timeseries models, to determine operations that best meet system objectives [*Raff et al.,* 2013]. Between long and short term is multi-year to decadal scale decisions to implement changes that

would take effect over several years and could benefit from projections based on understanding of multi-year to decadal scale variability [*Nowak,* 2011; *United States Department of the Interior*, 2001]. The sustained flow variability triggered the need for decadal scale planning and management of water resources [*Vera et al.,* 2010; *Meehl et al.,* 2009] and develop techniques to project the streamflow magnitude at decadal scale skillfully [*Switanek and Troch,* 2011]. The importance of decadal scale variability for planning and management of water resources for example in the CRB is recognized [*United States bureau of the Interior,* 2001]. This is an area that has recently gained traction among hydro climate scientists based on insights that relate streamflow variability at seasonal to multi-decadal time scales to climate forcings such as the El Nino Southern Oscillation (ENSO) [*Ropelewski and Halpert.,* 1986, 1989; *McCabe and Dettinger,* 1999; *Rajagopalan et al.,* 2000], the Pacific Decadal Oscillation (PDO) [*Latif and Barnett,* 1994; *Hidalgo,* 2004; *McCabe et al.,* 2007], and the Atlantic Multi-decadal Oscillation (AMO) [*Enfield,* 2001; *Tootle et al.,* 2005; *Timilsena et al.,* 2009]. Furthermore, these forcings are nonstationary and thus impart nonstationarity to the variability of precipitation and flow – this has been identified for Colorado River flows [e.g., *Nowak et al.,* 2012].

The WKNN simulation and projection model [Chapter 2] proved its suitability for simulation and projection of streamflow at decadal and multi decadal time scales. It simulates/projects streamflow sequences conditionally based on the variability of large scale climate indices. Similar studies suggest that the future flow conditions can be reasonably estimated using available tools and the choice of appropriate forcing [*Hughes,* 2015]. Climate indices such as ENSO, AMO and PDO are known to influence precipitation in the central and western United States. ENSO is known to have weak signal in the upper CRB [*Regonda et al.,* 2006*; Grantz et al.,* 2005], AMO and PDO signals, which have strong teleconnection with the

Colorado River flow, are used to conditionally simulate the naturalized flow at Lees Ferry. This modeling approach can be applied to any river basin where there exists a strong teleconnection of streamflow with climate indices such as Sea Surface Temperature (SST) anomalies.

5.1.2 Epochs of Predictability

Effective use of projections of future flow in water resources planning and management decisions depends on the skill of the projections. Because the natural processes underlying the variability of streamflow are not completely understood and include some degree of chaos, it is useful to quantify the time-varying predictability of streamflow projections using a nonlinear dynamical modeling approach [Chapter 4]. In this the underlying dynamics can be recovered [*Kennel et al.,* 1992; *Abarbanel and Lall,* 1996] and the time varying predictability of the projections can be determined through the Local Lyapunov Exponent (LLE) [*Abarbanel et al.,* 1992; *Bailey et al.,* 1995; *Guégan and Leroux, et al.,* 2011]. In Chapter 4 we applied this method in the CRB and demonstrated its suitability in identifying the predictable and non-predictable time epochs. In this phase of the research, the time varying predictability of the projections is used as a guide to using the projections in decision making. The projections are considered feasible and used in decision making in the predictable time epochs; otherwise, decisions are made without the projections.

5.1.3 The Colorado River Basin Supply and Demand Study

The CRB stakeholders anticipate increasing water demands in the basin in the coming decades [*Reclamation,* 2012]. This, along with the recent decade long dry spell and future drying from a warmer climate in the basin, leaves users at risk of unmet demands in the future. Under such circumstances, mid-term decisions may be considered either to increase the water availability through infrastructure development, transfers, etc., or to reduce demands through

conservation and other options to use the available water more efficiently. Reclamation recently undertook a major study, the Colorado River Basin Supply and Demand Study (Basin Study) to project future supply/demand imbalances in the CRB; in this they developed a decision making framework to explore the possibility of implementing options and strategies when the system shows signs of being vulnerable to the risk of not meeting demands[2]. For such decisions that take effect at decadal and multi-decadal time scales, the suitability of skillful decadal scale projections provided by the WKNN model should be considered.

The Basin Study simulated a range of supply-demand scenarios and explored the use of options and strategies such as infrastructure development, conservation and efficiency improvements to address anticipated supply-demand imbalances. The Colorado River Simulation System (CRSS) was used to simulate the rivers, reservoirs, diversions, return flows and operations, and determine the performance of the system in response to varying supplies and demands, both with and without the options and strategies to address supply-demand imbalances. CRSS is a monthly timestep, object oriented model capable of simulating the complex "law of the river" of the CRB [*Reclamation,* 2012], developed in the RiverWare modeling environment [*Zagona et al.,* 2001].

CRSS simulates each scenario to determine critical conditions of the system, indicating vulnerability with respect to impending shortage. Vulnerability is detected when combinations of metrics such as reservoir pool elevation and streamflow magnitudes - fall short of specified thresholds. Decisions are made each year of the simulation based on the values of the signposts as to whether or not to implement options and strategies to mitigate the risk of shortage

[2] http://www.usbr.gov/lc/region/programs/crbstudy/finalreport/

[*Reclamation,* 2012]. The decisions made to implement options and strategies are entirely based on the information from the current and past state of the system.

We propose to further inform the decisions with streamflow projection information generated by the WKNN model.

5.1.4 Study Objective

This final part of the research seeks to answer the question: Can the skill of the decisions in the Basin Study be improved by the use of decadal scale streamflow projection information based on the WKNN model, i.e., sensitive to variability driven by the large scale climate indices, PDO and AMO, along with information regarding the time varying predictability metric provided the LLE of the nonlinear dynamical model? To answer this question, we develop a technique for enhancing the Basin Study decision framework by incorporating the projections and the time varying predictability of the streamflow. We evaluate the skill of the integrated decision framework with respect to the costs of the options and strategies and the risk of system shortage.

5.1.5 Summary of approach

The time varying predictability of the streamflow is first determined for each year of the projections as the LLE to identify periods of non-predictability so that projections only within the predictable period can be used to influence the decision. An analysis of the skills of various projection window lengths is undertaken and the best is selected. The decision framework is modified to incorporate the projections: At the end of each simulation year, an ensemble of streamflow projections of the selected length is generated using the WKNN model which uses information about the climate signals in the current and previous years; the future flow is deemed likely to be either wet or dry relative to the long term mean of the Lees Ferry flow. A detailed

analysis of this determination and the effects of a range of wet/dry thresholds are presented. The existing decision logic of whether or not to implement options and strategies, and which to implement, is then conditioned on the wet or dry projection using two different logical approaches that either constrain or complement the decisions. The two approaches are compared. The skill of the enhanced decision framework is evaluated with respect to costs of implementing the options and strategies and system shortages, and a tradeoff curve is developed. The new decision methods are demonstrated first on a single trace of observed hydrology, then on an ensemble of plausible future supply scenarios. A single constant demand scenario from the Basin Study is used.

The chapter is organized as follows. First the methodology of applying the stochastic streamflow simulation and projection is presented followed by the detailed methodology of generating the decision metrics from the projections and their time varying predictabilities. Then, two proposed approaches for integrating the projection decision metrics with the existing Basin Study decision framework are described. The methods are demonstrated on a single trace of observed streamflow data. A process for generating an ensemble of plausible future hydrologic scenarios using WKNN simulations is presented. The two integration approaches are applied to the ensemble, and the results are described. A summary and discussion of results concludes the chapter.

5.2 Methodology: Streamflow simulations and projections

The CRSS, maintained by Reclamation, models the most important aspects of the CRB: the major reservoirs, hydrological inflows, demands, diversions and return flows, and operational rules (the Law of the River) [*Reclamation,* 2012] and is developed in the RiverWare modeling environment at monthly time step [*Zagona et al.,* 2001]. The Colorado River upper and lower

basins are divided by the Lees Ferry gauge, shown by red arrow in Figure 5.1 with the locations of the model's 29 hydrological input nodes: 20 in the upper basin (green dots) and 9 in the lower basin (purple dots). In addition to hydrology, inputs include demands and the operating policies. Model outputs include reservoir pool elevations and releases, diversions and deliveries, hydropower generation, occurrences of shortages, and other data of interest such as compliance with environmental flows, and salinity. The model is used extensively for long term planning studies such as the recent Basin Study [*Reclamation,* 2012], annual operating plans, and to share information with stakeholders.

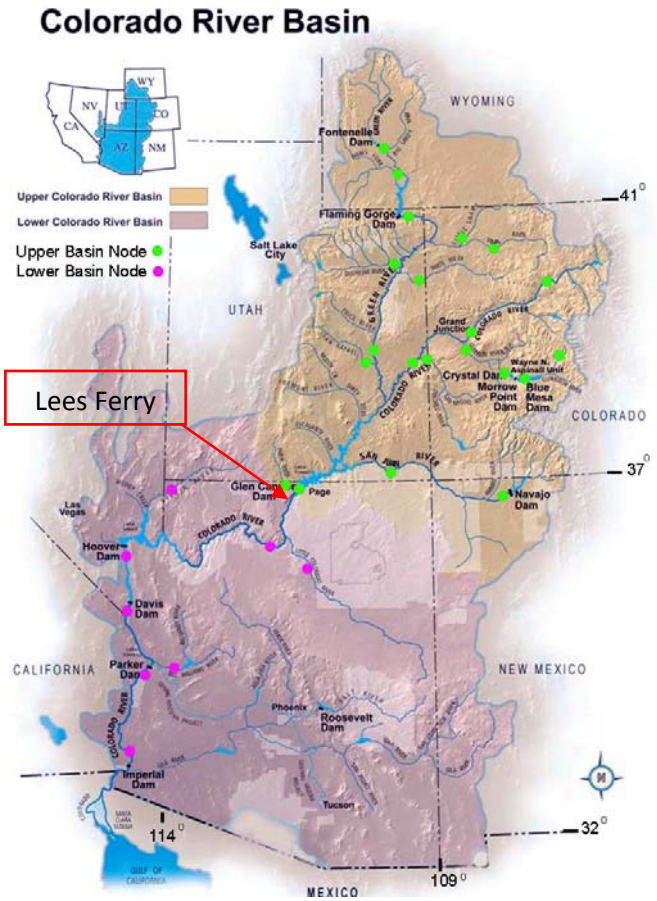

Figure 5.1: The CRB with upper and lower basin hydrological nodes used in the CRSS model and the location of the Les Ferry gauge and the basin states. The green dots are the upper basin natural flow nodes and the purple dots are the lower basin natural flow input nodes (adapted from *Nowak* [2011])

5.2.1 Simulating the future flow scenarios

The Lees Ferry flow gauge passes about 90% of the naturalized flow. Generating plausible future flow scenarios is a basis for robust decision making [*Groves et al.,* 2013]. Utilizing the strong teleconnection of the Lees Ferry naturalized flow with AMO and PDO, the future plausible streamflow scenarios are generated using the WKNN model (details in Chapter 2). The WKNN model is a streamflow simulation and projection model, conditioned on climate indices (in this case AMO and PDO), capable of representing the non-Gaussian and nonstationary characteristics of the Lees Ferry flow. Its suitability for simulation and projection at decadal and multi decadal time scales and its relative performance in comparison with the recently developed timeseries models such as the Wavelet based Autoregressive Model (WARM) and Conditional Hidden Markov Model (CHMM) are performed. Details are presented in Chapter 3.

To demonstrate the relative performance of integrating the future state of the flow on the Basin Study decision framework, decadal scale projections are performed for each simulation time step and for each of the plausible future scenarios. The plausible future flow scenarios are generated using the WKNN simulation approach. In this, 1000 streamflow scenarios of annual Lees Ferry flow are generated for the time span 2012 to 2060. The simulation timespan is chosen to match with the Basin Study so that the relative decisions of the proposed integration approach with the existing decision framework can be evaluated. From the generated 1000 simulations, a representative set of 120 traces are selected as follows:

i. First, the means of each of the generated 1000 plausible flow scenarios are computed.
ii. The simulations are grouped into 10 categories according to their means.
iii. From each category, representative traces are randomly sampled.

The selected 120 traces represent a wide range of plausible future flow scenarios. The mean values of the generated 1000 future plausible flow traces (blue dots) and the selected 120 traces (red dots) are shown in Figure 5.2.

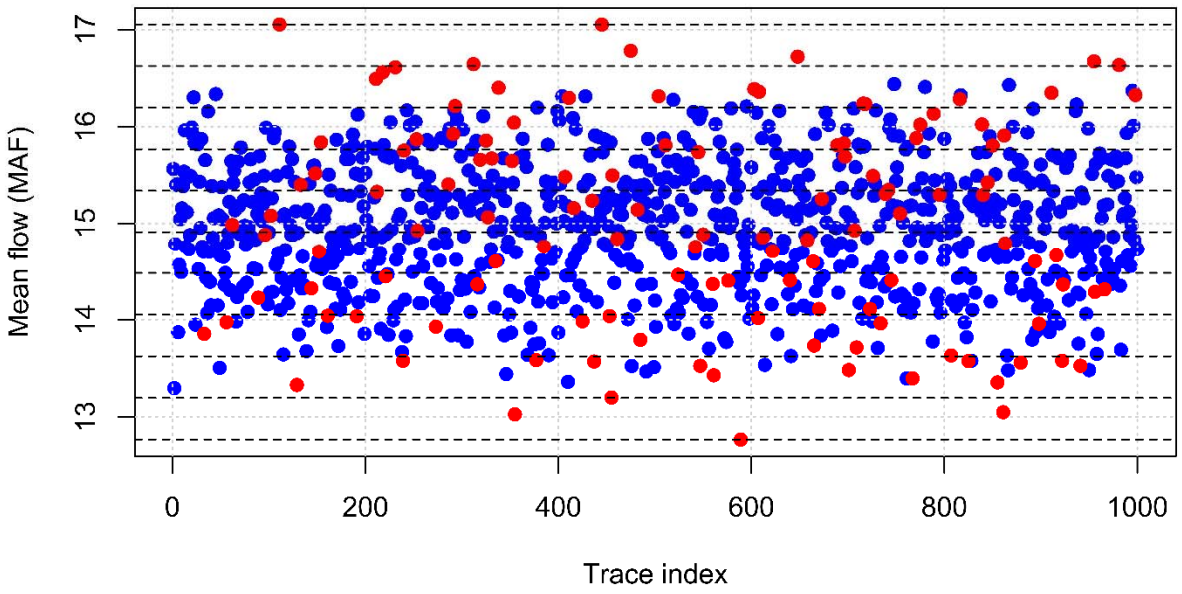

Figure 5.2: The mean values of the generated plausible 100 flow scenarios (blue dots) and the selected representative traces (red dots). The horizontal black dashed lines demarcate categories from which representative traces are sampled.

5.2.2 Spatial and temporal disaggregation of the selected traces

Each simulation of annual Lees Ferry flows must be disaggregated spatially to the 29 input nodes and temporally to monthly timesteps in order to be used for CRSS simulations. For this, the non-parametric space time disaggregation technique [*Bracken et al.,* 2010; *Nowak et al.,* 2010] is applied for the 20 upper basin nodes (shown green in Figure 5.2) and temporally into monthly time scale. The application of the non-parametric disaggregation technique is extended to estimate the 9 flows at the lower basin hydrological input nodes. In this, a proposition matrix is first generated based on the historic data as a ratio of the Lees Ferry flow (key station) with the

downstream flow nodes under consideration. Then the K-Nearest Neighbors (K-NN) of the generated annual streamflow of the key station are identified through the weighting metric as in *Lall and Sharma,* [1996] and one of the nearest neighbors are resampled. The downstream flow is estimated as the multiple of the proportion vector [*Bracken et al.,* 2010; *Nowak et al.,* 2010] with the resampled streamflow or simply the downstream historical flow that correspond to the selected nearest neighbor. This technique estimates the downstream flow much better in terms of representing the nonstationarity of the streamflow when compared with linear autoregressive model. The estimated downstream flows in the 9 lower basin nodes are then subjected to the non-parametric temporal disaggregation technique [*Bracken et al.,* 2010; *Nowak et al.,* 2010] to generate monthly flows.

5.2.3 Selection of the best projection period

To incorporate future streamflow projections in the decision model, we use paleo data with historical observed to select the projection window length with highest skill as follows:

i. For each year from 1750 to 2012 of the timeseries of annual naturalized Lees Ferry flows, 200 projections are performed using the WKNN modeling approach for projection windows ranging from 1 to 20 years.
ii. The means and medians of the 200 projections are computed for each of the projections windows for each year.
iii. Correlations of the means and medians of the projections are performed with the means and medians of the observed streamflow.
iv. The projection window length with highest skill is selected to generate projections that will be used in the decision metrics. The projection windows and associated skills are shown in Figure 5.3.

Chapter 3 compares the performance of the three timeseries models for simulation and projection. The three models perform well on simulation. The performance of the projection, measured in terms global correlation coefficient (details of the correlation is presented in Chapter 3) shows that the HMM tends to have higher skill than the wavelet based models (WARM and WKNN conditional projections) for annual and inter annual time scales. The HMM model appears to consistently perform better for these timescales regardless of where in time it is applied. This is because recursive use of TPM in the HMM projection approach results in a constant value after a number of estimates of the future values. This limits the projection window to be shorter when compared to wavelet based projection approaches. The skill of the wavelet based models outperforms that of the HMM based projections for longer projection periods (15-20 years). The wavelet based methods are applied on the signal components of climate indices. These components are quasi periodic and are of low frequency with periodicities from 16 years to 64 years. Applying Auto Regressive (AR) and block KNN models give skillful projections at decadal and multi decadal timescales. Conditional simulation of the streamflow using the AMO and PDO signal projections exhibits better skill for longer projection windows (decadal and multi decadal time scales) when compared to shorter periods (less than ten years). This is because the streamflow projections are conditioned by the projected low frequency climate signals. These long term (50-70 years) and decadal (~ 16 years) variability characteristics of the climate indices are known to have strong teleconnection with the Colorado River flow (see Chapter 2 for details). Application of the wavelet based projection that exhibits better skill for a longer projection period is relevant for the CRB and chosen for projection.

Among the wavelet based techniques, the WKNN approach performs better than the WARM (See Chapter 3 for details) and is used for further analysis to identify a robust projection

window by considering a range of projections. The 11 year projection shown in Figure 5.3 has the maximum correlation coefficient, indicating the best performance of the projections. This figure demonstrates the robustness of the 11year projection window.

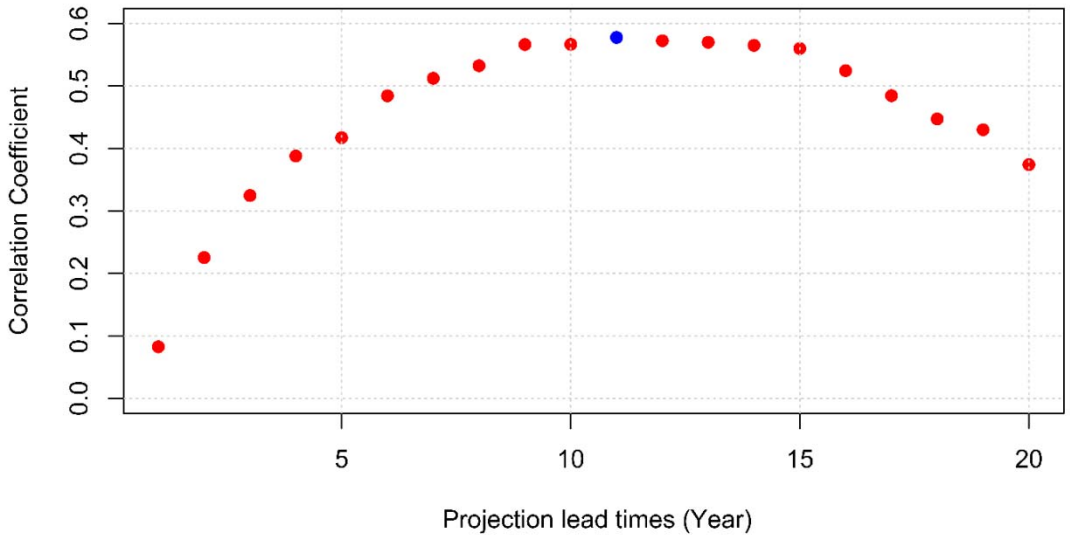

Figure 5.3: Correlation coefficients of the WKNN model projections with the observed flow. The blue dot is the maximum correlation coefficient at 11 years projection window. Each dot represents the median of the mean projections for different projection windows.

5.2.4 Streamflow projections

The WKNN streamflow projection approach with 11 year projection window is applied to determine 200 projections for each year of each streamflow scenario. These annual projections are performed for all the 120 traces to determine the state of the projected streamflow as wet or dry determined as follows.

i. The long term (observed) mean of the Lees Ferry flow is computed to be used as a reference value to determine the mean of the projections as wet and dry. If the projection mean is above this reference, it will be considered as wet and vice versa for dry [*Prairie et al.,* 2008].

The means of the 200 projections are then computed and the numbers of projections which fall above (wet) and below (dry) the reference value are determined. If the number of wet projections is greater than the number of dry projections, then the overall projection is considered to be wet, and vice versa for dry.

ii. Wet projection ensembles are further classified as wet and dry depending on the severity of wetness. For this we introduce a Reference Percentage Threshold (RPT) - a threshold higher than 50% - that requires the ensemble to have a greater percentage of wet projections in order to be considered wet. For example, for RPT of 75%, the ensemble would need at least 75% of its projections to be wet in order for the ensemble projection to be considered wet, otherwise it is considered dry. With increased RPT, fewer projections are classified in the wet category and the projection period is more likely to be dry, necessitating implementation of options and strategies to mitigate a shortfall.

The dry and wet projections are represented by numeric values of 0 and 1, respectively, for ease of integration with the existing decision framework. For a wet projection of 75% in step (i), the decision metrics would be as shown in Table 5.1 for RPTs (step ii) ranging from 51% to 100%.

Table 5-1: Wet projections from (i) and their representation for varying RPTs from (ii)

	(i)	(ii) (RPTs)						
	75%	51%	52%	…	75%	76%	…	100%
	wet	wet	wet	wet	wet	dry	dry	dry
Decision metric (2012)	-	1	1	1	1	0	0	0

If more than 50% of the projections in the ensemble are less than the historical mean the ensemble is dry regardless of the RPT. For each of the years in the planning period and for each of the possible futures, a decision metric Table is generated as shown in Table 1.

5.2.5 Nonlinear dynamical model identification of predictable and less predictable epochs and decision metrics

The divergence and convergence of trajectories locally in the phase space (reconstructed through proper embedding) are computed for every year of the 120 traces as LLE to determine the time varying predictability of the traces (details are presented in Chapter 4). This predictability information is used to guide decisions in the predictable and less predictable time epochs. To ease the integration of the predictable and less predictable time epochs in the existing decision making metric, the less predictable time epochs (LLE positive or negative but close to zero) are tagged with a numeric value of 2. The predictable time epochs however are tagged with the projection metrics as shown in Table 5.1: 0 or 1 for dry or wet. Sequences of zeros and ones in the predictable epochs and twos in the less predictable epochs form the decision metric as shown in Figure 5.4. The sequence of annual projection decision metrics (dry, wet or unpredictable) for each scenario can be developed in advance of the CRSS decision simulations, based on the WKNN projections and LLEs for each year, and later used in the integration of these with the signpost information in the decision model.

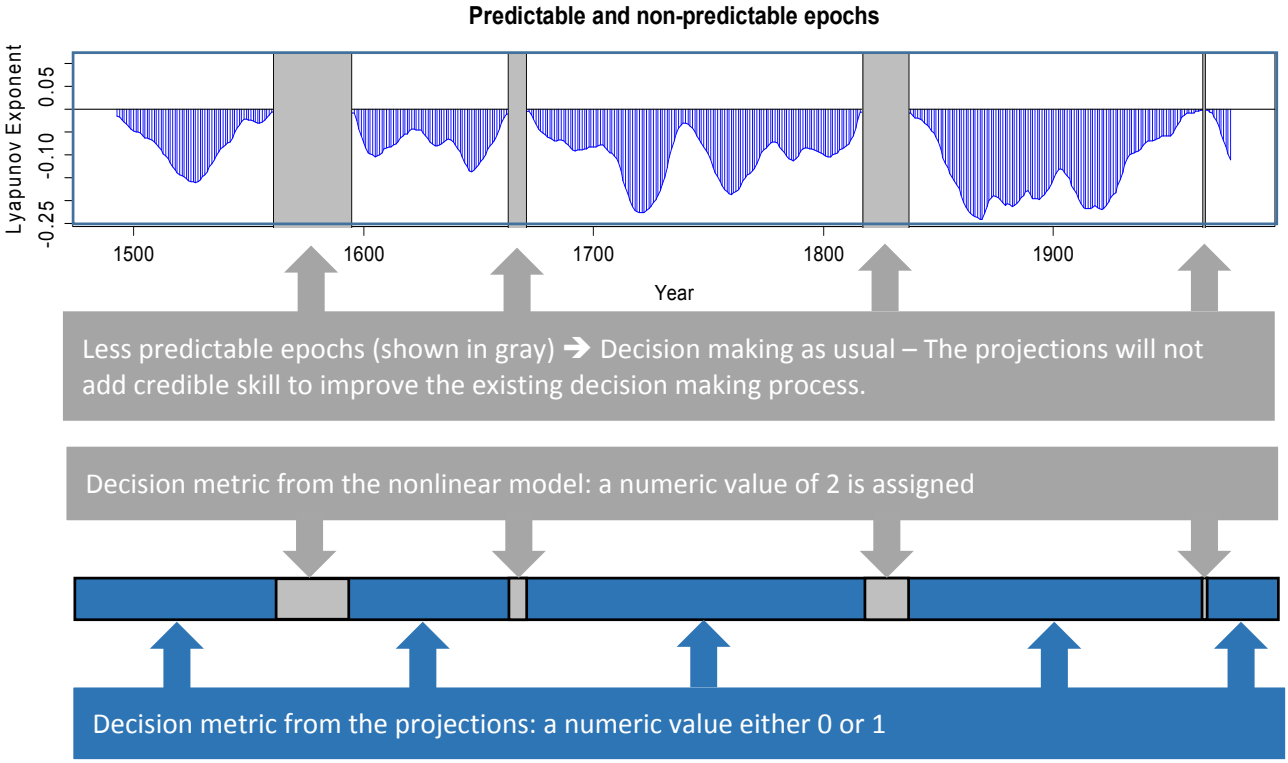

Figure 5.4: Decision metrics applied to the paleo and observed data from the nonlinear dynamical model. Gray shaded regions are time epochs when projections would not add credible information to improve the existing decision making. These regions are assigned a decision metric value of 2, whereas decision metrics 0 or 1 (dry or wet) are used during the predictable epochs.

During times when the projections are in the less predictable (gray) region, the wet/dry (1 or 0) projection decision metrics will be replaced by a value of 2 as shown in Table 5.2.

Table 5.2 demonstrates how the time varying predictability of the trace guides the inclusion and exclusion of the projections into the existing decision framework. For a given year the RPTs generated for a particular year (Table 1) are modified based on the time varying predictabilities using a numeric value of 2.

Table 5-2: Typical representation of decision metrics for a single trace from the projections and the nonlinear model. Columns are RPTs and rows are years. Values for each year are determined as shown in Table 1 and then decision metrics are updated based on the time varying predictability. Shaded region with a numeric value of 2 is the less predictable epoch.

Year	51%	52%	…	60%	…	99%	100%
2012	1	1	1	1	0	0	0
2013	1	1	1	0	0	0	0
…	1	1	1	0	0	0	0
…	2	2	2	2	2	2	2
…	2	2	2	2	2	2	2
…	2	2	2	2	2	2	2
…	…	…	…	…	…	…	…
...	…	…	…	…	…	…	…
…	1	1	0	0	0	0	0
…	1	1	1	1	0	0	0
2060	1	1	1	1	1	0	0

5.3 Methodology: Integration of Projections in Decision Framework

5.3.1 Existing decision model (baseline model)

Reclamation used scenario analysis in the Basin Study to understand possible future supply and demand conditions and propose ways to mitigate possible shortfalls through various options and strategies [*Groves at al.,* 2013; *Reclamation,* 2012]. CRSS simulations of the system performance with the various supply, demand and operations combinations were used to evaluate the scenarios for the possible future supply-demand imbalances. Depending on the severity of

shortfall, mitigation measures were applied to minimize the supply-demand gap. Indicator metrics – observable quantities that indicate how well the system will perform – are used to signal vulnerable conditions and the need for mitigation. For this, the Basin Study conducted "system reliability analysis" to determine the signposts that indicate the reliability of meeting demands. Signposts are features or combinations of features of the observable system that are good predictors of impending vulnerabilities. Signposts can inform the system that a vulnerable condition is likely to occur so that appropriate actions will be taken to mitigate the shortfall. For the Basin Study, Reclamation ran CRSS through thousands of plausible future scenarios [*Reclamation,* 2012] and then used cluster analysis to identify key signposts and threshold values to use as indicators of vulnerability. They found that a combination of Lakes Mead and Powell pool elevations and Lees Ferry flow are good signposts. Depending on the supply – demand imbalances determined from the plausible future demand and supply scenarios, appropriate options and strategies were identified to address the system vulnerability. The CRSS model was then used to evaluate the system reliability of implementing options and strategies. Table 5.3 shows indicator metrics and their vulnerability thresholds.

Table 5-3 Vulnerability thresholds for indicator metrics

Indicator Metrics	LNF (MAF)	PPE (ft)	MPE (ft)	UBS (%)	LBDAP (acfr-ft)
Lees Ferry deficit	12.39	3490	-		
Mead Pool Elevation	13.35	-	1040		
Lower Basin shortage (2 yrs)	13.51	-	1060		
Lower Basin shortage (5 yrs)	13.51	-	1075		
Upper Basin Shortage				25	
Lower Basin Shortage Above Proposition					900,000

Vulnerability indicators based on reservoir elevations and Lees Ferry flow are summarized in Table 5.4 and shortage based vulnerabilities are shown in Table 5.5. The vulnerability combinations are marked “Vulnerable” in each table.

Table 5-4: Signposts based on combination of pool elevations and streamflow magnitudes

	LNF < 12.39 (MAF)	LNF < 13.35 (MAF)	LNF < 13.51 (MAF)	LNF < 13.51 (MAF)
PPE < 3490 ft.	Vulnerable	-	-	-
MPE < 1040 ft.	-	Vulnerable	-	-
MPE < 1060 ft.	-	-	Vulnerable	-
MPE < 1075 ft.	-	-	-	Vulnerable

Table 5-5 Vulnerability based on shortage

	UBS < 25%	LBDAP < 900,000 (acre-ft)
UBS	Vulnerable	-
LBDAP	-	Vulnerable

5.3.2 Options and strategies

The options and strategies which are proposed to mitigate the detected vulnerabilities can be broadly grouped as follows;

i. Increasing the availability of water supply through infrastructure development,

ii. Reduce demand through conservation strategies and improved efficiency,

iii. Modification of operational strategies.

From a list of 150 options and strategies the Basin Study identified about 30 options and strategies as technically and economically feasible and grouped them into 4 portfolios, each with a specific adaptation strategy. The Basin Study evaluates and compares the future reliability of

the system with all four portfolios; in this study we consider only Portfolio A because it has most of the options and strategies and also incorporates the options and strategies of Portfolios B and C.

During the simulation runs, when signposts are triggered, specific vulnerability can be mitigated by activating options from the available list in the active portfolio. For example, vulnerability in the year 2025 can be mitigated by options that are available in 2025 and earlier. The option, once implemented, remains in effect until the end of the simulation period and cannot be implemented again. Suppose the next available option is in 2030 and all the options in and before 2025 are implemented, then any vulnerability between 2026 and 2030 cannot be mitigated.

5.3.3 Integration of the decision metrics with the existing framework

The implementation of options in the Basin Study's decision model is entirely dependent on the signposts that signal potential vulnerabilities detected each year in the simulation based on the current state of the system. The research addresses the question of whether using skillful projections along with the existing signposts can further inform the decisions. A triggered signpost this year may not be followed by a vulnerable condition, for example, if the future hydrology is high (wet) enough.

The decision metrics (wet or dry) generated from the streamflow projections and their time varying predictability (hereafter "projection metrics") are proposed to be incorporated in the Basin Study decision logic (hereafter "baseline") such that if the projection is wet enough, more water is expected into the system, thereby minimizing the anticipated supply and demand imbalences so that a more appropriate decision can be made. Two different integration approaches are considered as follows.

The AND approach

In this approach, the baseline signposts are coupled with the projection metrics with "AND," forming a necessary condition. To implement options the signpost is triggered AND the projection is dry, otherwise no option is implemented. If a very high RPT is used, few wet projections will be made and decisions are similar to the baseline, whereas a low RPT will result in many wet projections that could potentially constrain the baseline, i.e., some options will not be activated. There is only one possible combination of the signposts and projection metrics that allows the implementation of options and strategies as shown in Table 5.6.

Table 5-6: The AND approach decision metrics

Signpost	Projection Metric	Overall decision: Implement options and strategies?	
		Yes	No
True	0 or 2	✓	
True	1		✓
False	0		✓
False	1		✓

Because fewer options are implemented, especially with low RPT, there is a potential for higher risk of shortage than for the baseline, but with more potential for cost savings, avoiding investment in unneeded options.

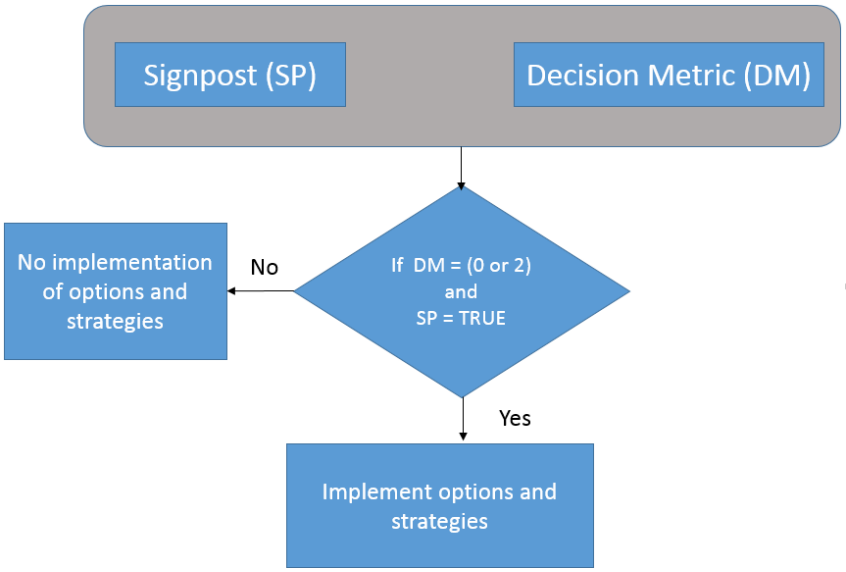

Figure 5.5: the AND integration logic

The OR approach

This approach allows the implementation of options if either the signpost is triggered or the projection metrics is dry. This approach could potentially result in more options executed than the baseline, especially if the RPT is high, resulting in lower risk of shortage, but higher costs. With low RPT, the results will be similar to the baseline. The possible combinations of the signposts and projection metrics for this approach are summarized in Table 5.7.

Table 5-7: The OR integration approach decision metrics

Signpost	Projection Metric	Overall decision: Implement options and strategies?	
		Yes	No
True	0 or 2	✓	
True	1	✓	
False	0	✓	
False	1		✓

The logical representation of the OR approach is presented in Figure 5.6

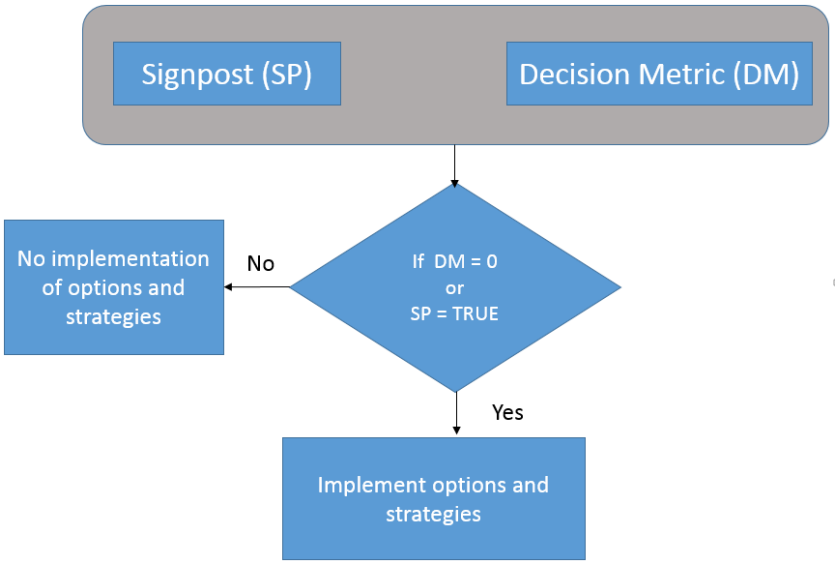

Figure 5.6: The OR integration logic

To evaluate these two approaches across a range of RPTs, we executed the baseline model, then added the projection metrics and compared the results.

5.4 Results

The effect of the proposed decision approach is demonstrated by considering a single hydrology from the historic period, and then its application to the ensemble of plausible future scenarios is presented.

5.4.1 Single run with observed data

The single trace uses the observed flow for the time period from 1964 – 2012 at Lees Ferry (Figure 5.7), Portfolio 1 (the portfolio with the broadest range of options and strategies in the Basin Study), a constant demand scenario of 14.03 MAF per year (the 2060 demand level of the demand scenario B (slow growth) of the basin study), and the rule set that represents the current Law of the River.

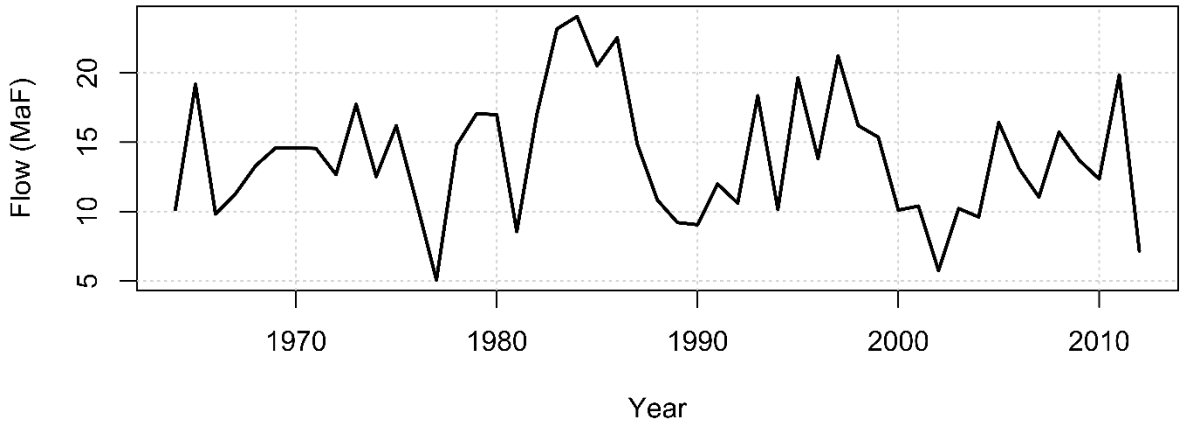

Figure 5.7: The Lees Ferry annual flow timeseries from 1964 – 2012.

The observed period hydrology is chosen to better demonstrate the decisions for the known hydrology in the basin. Decision metrics with RPT of 51%, 55%, 60%, 65%, 70%, 75% and 80% are tested for both AND & OR approaches. (It was found that RPT greater than 80% does not result in decisions different than RPT equal to 80%, most likely because there are no scenarios that are that wet.) CRSS was executed with the projection decision metrics for each of the 7 RPT values, for both AND & OR approaches, and one additional run for the baseline to 15 simulation runs performed. Each uses unique decision logic and has the possibility of executing a different set of options.

To evaluate the results, we plot of Mead pool elevation, as that metric has significance for Lower Basin shortage. Figure 5.8 demonstrates the effects of the two integration approaches. As expected, the AND approach limits the implementation of options resulting in lower pool elevations (blue) relative to the baseline pool elevation (black). The OR approach complements the baseline decisions resulting in higher pool elevations (red) than the baseline. The lower

Mead pool elevations (blue) are with fewer options than the baseline decisions, indicating how severe the supply – demand imbalances can be without implementation of options for this supply and demand scenario.

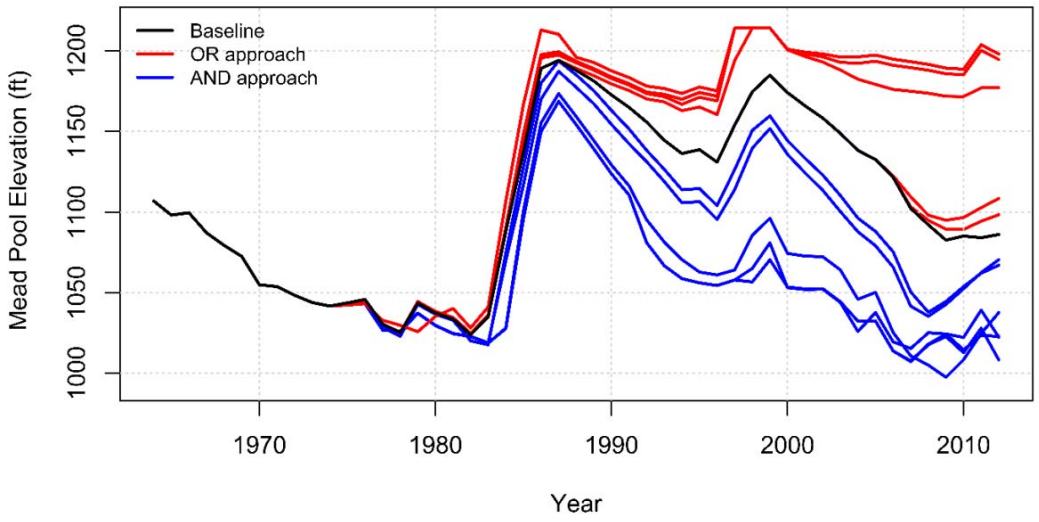

Figure 5.8: Lake Mead pool elevation from the two integration approaches. Higher pool elevations are associated with higher RPTs with respect to each of the integration approaches. The pool elevations are the December values of each year.

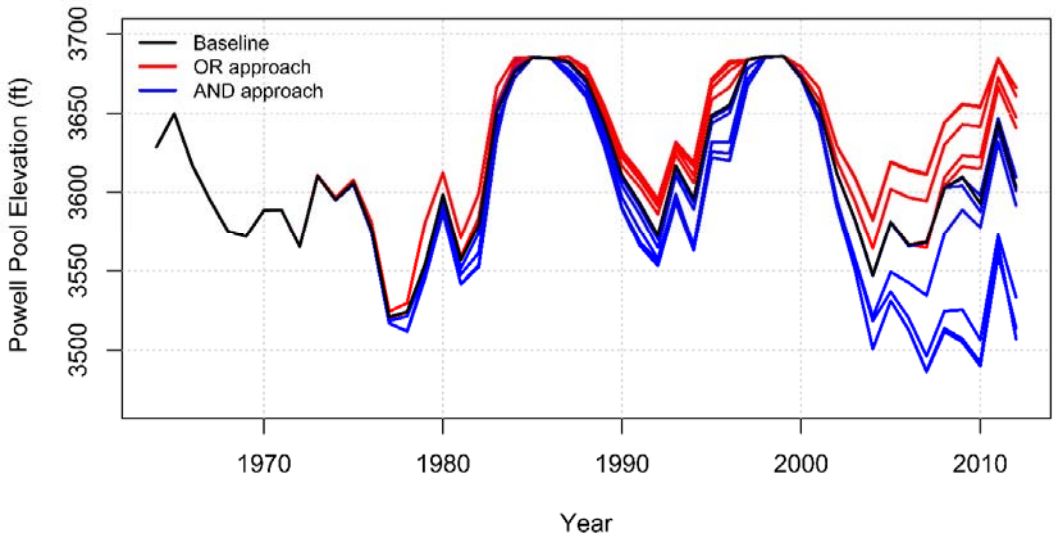

Figure 5.9 Lake Powell pool elevation from the two integration approaches. Higher pool elevations are associated with higher RPTs with respect to each of the integration approaches. The pool elevations are the December values of each year.

Each of the pool elevations shown above results from the options and executed by the decision logic as indicated. Higher pool elevations are associated with greater numbers of options and vice versa for lower pool elevations.

Shortages from the 51% RPT AND logic, the baseline and the 80%RPT OR logic are presented in Figure 5.10 to show the extremes and the relative shortages of the baseline options. The remaining solutions from the RPTs and the integration approaches are in between and for the interest of space they are not presented here. However, the total system shortages (cumulative shortages throughout the planning period) are presented separately.

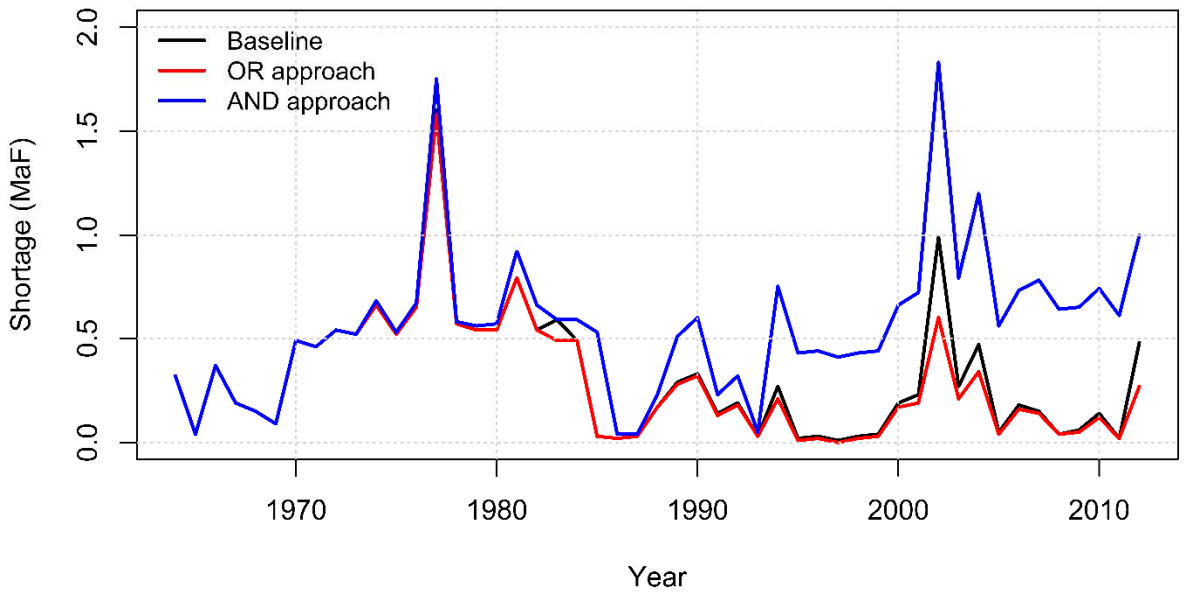

Figure 5.10: Shortages of the AND logic with 51% RPT (blue), baseline (black) and from the OR logic (red). . Highest shortage from the AND approach with 51% RPT (blue) as expected and the lowest shortage from the OR approach with 80% RPT.

The 51% AND logic is the most restrictive in terms of allowing the implantation of options and strategies because the 51% projection metrics are mostly wet and the AND approach with wet projection is "no implementation" combination (Table 5.6). On the other hand, the OR logic with the highest RPT is the most allowing logic because higher RPTs are dryer and any dry combination in the OR logic allows implementation of options and strategies (Table 5.7). Therefore the magnitudes of shortages and costs range from the 51% AND logic with least possible cost and highest possible shortage to highest RPTs OR logic with least possible shortage and highest possible cost.

The shortages from the AND 51% RPT in Figure 5.10 are the highest for most of the times, especially starting from the mid-1970s. This is mainly because the least number of options

are implemented during these periods because the implementation of options and strategies are suppressed by the 51% wet projection metrics. The baseline shortages (shown black in Figure 5.10) are as low as the least possible shortages (shortages from the OR highest RPT logic- shown red in Figure 5.10). This implies incremental implementation of options with the OR logic is not reducing the shortages significantly. The options that correspond to the shortages in Figure 5.10 are shown in Figure 5.11. As expected many more options are implemented under the OR approach compared with the AND & baseline approaches. Even though the shortages don't seem to be significantly different between the baseline and the OR decisions, the implemented options are significantly higher as shown in Figure 5.11.

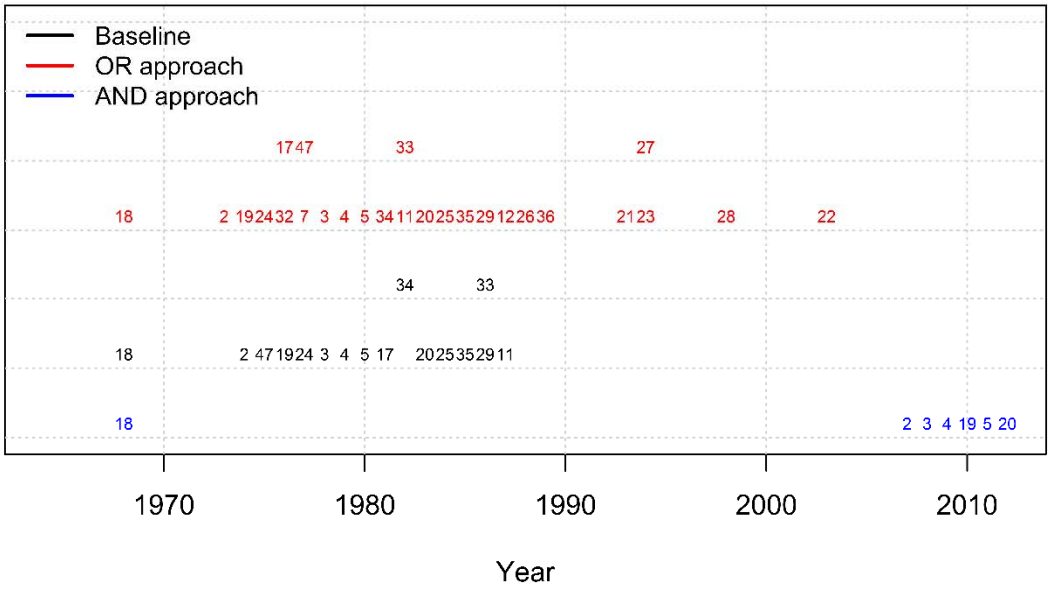

Figure 5.11: Options and strategies from the baseline (black), OR logic (red) and the AND logic (blue). The numbers indicate the option or strategy numbers implemented to address the vulnerabilities. The option numbers can be used to read options and strategies from Table 5.8.

The present costs of all the options are computed and summed to get the overall cost of the particular approach. The costs of options or strategies used in this analysis are taken from *Reclamation,* [2012], estimated as the cost of both investment and maintenance (see Table 5-8 for the list of costs for a particular option or strategy). For example, the annual costs of each of the options of the OR logic (shown red in Figure 5.10) are identified from Table 5.8 and then discounted with the rate of 7% to get the present values. The present values are then summed to get the total cost of all the options over the planning period. The costs for each of the 15 simulation runs are similarly determined and their cumulative costs are shown in Figure 5.12. Because the higher RPT AND decisions and the lower RPT OR decisions are very close, there could be an overlap of curves in Figure 5.12 and Figure 5.13.

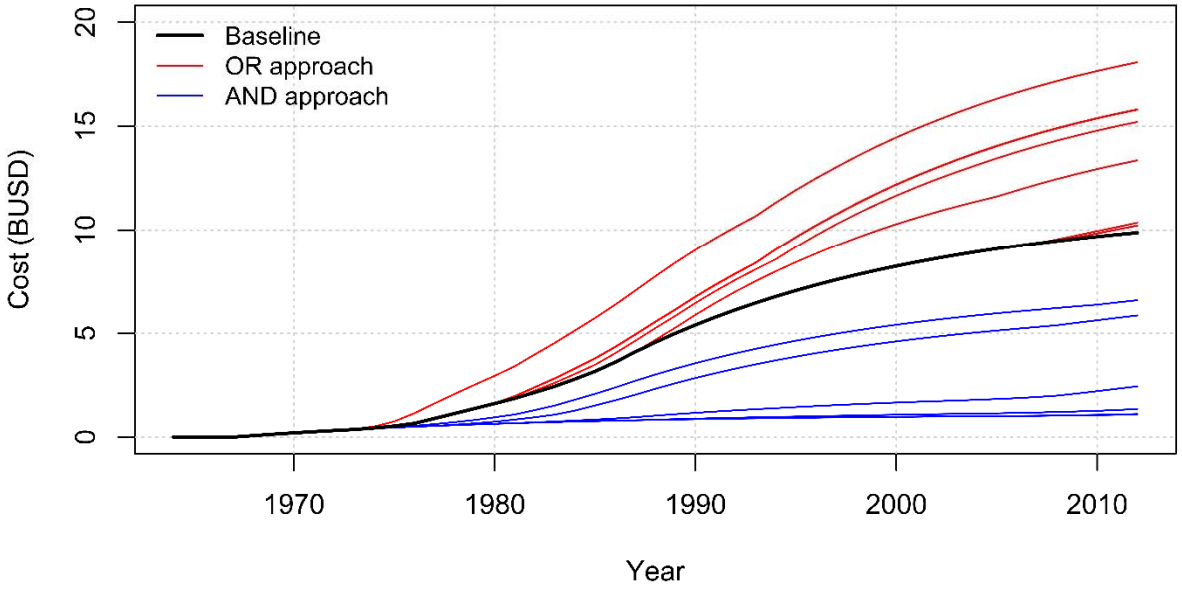

Figure 5.12: Cumulative costs of options and strategies implemented based on the wet percentage thresholds and the two integration approaches.

Table 5-8: Options and strategies under portfolio 1 (Reclamation study, 2012)

Options (Portfolio 1)	Option numbers	Year of availability	Magnitude (Acre-ft)	Estimated annual cost ($/afy)	
				Min	Max
AgCons-Transfer2	2	2021	200000	250	750
AgCons-Transfer3	3	2026	200000	250	750
M&IConservation1	18	2016	200000	500	900
AgCons-Transfer4	4	2026	200000	250	750
Desal-Yuma	47	2021	100000	600	
M&IConservation2	19	2021	200000	500	900
AgCons-Transfer5	5	2026	200000	250	750
Desal-SoCalgroundwater	37	2021	20000	750	
M&IConservation3	20	2031	200000	500	900
M&IConservation4	21	2041	200000	500	900
M&IConservation5	22	2051	200000	500	900
Desal-SaltonSea1	34	2026	200000	1000	
Desal-SaltonSea2	35	2031	200000	1000	
Desal-SaltonSea3	36	2036	100000	1000	
Desal-PacificOcean-MX	33	2026	56000	1500	
Reuse-Municipal1	24	2021	200000	1500	1800
Reuse-Municipal2	25	2031	200000	1500	1800
Import-FrontRange-Missouri	23	2041	600000	1700	2300
Reuse-Municipal3	26	2036	200000	1500	1800
Reuse-Municipal4	27	2041	200000	1500	1800
Reuse-Municipal5	28	2046	132000	1500	1800
Desal-PacificOcean1	29	2031	200000	1850	2100
Desal-PacificOcean2	30	2036	200000	1850	2100
EnergyConservation	32	2021	160000	2000	
Local-CoalbedMethane	7	2021	100000	2000	
Reuse-Industrial	17	2021	40000	2000	
Desal-Gulf1	11	2028	200000	2100	
Desal-Gulf2	12	2033	200000	2100	

The highest cost value is associated with higher RPT with OR approach and the smallest cost is associated with the lower RPT with AND approach. The highest cost of the AND approach is associated with the baseline cost and at the same time with the lowest RPT of the OR approach.

To evaluate the relative performances of the decisions from the two integration approaches with the baseline, the shortages are computed similarly. With increased investment, there is expected reduction in shortage as the implemented options are addressing the shortfall. The cumulative shortages of all planning decisions (options implemented based on the particular approach and decision metric) are computed to determine the overall shortages in the planning period and are shown in Figure 5.13.

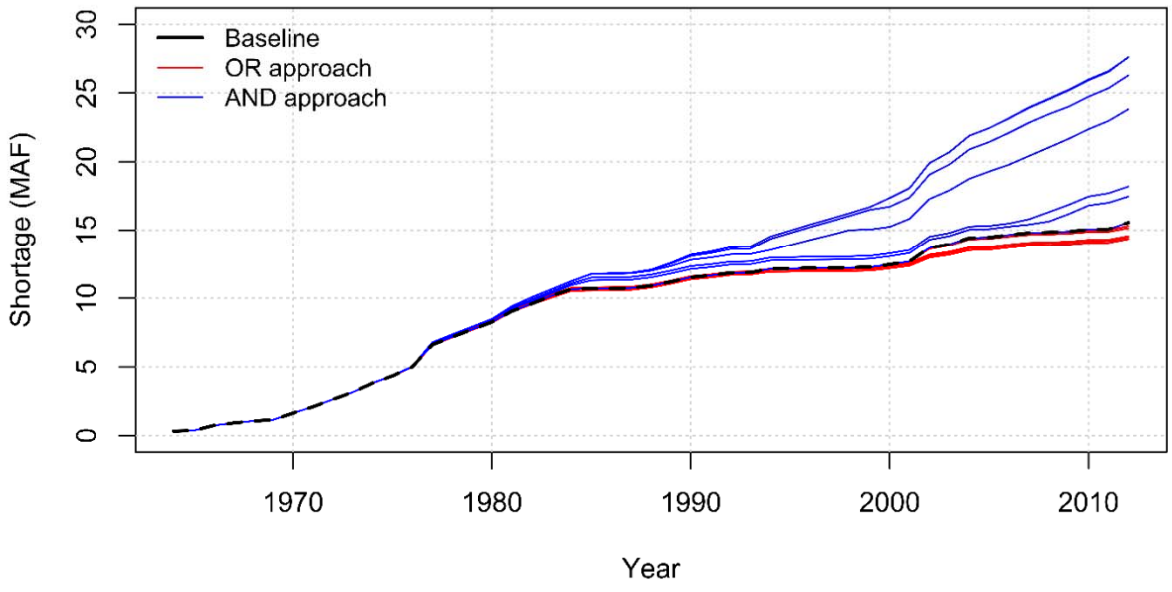

Figure 5.13: Cumulative shortages of options and strategies implemented based on the RPTs and the two integration approaches.

Shortages from the AND approach (shown in blue) show a significant variation with different RPTs. The highest shortage in Figure 5.13 is associated with the AND approach with the lowest RPT and it is also associated with the least cost in Figure 5.12. Similar to the cost, decisions of the AND approach with the highest RPT (> = 80%) are similar to the baseline and the OR approach with the lowest RPT (51%). The OR approach however, shows little variation in shortage when compared with its variation in the cost.

The costs and shortages exhibit a clear tradeoff. The tradeoff curve is determined by taking the overall costs and shortages of the decisions made by the AND & OR approach with each approach of 7 RPT decision metrics. The baseline overall cost is also determined to evaluate the relative performance of the decisions. Shortage vs. cost tradeoff is shown in Figure 5.14. As expected, with an increase in investment, the AND approach exhibits significant reduction of shortage from the 51% RPT to its maximum 80% RPT. The baseline is at the boundary between the AND & OR approach outcomes. With increased investment beyond the baseline, there is little reduction in shortage even if a significant increase in investment.

The underlying assumption of incorporating flow projections in to the baseline decision framework is to inform the system about the future state of the flow so that the baseline supply-demand imbalances will be modified. The new supply- demand imbalance triggers the need for implementation of more numbers of options and strategies if the future flow is dry when compared with the imbalances are modified by the future wet flow. The decision of implementing the required option or strategy from the active portfolio is, however, constrained by the availability of the option and/ or strategy during the need and the suitability of the option/strategy for the detected vulnerability. This brings less flexibility to implement suitable options and strategies for the projection conditioned supply- demand imbalance. In the worst

case, options and strategies may not be available for implementation. This limits the efficiency of the projections in the decision framework to improve the baseline options both in terms of shortage and cost at the same time.

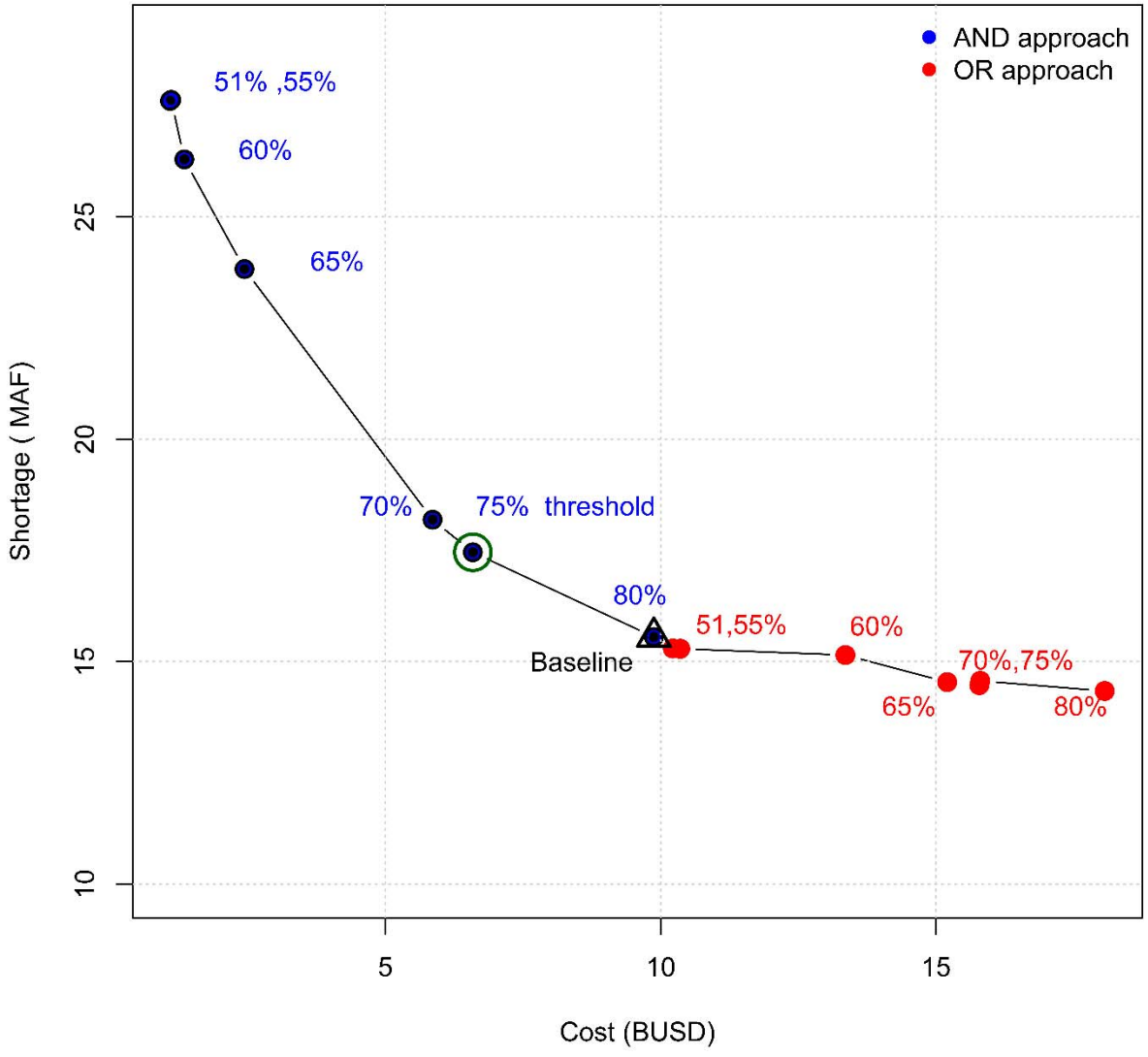

Figure 5.14: Shortage – cost tradeoff curve. The blue dots are from the AND approach with RPT as labelled and the same for the OR approach with red dots. The baseline (black triangle) is shown at the interface between the AND & OR logic options and strategies.

The marginal benefit of implementing more options and strategies beyond the baseline options does not seem to be attractive. Moving from baseline to, for example, the 60% OR, there is ~ 26% increase in cost while reducing the shortage by only ~2.6%. The baseline is as close as the inflection point where any more investment will not bring noticeable benefit. The ideal solution for this type of problem is the 0, 0 coordinate (no shortage and no cost). A point close to the ideal solution is preferred. For this, the Euclidean distances are computed for each of the points in Figure 5.14 and the closest point is selected. For this particular scenario, the AND logic with the 75% RPT is favored. The points shown in Figure 5.14 illustrate the relative benefits of the implemented options and strategies under the RPTs. The AND 75% RPT for example shows an increase in shortage of 11% while the cost is reduced by 33%.

Each of the RPTs can be associated with a range of streamflow magnitudes. For the streamflow projections for a given year of a given hydrologic scenario, the streamflow magnitude that corresponds to a specific RPT is computed as the streamflow magnitude for which 50% of the projections are greater. Higher percentage thresholds are associated with high flow magnitudes and vice versa for low RPT. This procedure is applied to each of the projections ensembles for each year. The scatterplot shown in Figure 15 shows the relationship of the wet percentage thresholds with their corresponding flow magnitudes.

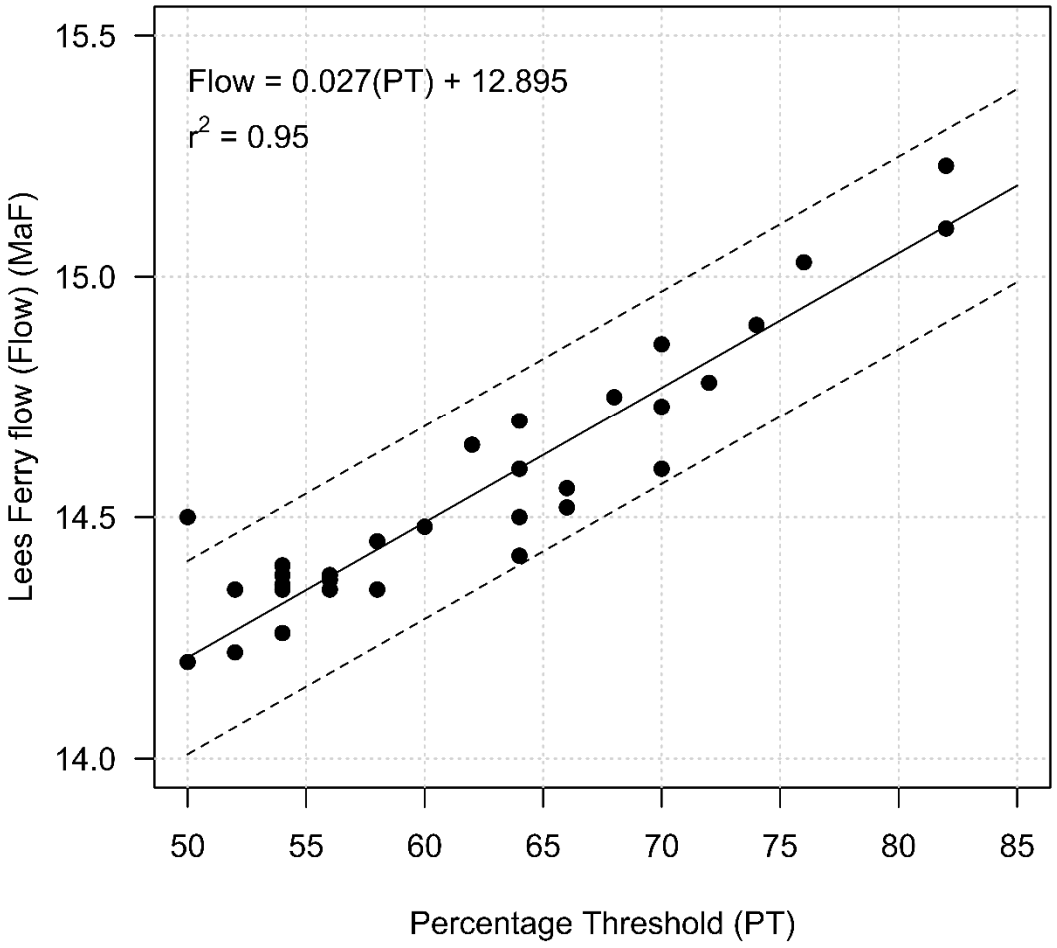

Figure 5.15: Relationship between the PT and the Lees Ferry flow. The straight line that connects the dots is a linear regression model fit and the dashed lines are the linear model fit with +/- 0.2 MAF

The relationship shown in Figure 15 is determined by taking 50 projections from the historic Lees Ferry flow (1964-2012) which can cover a wide range of RPTs. The established relationship can be used to estimate flow magnitude for the chosen or preferred RPT.

For example, for the 75% preferred solution for this flow scenario, the corresponding flow magnitude is:

$$\text{Flow} = 75 * 0.027 + 12.895 = 14.92 \text{ MAF}$$

This flow magnitude can be related to the demand as follows. The preferred solution for the demand level of 14.03 MAF is found to be the 75% RPT. The same analysis performed for a constant demand level of 13.72 MAF (the middle third of the slow growth scenario) shows the preferred solution 70% RPT with the corresponding flow magnitude of 14.78 MAF.

5.4.2 Multiple run with ensemble of plausible future flow scenarios

The RPT that performs the best may vary with hydrology; without knowing the hydrology in advance, it is not possible to take advantage of a tradeoff curve like the one in Figure 5.14 to make a decision about selection of an RPT. With that in mind, we analyze an ensemble of plausible future hydrologic scenarios with a wide range of mean flows and look for robust performance across a range of RPT values.

The AND & OR decision frameworks are applied on the 120 plausible future flow scenarios. The 120 traces are disaggregated both spatially and temporally so they can be used in the CRSS. For each of the ensembles, the time varying predictability is determined through the nonlinear modeling approach to identify the predictable and less predictable time epochs. The decision metrics are then generated with sequences of zeros, ones and twos for dry, wet and less predictable respectively.

Using the constant demand of 14.03 MAF, the CRSS model simulation is performed with and without the projection metrics for the 120 traces. From the simulation run, the costs of implementing the options and strategies and the corresponding shortages are determined for the

three decision making approaches – the AND, OR and baseline. Using the computed costs and shortages, tradeoff curves are generated for each of the traces as shown in Figure 5.16. Future flow scenarios with high flow magnitude tend to show smaller shortages because the supply demand imbalances are low. Implementing additional options and/or strategy does not seem to make changes. However, traces with low flow magnitudes exhibit higher shortages when compared to high flow traces because the supply demand imbalances are higher. For these traces, implementation of options and/or strategies tend to show a decrease in shortages.

The AND approach (shown in blue) generally shows the performance of implementing options and / or strategies in reducing the shortage with increasing RPT when compared to the OR approach. This is not a surprise because the AND approach constrains the implementation of options and strategies (high for low RPT and less for high RPT). Increased numbers of options and strategies implemented under the OR approach (shown by red line) does not reduce the shortage even at high RPT.

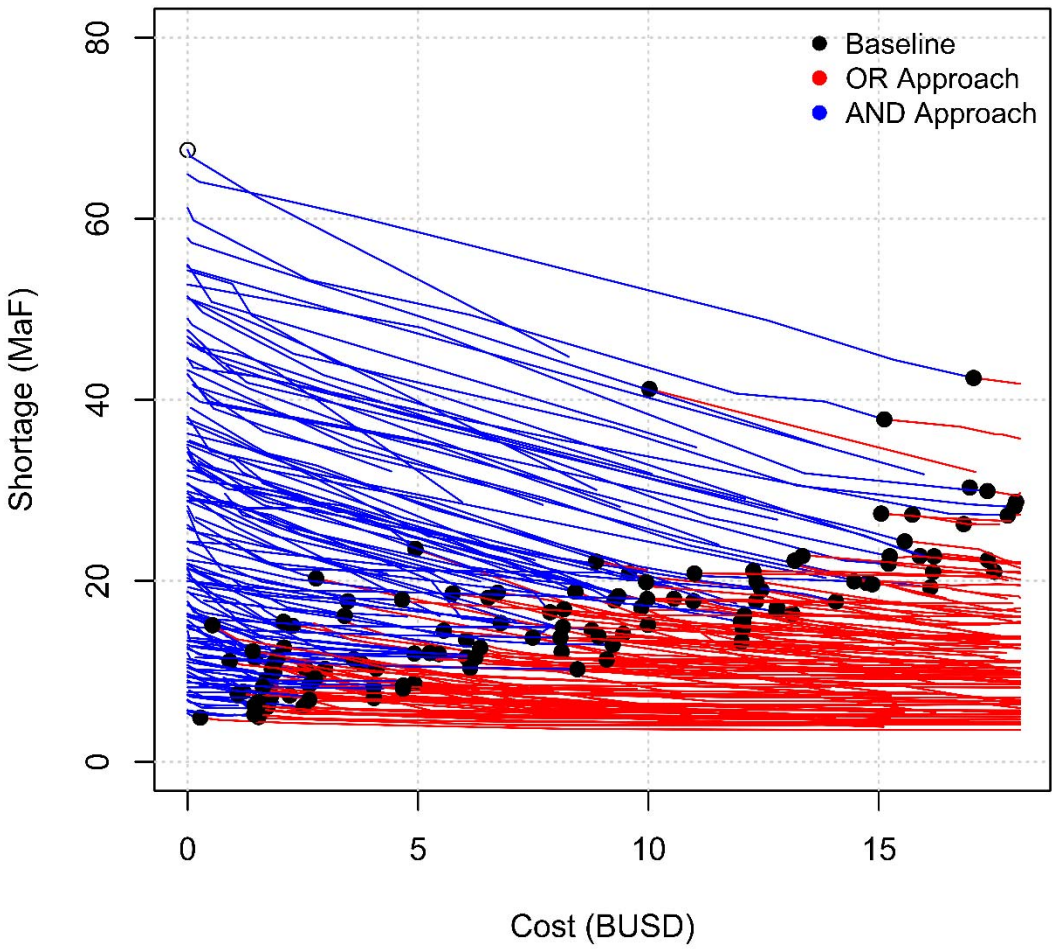

Figure 5.16: Tradeoff curves of the 120 ensemble simulation runs of the OR (red), AND (blue) and the baseline (black)

To investigate the relative performances of the ensemble simulations, changes in shortages of the RPTs of the 120 traces in reference to the baseline are calculated as arithmetic difference between the baseline shortages and the RPTs. For example the increased shortage of the 51% AND RPT is calculated as baseline shortage minus the 51% AND RPT shortage. If the RPT's shortage is greater than the baseline shortage, the value is negative and represented as negative to

show how bad the alternative is with respect to the baseline. The same analysis is performed for the cost, negative cost values indicate how bad the RPT is in reference to the baseline. This analysis is performed for all the 120 traces for each of the OR and AND approaches. Repeating the above analysis for all the 120 traces and RPTs, the results are presented in Figure 5.17. Regions shown by roman numerals in Figure 5.17 represent the solution spaces. Solutions in space I show improvements both in shortage and cost, space II is the region where reduction in shortage at the expense of cost (the OR solution space), space III is a dominated space in which both shortage and costs are increased relative to the baseline. In Region IV, the cost is reduced at the expense of increased shortage (predominantly the AND solution space). The 51% RPT solutions show that the OR approach has almost the same solution as the baseline (region II). This is because at the 51% threshold, the projection metrics are most of the time wet and the decisions are mainly made by the baseline logic. The 51% AND approach solutions show however a significant increase of shortage with a significantly reduction in cost (region IV). Looking at the 90% RPT solutions, the range of values seems to shift from region IV to region II. The question may be asked as to why the projection metrics do not have solutions in region I?

The projection metrics are integrated in the baseline logic in such a way that the options and strategies are identified and triggered by the baseline logic based on the severity of vulnerability and the supply- demand imbalances. In the baseline logic, the numbers and availability of options and strategies are predetermined and are set to be available at a specific time. For example, vulnerability detected at the current time can be mitigated from the available options and strategies at the current time or from the past. The baseline logic identifies options and strategies based on the supply-demand imbalance and a suitable option for the vulnerability.

The OR and AND approaches have the potential to determine the supply-demand imbalances and/or the severity of vulnerability at a given time based on the projection metric. However, the search for appropriate options and strategies is made by the baseline logic. The fewer numbers of available and range of options during the time of implementing options and strategies tend to force the same options or strategies to be selected for different levels of supply demand imbalances and severity of vulnerability. For example, the simulation being made by the baseline logic identifies a supply demand imbalance of 100 units of shortage at time t. The baseline logic search from the available options and strategies and implements the option or strategy that can mitigate the 100 units of shortage say with 100 units capacity and cost of 100 units. For the same hydrology and demand conditions but with the AND approach, the supply-demand imbalance at time t+1 is found to be say 110 units. To mitigate this level of vulnerability the baseline logic look for the option to address the 110 unit imbalance and implements the available 100 unit option, leaving it with 10 units of imbalance for the next time step. For the same cost, the shortages of the AND approach will go higher by 10 units when compared with the baseline and so on. Therefore, the scale of available options and more range of options and strategies can affect the efficiency of the integration approach explained by one example. This being said, cluster analysis used to identify key signposts and threshold values in the baseline decision framework is so skillful that it leaves little room for improving decisions made by our model in terms of reducing both cost and shortage.

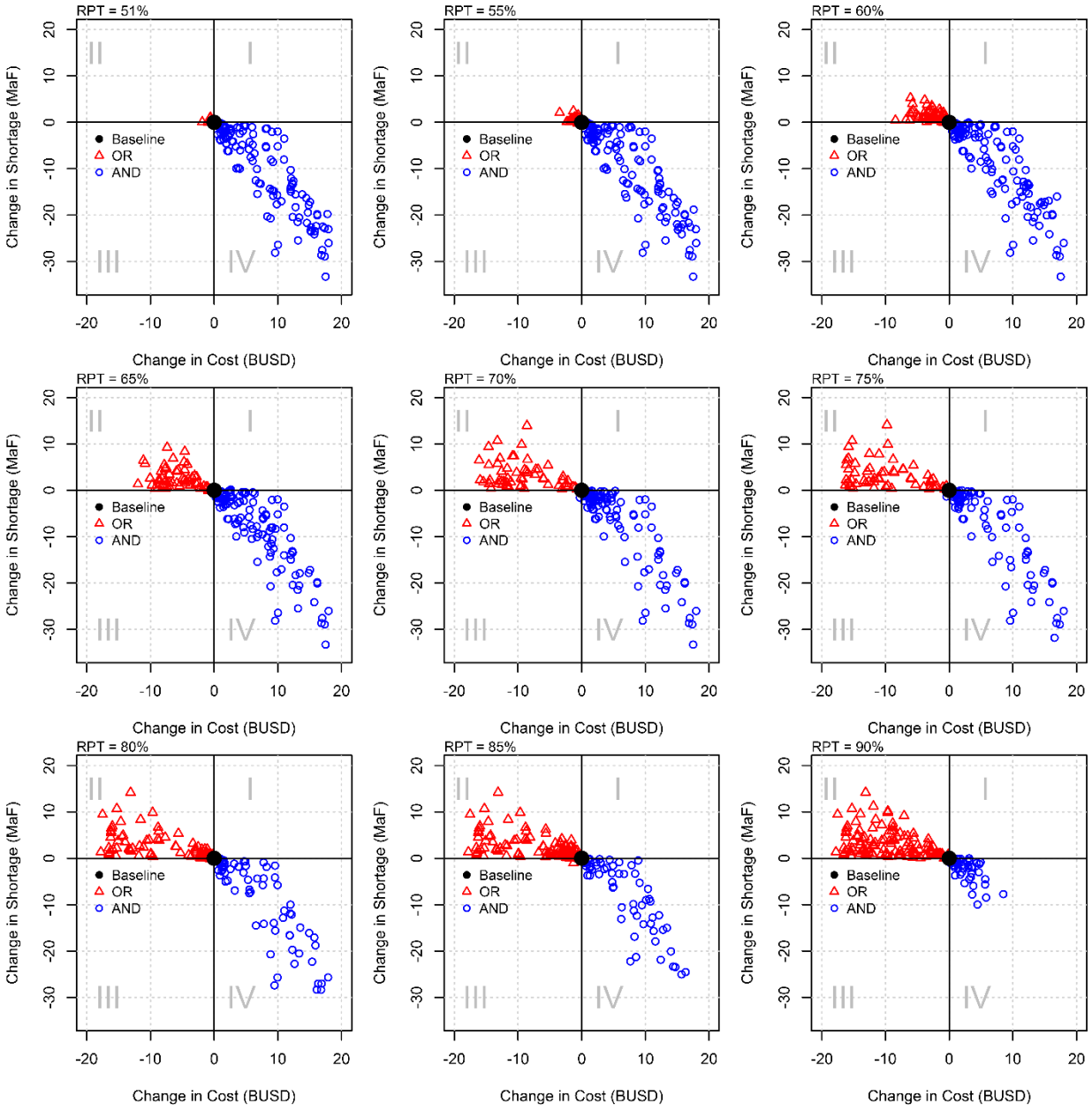

Figure 5.17 scatter plots showing normalized shortage-cost tradeoff for each of the RPTs from the 120 traces. The red triangles are solutions from the OR approach and the blue circles are from the AND approach. The black dot at the (0, 0) point is the baseline solution. The roman numerals show solution spaces (I) Improved shortage and cost (II) Improved shortage with increased cost, (III) Increased cost and shortage (Dominated solution) and (IV) Reduced cost but with increased shortage.

Shortages and costs are determined based on the cumulative values – indicating the overall costs and shortages through the entire planning period. The wide range of RPTs observed for high mean values in Figure 5.18 is because of the variabilities of the traces with time. Two traces with the same mean values can result in entirely with different shortages and costs because of different nonstationarity in the traces. A trace without a significant upward or downward trend is more likely to have less shortage and cost than the trace with a trend. Let's take a trace with upward trend. In this, at the beginning there will be a higher shortage because of the low flow implying implementation of options and strategies and/or shortage as well as higher cost than the down ward trend traces because of the effect of discounting.

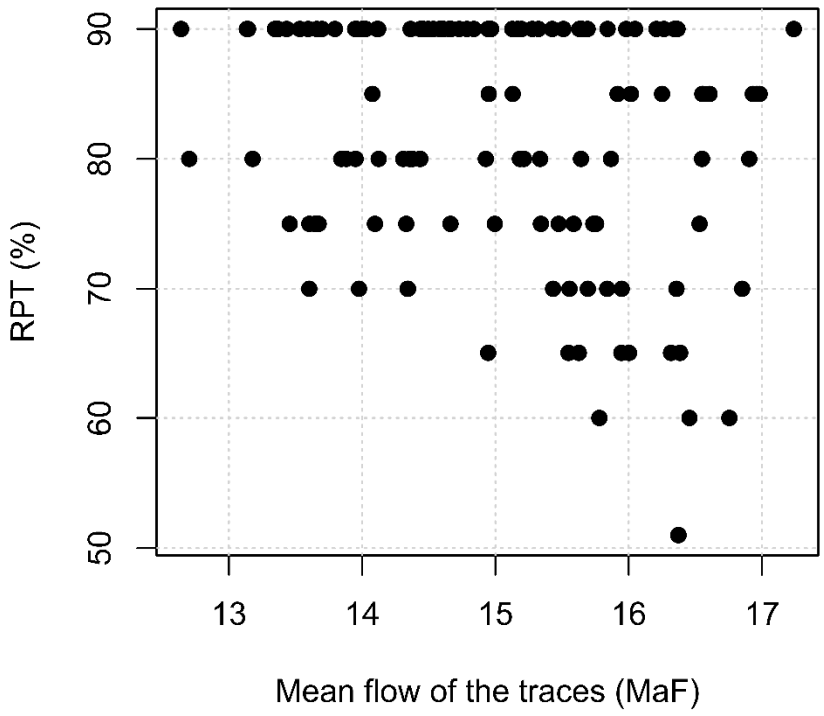

Figure 5.18 Scatterplot of the RPTs with the 49 year means of the 120 traces

If the flow magnitude is low, the effect of either upward or downward trends does not cause a significant shift in RPTs when compared to the high mean flows. It is mainly because the vulnerability is detected most of the times during the simulation and more implementation of options and strategies leading to higher RPT.

5.5 Conclusions

The WKNN simulation and projection model as developed in Chapter 2 is found to be skillful for simulation as well as for projection of streamflow at decadal and multi decadal time scales. This model has been used to generate the plausible future flow scenarios for the CRB and project annual streamflows to incorporate in decision making. The nonlinear dynamical modeling as developed in Chapter 4 provides a novel approach to determine the credibility of the projections. In this application, it has been used as a guide to identify predictable time epochs of the projections

The reference percentage threshold provides a mechanism to modulate and calibrate the magnitude of flow projections that potentially influence the decisions. The threshold value determines the implementation of options and strategies with resulting increased or decreased shortage/cost relative to the baseline options and strategies.

The best performing RPTs from each trace are identified which demonstrate the most balanced solution between shortage and cost with values range from 51 % to 90 %. Figure 5.18 demonstrates the general trend that lower preferred RPTs are more present in the high mean flow values than the low mean valued traces. From Figure 5.15 the wide range of RPTs for a given mean flow particularly for higher mean flows, indicates mean values do not have a direct relation with RPTs. This can be because of the time variability of the traces and trends.

The AND & OR approaches of integration of streamflow projections, along with time varying predictabilities, allow implementation of a range of alternative options and strategies unique for each RPT, whose relative benefits can be assessed with respect to the baseline options and strategies. In the AND approach, options and strategies can be implemented if and only if the projections metrics indicate a dry future and if the signposts are triggered for probably vulnerability; it avoids implementation of unnecessary options and can save in unnecessary costs. The OR approach on the other hand, allows implementation of more options and strategies than the baseline, potentially decreasing shortage.

For the single trace scenario of 1964 – 2012 observed flows, the RPT that gives the most balanced solution between shortage and cost was identified on a tradeoff curve as 75%. Reducing options and strategies using the AND approach demonstrates a significant benefit of reducing shortages for the investment when compared to reductions of shortages with the OR approach. The RPT that performs the best may vary with hydrology; without knowing the hydrology in advance, it is not possible to take advantage of a tradeoff curve like the one in Figure 5.14 to make a decision about selection of an RPT. With that in mind, we analyze an ensemble of plausible future hydrologic scenarios with a wide range of mean flows and look for robust performance across a range of RPT values.

Integration of the projections and their time varying predictabilities are made by utilizing the baseline logic to identify and implement from the available options and strategies. The severity of shortage /vulnerability informed to the baseline logic through the signposts look for appropriate options and strategies to implement and mitigate the vulnerability.

The severity of vulnerability is generally modified by the projections: it will most likely be higher for the AND approach with smaller RPTs because it constrains the baseline logic

implying the need for higher capacity options than the OR approach. Conditioning the severity of vulnerability by the projections provide additional information to identify and select a more suitable options and strategies than the baseline logic alone.

This being said, the limited availability and time constrained options and strategies limit the appropriate choice of options and strategies for vulnerabilities conditioned by the projections. This leads to relatively similar choices of options and strategies for both the baseline and projection conditioned vulnerabilities making the baseline solution one of the non-dominated solutions on the tradeoff curve. Because of this, the baseline solution is improved through tradeoff – either by increasing cost to reduce shortage or reducing cost by increasing shortage. The shortage and costs analyzed for each of the RPTs shown in Figure 5.17 demonstrate the influence of the baseline logic. Scatterplots in Figure 5.17 present regions with RPTs and integration approaches. The top left panel of Figure 5.17 is mainly the AND approach solution suggesting the possible level of shortage if the decision is made by 51% RPT. The worst case scenario in this case is the increase in a 30MAF increase of shortage over the 50 year period, which is 0.6 MAF per year on average. If cost is a constraint and the 0.6MAF average annual shortage is acceptable, the 51% and approach is the solution. On the other extreme, if shortage cannot be compromised, region II of the 90% RPT solution is suitable.

The integration approach used in the CRB decision framework could perform better if more options and strategies would be available with varying costs and capacities and could be selected based on the severity of the vulnerability. Alternatively, instead of selecting from the available options, the decision algorithm could propose options and strategies with a suitable capacity for the detected vulnerability so that a more efficient option could be implemented.

However, inclusion of additional options or strategies would require additional investigation to determine feasibility.

6 Conclusions and Discussion

6.1 Summary and Research Contributions

A novel wavelet-based time series bootstrap simulation model is developed to generate streamflow simulations/projections conditioned on the signals of large scale climate indices. The signals determined by the wavelet technique are simulated /projected using the skillful block bootstrap approach to generate ensembles. The ensembles of climate signals are then used to conditionally simulate/project the streamflow. This modeling approach is demonstrated on the Lees Ferry gauge on the Colorado River by using the two climate indices: AMO and PDO to condition the simulation. The model reproduced all the statistical properties of the naturalized Lees Ferry flow including its non-Gaussian and non-stationary characteristics. Traditional methods develop similar models on the flow timeseries and have limited skill in projections. Here, the climate indices are modeled and streamflow generated conditionally, exploiting the skill in climate indices. The ability to reproduce the nonstationarity characteristics of the flow plays a significant role in water resources management because it can determine the availability of water at a particular time. The WKNN model projections are suitable for water resources planning and management because of their projection skills at decadal and multi decadal timeframes

The performance of the WKNN model relative to two other recently developed timeseries models - the Hidden Markov and the Wavelet based Auto regressive models - is assessed in simulation and especially in projection for different projection times. This comparison is offered as a contribution to the community of water resources management to provide guidance in the suitability of these models for stochastic simulation and for projections over various timeframes.

The comparison is performed by using a conditional simulation approach using the Lees Ferry streamflow with AMO and PDO. In this, first each of the three modeling approaches is applied on the climate indices to generate ensembles (simulation /projection). Then the flow is conditionally realized based on the generated ensembles of climate indices. The WKNN and WARM models are applied on the signal components of each of the climate indices determined by wavelet function. However, the Hidden Markov Model was applied directly on the climate indices. In the simulation mode, the three models perform well in reproducing the distributional statistics (mean, variance, skew and lag 1), PDF and the wavelet spectra. The local wavelet spectra of the three simulations seems to reproduce the nonstationarity characteristics of the observed flow wavelet spectra. The PDFs of the simulations also captured the PDF of the observed flow implying the capabilities of the three models in reproducing the non-Gaussian distribution of the observed flow.

In the projection mode, several conditional streamflow projections were performed for different projection periods using each of the three models. The HMM model performed better for shorter lead times than the wavelet based approaches, so would be more appropriately used for projecting 1 to ~10 years. The WKNN model demonstrated its suitability for decadal and multi decadal time scales, so would be more useful in water resources planning and management at decadal and multi decadal time scales such as the Basin Study. The WARM projections showed similar skills for decadal and multi decadal time scales as the WKNN projections, but the WKNN projections perform slightly better.

A novel approach to stochastic time series simulation and determining epochal predictability of the time series based on reconstructing the phase space through the nonlinear dynamical modeling approach is presented. The multivariate version of a timeseries is

reconstructed through embedding to create the phase space. The reconstructed phase space is a proxy to the true phase space in which the underlying dynamics unfolds, enabling to take advantage of the system predictability via the Local Lyapunov Exponents (LLE) to determine the epochs when projections are not credible. Application to the CRB shows a negative global LLE, indicating the signal in the flow timeseries is generally predictable, but showed significant epochal variations – with some epochs exhibiting high predictability and some low predictability. Blind projections of stream flows during high predictable epochs show good skill and capture all the distributional, drought and surplus statistics, while the low predictability epochs had poor performance on these measures. The time varying predictability of the streamflow determined as LLE, provokes the tantalizing idea that water resources management should adapt in a flexible manner with regard to the epochs of good and poor predictability.

Skillful projections based on the new WKNN method and time varying predictabilities determined as LLE are demonstrated as additional information integrated with the decision making framework developed for the 2012 Colorado River Basin Supply and Demand Study which explores the use of options and strategies to address possible future supply-demand imbalances. Ensembles of 11-year projections are generated at every year of system simulations; these are translated into sequences of annual wet and dry depending on the percentage of projections in each ensemble falling above or below some reference threshold. Threshold based projection metrics, together with the predictability information, are integrated with the existing decision framework using two approaches. (i) Constrain the decisions based on the projections: decisions can be implemented only if the projection metric is dry and if vulnerability is detected by the existing decision ("AND" approach); (ii) Complement the decisions: implement options and strategies if either the projections are dry or the existing signposts detect vulnerability ("OR"

approach). The integrated decision metrics are applied to a single observed hydrologic trace, then to 120 plausible futures generated using the WKNN model. The implemented options and strategies using the projection information are compared with those generated by the original logic of the Basin Study in terms of the cost of implementation and the associated shortages. The tradeoff between the cost and shortages for different thresholds of wet/dry illustrates the possible effects of integrating the projections with the baseline framework through the two integration approaches.

6.2 Discussion

For water resources planning decisions to minimize demand-supply imbalances over several years to decades, information about the future flow conditions through skillful projections could be useful. The WKNN stochastic timeseries model, which simulates and projects the streamflow conditioned to the large scale climate indices, was shown to be suitable for planning and management of water resources because of its skill.

Incorporating the skillful decadal streamflow projections on the CRB decision framework is the main objective of this research. For this, two integration approaches are developed: (i) constraining the baseline decisions through the projections and (ii) complementing the baseline decisions by the projections. These two approaches have a potential to condition the supply-demand imbalances and the severity of vulnerability of the baseline framework so that a more appropriate option and strategy can be implemented.

Projection metrics determined from the skillful decadal projections and the time varying predictability of the streamflow utilize the baseline framework with better efficiency. The projections inform the baseline framework about the future flow as wet or dry through either the

AND approach or through the OR approach to modify the baseline vulnerabilities. The modified vulnerabilities are used to identify appropriate options and strategies. The AND and OR approaches utilize the capability of the baseline logic to identify a suitable option from the projection conditioned supply-demand imbalances and/or vulnerabilities. The baseline logic is designed to identify vulnerabilities through signposts based on the current or past conditions of the system. Severity of vulnerability and supply-demand imbalances are used as input to identify appropriate options and strategies from the active portfolio being used.

The OR approach allows implementation of options and strategies especially if the projections are dry. The OR-dry combination (the most allowing) and the AND-wet combination (the most constraining) marks the two extremes of implementing options and strategies and at the same time the extremes of shortages and costs.

Conditioning the baseline options and strategies provides wide options in terms utilizing the available resources in a number of ways through the RPT. The applications of these integration approaches for a robust water resources planning and management is demonstrated by presenting the relative performances of costs and shortages with respect to the baseline costs and shortages. Alternatives of options and strategies from the AND approach tend to increase shortages relative to the baseline while reducing the cost. The OR alternative on the other hand exhibit increasing cost with reduces shortage. For cases where shortages have a highest priority over cost, the OR approach with higher RPT is a solution. If the shortages can be tolerated because of cost constraints, the AND approach with lower RPT show a solution. However, improved performance both in terms of cost and shortage is not demonstrated either through the AND or OR approaches. One of the main reasons, as explained in Chapter 5, is related to availability of options and strategies that closely address the scale of vulnerability or the supply-

demand imbalance conditioned by the projections. Similar options and strategies tend to be implemented despite the differences in the scale of vulnerability or the supply-demand imbalances of the baseline and the projection conditioned imbalances.

6.3 Future Work

The WKNN Streamflow time series model utilizes the block bootstrap approach to simulate and project the large scale climate indices. The choice of the block size has a significant effect on the skill of the timeseries simulations and projections. In this research, a block size of about half the period (B) of the signal component of the climate index was used. This block size is long enough to represent the periodicity and pattern of the data and it is used to identify other blocks of size B from the timeseries with similar patterns and periodicity. This method uses the block size to divide the timeseries into n numbers of blocks. For example, a timeseries with L years of data will have n=L/B blocks. With increased block size the numbers of blocks decrease, resulting in fewer blocks from which to resample, hence less variety of the simulation. Developing criteria for the selection of block size is a potential research area.

Significant changes in flow regime such as the Lees Ferry flow from wet in the early 1900s to low flow in ~ 1935, were not captured by the conditional simulation models used in this research. Applying a Hidden Markov model on the timeseries to identify the flow states and then using the block bootstrap approach could improve the simulation changes observed in the Lees Ferry flow. For example, the flow could shift from state 1 to state 2 or 3. With the known state transition from the HM model, KNN bootstrap could be applied to identify and resample values from the same state from the past. This hybrid approach could benefit in capturing transitions observed like in the Lees Ferry flow.

This research demonstrated the performance of incorporating the streamflow projections in the CRB decision framework through the two integration approaches. The integration approach has a potential to improve the performance of the baseline framework alternatives more through consideration of a more flexible implantation of options and strategies. Applying the integration of the projections could benefit on decision making frameworks other than the CRB framework. The integration logic has a potential to condition the demand-supply imbalances through constraining the implementation of options and strategies.

The decision making approach presented in this research is demonstrated by using constant demand throughout the planning period. For this demand level the 75% RPT is computed to be the most balancing option. Developing a relationship between demand and streamflow magnitude and the associated preferred flow magnitudes can be used as a guide to determine the conditions of the system as critical, wet, or dry depending on the demand and supply levels at the current time.

7 References

Colorado River Compact, 1922: http://www.usbr.gov/lc/region/g1000/pdfiles/crcompct.pdf

Abarbanel H. D. I, R. Brown, and M. B. Kennel, 1992: Local Lyapunov Exponents Computed from Observed Data, J. *Nonlinear Sci. gol. 2: pp. 343-365*

Abarbanel, H.D.I, R. Brown, J. J. Sidorowich, L. S. Tsimring, 1993: The analysis of observed chaotic data in physical systems, Reviews of modern physics 65 (4), 1331Abarbanel H. D. I. and U. Lall, 1996: Nonlinear dynamics of the Great Salt Lake: system identification and prediction, *Climate Dynamics 12: 287–297*

Abarbanel H, D. I., U Lall, 1996: Nonlinear dynamics of the Great Salt Lake: system identification and prediction, *Climate Dynamics 12: 287–297*

Asefa, T., M. Kemblowski, U. Lall, and G. Urroz, 2005: Support vector machines for nonlinear state space reconstruction: Application to the Great Salt Lake time series, *Water Resour. Res., 41, W12422, doi:10.1029/2004WR00378*

Bailey, B. A. and D. W. Nychka, 1995: Local Lyapunov Exponents: Predictability depends on where you are, *Biomathematics Graduate Program, Department of Statistics North Carolina State University, Raleigh NC 27695-8203*

Barnett, T.P. et al., 2008: Human-induced changes in the hydrology of the western United States, *Science, 319, 1080-1083*

Bracken, C., B. Rajagopalan and E. Zagona, 2014: A Hidden Markov Model Combined with Climate Indices for Multi-decadal Streamflow Simulation, *Water Resour. Res., 50, 7836-7846, doi: 10.1002/2014WR015567*

Bracken, C., B. Rajagopalan, and J. Prairie, 2010: A Multisite Seasonal Ensemble Streamflow Forecasting Technique, *Water Resour. Res., 46, 3, DOI: 10.1029/2009WR007965*

Brown, C., Y. Ghile, M. Laverty and K. Li , 2012: Decision scaling: Linking bottom-up vulnerability analysis with climate projections in the water sector, Water Resour. Res., 48, DOI: 10.1029/2011WR011212

Caraway, N. M., J.L. McCreight, B. Rajagopalan, 2014: Multisite stochastic weather generation using cluster analysis and k-nearest neighbor time series resampling, *Journal of Hydrology 508 (2014) 197–213*

Carlson, R.F., A.J. MacCormick, D.G. Watts, 1970: Application of linear models to four annual streamflow series, *J. Wat. Resour. Res., 6,4,1070-1078*

Casdagli, M., S. Eubank, J. D. Farmer, J. Gibson, D. Des Dardins, N. Hunter, and J. Theiler, 1990: Nonlinear modeling of chaotic time series: theory and applications, *Los Alamos National Laboratories, LA-UR-91-1637*

Chao, Y., M. Ghil and J.C. Mcwilliams 2000: Pacific interdecadal variability in the century's Sea Surface Temperatures, *Geophys. Res. Lett., 27, 2261-2264.*

Cook, E. R., C. A. Woodhouse, C. M. Eakin, D. M. Meko, and D. W. Stahle , 2004: Long-term aridity changes in the western United States, *Science, 306, 1015–1018, doi:10.1126/ science.1102586.*

Dracup, J. A., and E. Kahya, 1994: The relationships between United States streamflow and La Niña events. *Water Resour. Res., 30, 2133–2141*

Efron, B., and R. Tibishirani 1993: An Introduction to the Bootstrap, *Chapman and Hall, New York*

Elsner J. B. and A. A. Tsonis, 1992: Nonlinear Prediction, Chaos, and Noise, *American Meteorological Society*

Enfield, D. B., A. M. Mestas-Nunez, and P. J. Trimble, 2001: The Atlantic multidecadal oscillation and its relation to rainfall and river flows in the continental US. *Geophys. Res. Lett., 28, 2077–2080.*

Erkyihun S. T., B. Rajagopalan, E. Zagona, U. Lall, K. Nowak, 2015: Wavelet-based Time Series Bootstrap Model for Multi-decadal Streamflow Simulation Using Climate Indicators. *Water Resour. Res., Submitted*

Fraser A. M. and H. L. Swinney, 1986: Independent coordinates for strange attractors from mutual information, *The American Physical Society*

Farmer J.D. and J. J. Sidorowich, 1987: Predicting chaotic time series. *Phys. Rev. Lett., 59(8), 845-848*

Foufoula-Georgiou E., P. Kumar, 1994: Wavelets in Geophysics, *Academic press*

Gangopadhyay, S., B. L. Harding, B. Rajagopalan, 2009: A nonparametric approach for paleohydrologic reconstruction of annual streamflow ensembles, *Water Resour. Res., 45, W06417, doi: 10.1029/2008WR007201*

Gershunov, A. and Tim P. Barnett, 1998: Interdecadal Modulation of ENSO Teleconnections, *the American Meteorological Society, Vol. 79, No. 12.*

Grantz K. and Rajagopalan B., M. Clark, E. Zagona, 2005: A technique for incorporating large-scale climate information in basin-scale ensemble streamflow forecasts, *Water Resour. Res., 41, W10410, doi: 10.1029/2004WR003467*

Grassberger P., and I. Procaccia, 1983a: Characterization of strange attractors. *Phys. Rev. Lett., 50, 346-349.*

Grassberger P., and I. Procaccia, 1983b: Measuring the strangeness of strange attractors, *Physica D, 9, 189-208*

Grassberger P., T. Schreiber, and C. Schaffrath, 1991: Nonlinear time sequence analysis, *Int. J. Bifurcation Chaos, 1(3), 521– 547.*

Gray S. T., L. J. Graumlich, J. L. Betancourt, and G. T. Pederson, 2004: A tree-ring based reconstruction of the Atlantic Multidecadal Oscillation since 1567 A.D., *Geophys. Res. Lett., VOL. 31, L12205, doi: 10.1029/2004GL019932*

Guégan D. and J. Leroux, 2009: Forecasting chaotic systems: The role of local Lyapunov exponents, *Elsevier Ltd. All rights reserved.doi:10.1016/j.chaos.2008.09.017*

Guégan D. and J. Leroux , 2011: Predicting Chaos with Lyapunov Exponents: Zero Plays no Role in Forecasting Chaotic Systems, Chaotic Systems, *Prof. Esteban Tlelo-Cuautle (Ed.), ISBN: 978-953-307-564-8, InTech*

Gupta H.V., Brookshire, D.S., Tidwell, V. & Boyle, D., 2011: Modeling: A Basis for Linking Policy to Adaptive Water Management, Chapter 2 in Brookshire D, HV Gupta, and P. Matthews (Editors), Water Policy in New Mexico: Addressing the Challenge of an Uncertain Future, RFF Press, Resources for the Future Book Series: *Issues in Water Resources Policy Series.*

Gray S. T., L. J. Graumlich, J. L. Betancourt, and G. T. Pederson, 2004: A tree-ring based reconstruction of the Atlantic Multidecadal Oscillation since 1567 A.D., *Geophys. Res. Lett., VOL. 31, L12205, doi: 10.1029/2004GL019932*

Groves, D.,E. Bloom, R. Lempert, J. Fischbach, J.Nevills, and B. Goshi, 2015: Developing Key Indicators for Adaptive Water Planning, *Journal of Water Resources Planning and Management 2015 141:7*

Groves, D. G., J. R. Fischbach, E. Bloom, D. Knopman, and R. Keefe, 2013: Adapting to a changing Colorado River, *RAND, Santa Monica, CA.*

Groves, D., D. Yates and c. Tebaldi, (2008) Developing and applying uncertain global climate change projections for regional water management planning, *Water Resour. Res., 44.*

Hall J., R.J. Lempert, K. Keller, Hachbarth, C. Mijere, D.J. McInerney, 2012: Robust climate policies under uncertainity a comparison of robust decision making and info-gap methods, *Risk Analysis, 32 (10) (2012), pp 1657-1672*

Hallegatte S., 2009: Global Environmental Change, *Science Direct, 19 (2009) 240-247, doi:10.1016/j.gloenvcha.2008.12.003*

Hashimoto, T., J.R. Stedinger, D.P. Loucks, 1982: Reliability, resiliency and vulnerability criteria for water resource system performance evaluation, *Water Resour. Res., 18 (1982), pp. 14–20*

Hidalgo, H.G., 2004: Climate precursors of multidecadal drought variability in the western United States, Water Resour. Res., 40, W12504, doi: 10.1029/2004WR003350Hughes D. A., 2015: Scientific and practical tools for dealing with water resource estimations for the future, *Hydrologic Nonstationarity and Extrapolating Models to Predict the Future (HS02 – IUGG2015), Proc. IAHS, 371, 23–28, 2015 proc-iahs.net/371/23/2015/ doi:10.5194/piahs-371-23-2015*

Hidalgo H.G.; Dracup J.A., 2003: ENSO and PDO effects on hydroclimatic variations of the Upper Colorado River Basin, *Journal of Hydrometeorology, 4, 5-23*

Hughes D. A., 2015: Scientific and practical tools for dealing with water resource estimations for the future, *Hydrologic Nonstationarity and Extrapolating Models to Predict the Future (HS02 – IUGG2015), Proc. IAHS, 371, 23–28, 2015 proc-iahs.net/371/23/2015/ doi:10.5194/piahs-371-23-2015*

Ibe, O.C, 2009: Markov Processes for Stochastic Modeling, *University of Massachusetts, Academic Press*

Kantz H., 1994: A robust method to estimate the maximal Lyapunov exponent of a time series. *Physics Letters A, 185, 77–87*

Kantz H., and T. Schreiber, 1997: Nonlinear Time Series Analysis, *Cambridge Univ. Press, New York.*

Kantz H. and T. Schreiber, 1998: Human ECG, Nonlinear deterministic versus stochastic aspects, *IEE Proc. Science, Measurement and Technology*

Kaplan, A., M. Cane, Y. Kushnir, A. Clement, M. Blumenthal, and B. Rajagopalan, , 1998: Analyses of global sea surface temperature 1856-1991, *Journal of Geophysical Res., 103, 18,567-18,589*

Kahya E., J. A. Dracup, 1993 : U.S. streamflow patterns in relation to the El Niño/Southern Oscillation, *Water Resour., Res., 29,8, DOI: 10.1029/93WR00744*

Kasprzyk J.R, S. Nataraj, P.M. Reed, R.J. Lempert, 2013: Many objective robust decision making for complex environmental systems undergoing change, *Environmental Modelling & Software Volume 42, April 2013, Pages 55–71*

Kennel M.B., R. Brown and H.D.I Abarbanel, 1992: Determining embedding dimension for phase-space reconstruction using a geometrical construction, *The American Physical Society*

Kirchner J. W., 2009: Catchments as simple dynamical systems: Catchment characterization, rainfall-runoff modeling, and doing hydrology backward, *Water Resour. Res., 45, W02429, doi: 10.1029/2008WR006912*

Kirtman, B.P and P. S. Schopf, 1998: Decadal Variability in ENSO Predictability and Prediction. *J. Climate, 11, 2804–2822*

Kumar P., E. Foufoula-Georgiou, 1997: Wavelet analysis for geophysical applications, *Reviews of Geophysics.*

Kwon, H.H., U. Lall, and A. F. Khalil, 2007: stochastic simulation model for nonstationary time series using anautoregressive wavelet decomposition: Applications to rainfall and temperature, *Water Resour. Res., 43, W05407, doi: 10.1029/2006WR005258.*

Kwon, H. H., Lall, U., & Obeysekera, J. 2009: Simulation of daily rainfall scenarios with interannual and multidecadal climate cycles for South Florida.*Stochastic Environmental Research and Risk Assessment, Springer, 23(7), 879-896, doi 10.1007/s00477-008-0270-2*

Lahdelma, R., Salminen, P., Hokkanen, J., 2000: Using multicriteria methods in environmental planning and management*, Environmental Management Vol. 26, No. 6, pp. 595– 605.*

Lall, U. 1995: Recent advances in nonparametric function estimation: hydraulic applications, *U.S. Natl. Rep. Int. Union Geod. Geophys. 1991-1994, Rev. Geophys., 33, 1093-1102.*

Lall,U. and, A. Sharma 1996: a nearest Neighbor bootstrap for resampling hydrologic time series, Water Resour. Res., 32, NO. 3, PAGES 679–693

Lall, U., T. Sangoyomi, and H.D.I. Abarbanel, 1996: Nonlinear dynamics of the Great Salt Lake: Nonparametric short-term forecasting. *Water Resour. Res., 32(4), 975-985.*

Lall, U., Devineni, N., & Kaheil, Y. 2015: An Empirical, Nonparametric Simulator for Multivariate Random Variables with Differing Marginal Densities and Nonlinear Dependence with Hydroclimatic Applications. *Risk Analysis. doi: 10.1111/risa.12432*

Latif, M and T.P. Barnett 1994: Causes of Decadal Climate Variability over the North Pacific and North America, *Science 266: 634-637*

Lempert R.J., D. G. Groves, S. W. Popper, S. C. Bankes, 2006: A General, Analytic Method for Generating Robust Strategies and Narrative Scenarios. *Management Science 52(4):514-528.*

Lempert, R., J. and Myles T. Collins, 2007: Managing the Risk of Uncertain Threshold Responses: Comparison of Robust, Optimum, and Precautionary Approaches, *Risk Analysis, Vol. 27, No. 4, 2007, DOI: 10.1111/j.1539-6924.2007.00940.x*

Lempert, R. J., 2002a: New Decision Sciences for Complex Systems, *Proceedings of the National Academy of Sciences, Vol. 99, supplement 3, 2002a, pp. 7309–7313.*

Lempert R.J., D.G. Groves, 2010: Identifying and evaluating robust adaptive policy responses to climate change for water management agencies in the American west, *Technological Forecasting and Social Change Volume 77, Issue 6, July 2010, Pages 960–974*

Loucks, D. P. and E.Van Beek 2005: Water Resources Systems Planning and Management, *United Nations Educational, Scientific and Cultural Organization, 7, place de Fontenoy F-75352 Paris 07 SP and WL | Delft Hydraulics, The Netherlands*

Loucks, D. P. and E.Van Beek 2005: Concepts in Probability, Statistics and Stochastic Modelling, in Water Resources Systems Planning and Management, 169-229, UNESCO PUBLISHING, *United Nations Educational, Scientific and Cultural Organization, 7, place de Fontenoy F-75352 Paris 07 SP and WL | Delft Hydraulics, The Netherlands*

Lorenz E. N., 1963: Deterministic Nonperiodic Flow, J. *of the Atmosphere Sciences*

MacDonald, G.M., and R.A. Case. 2005. Variations in the Pacific Decadal Oscillation over the past millennium. *Geophys. Res. Lett., 32, L08703, doi: 10.1029/2005GL022478*

MacDonald, G.M., and R.A. Case. 2006: Pacific Decadal Oscillation Reconstruction for the Past Millennium. *IGBP PAGES/World Data Center for Paleoclimatology Data Contribution Series # 2006-023. NOAA/NCDC Paleoclimatology Program, Boulder CO, USA.*

Mann, M.E., E.P. Gille, R.S. Bradley, M.K. Hughes, J.T. Overpeck, F.T. Keimig, and W.S. Gross, 2000: *Global Temperature Patterns in Past Centuries: An Interactive Presentation, Earth Interactions: Vol. 4, Paper 4*

Mantua, N.J. and S.R. Hare, Y. Zhang, J.M. Wallace, and R.C. Francis, 1997: A Pacific interdecadal climate oscillation with impacts on salmon production. *Bulletin of the American Meteorological Society, Vol. 78, pp. 1069-1079.*

Matrosov, E. S., A. M. Woods, and J. Harou 2013: Robust Decision Making and Info-Gap Decision Theory for water resources system planning, J. *Hydrol., 494, 43–58.*

Means, E., M. Laugier, J. Daw, L. Kaatz, and M. Waage, 2010: Decision support planning methods: Incorporating climate change into water planning, *Water Utility Climate Alliance, Clear Water, FL*

Meehl A.G, L. Goddard, J. Murphy, R. J. Stouffer, G. Boer, G. Danabasoglu, K. Dixon, M. A. Giorgetta, A.M. Greene, Ed H., G. Hegerl, D. Karoly, N. Keenlyside, M. Kimoto, B. Kirtman, A. Navarra, R. Pulwarty, D. Smith, D. Stammer, and T. Stockdale, 2009: *Decadal prediction. Bull. Amer. Meteor. Soc., 90, 1467–1485. doi: http://dx.doi.org/10.1175/2009BAMS2778.1*

Meko, D. M., C. A. Woodhouse, C. A. Baisan, T. Knight, J. J. Lukas, M. K. Hughes, and M. W. Salzer (2007), Medieval drought in the upper Colorado River basin, *Geophys. Res. Lett., 34, L10705, doi:10.1029/2007GL029988.*

Miller, W., R. Butler, T. Piechota, J. Prairie, K. Grantz, and G. DeRosa, 2012: Water Management Decisions Using Multiple Hydrologic Models within the San Juan River Basin under Changing Climate Conditions, *Journal of Water Resources Planning and Management, 138 (5), 412-420.*

Minobe, S. 1997: A 50-70 year climatic oscillation over the north pacific and North America. *Geophys. Re. Lett., 24, 683-686.*

Mccabe, G. J. And M. D. Dettinger 1999: Decadal Variations in the Strength of ENSO teleconnections with Precipitation in the western United States. *Int J of Climatology 19 1399-1410*

McCabe, G.J. And M.D. Dettinger, 2002: Primary Modes and Predictability of Year-To-Year Snowpack Variations in the Western United States from teleconnections with Pacific Ocean climate. *Journal of Hydrometeorology, 3(1):13-25.*

McCabe, G. J., M. A. Palecki, J. L. Betancourt, 2004: Pacific and Atlantic Ocean influences on multidecadal drought frequency in the United States, *The National Academy of Sciences of the USA, vol. 101 no. 12.*

McCabe, G. J., M. D. Dettinger, J. L. Betancourt, and H. G. Hidalgo, 2007: Associations of decadal to multidecadal sea surface temperature variability with Upper Colorado River flow. *J. Amer. Water Resour. Assoc., 43, 183–192.*

McCabe, G. J., M. D. Dettinger, S. T. Gray, M. A. Palecki, and H. G. Hidalgo, 2008: Associations of multi-decadal sea surface temperature variability with US drought. Quat. Int., 188, 31–40.Means, E., M. Laugier, J. Daw, L. Kaatz, and M. Waage, 2010: Decision support planning methods: Incorporating climate change into water planning, *Water Utility Climate Alliance, Clear Water, FL*

Moon Y., B. Rajagopalan, and U. Lall., 1995: Estimation of Mutual Information Using Kernel Density Estimators, *Physical Review E, 52(n3B), 2318-2321*

Moon, Y., U. Lall and H.H. Kwon, 2008: Non-parametric short-term forecasts of the Great Salt Lake using atmospheric indices. *International Journal of Climatology, 28(3), 361-370.*

Murphy J., V. Kattsov N. Keenlyside, M. Kimoto, G. Meehl, V. Mehta, H. Pohlmann, A. Scaife, D. Smith, 2010: Towards Prediction of Decadal Climate Variability and Change, *Procedia Environmental Sciences, Volume 1, 2010, Pages 287–304, doi:10.1016/j.proenv.2010.09.018*

Mysiak J. , C. Giupponi , P. Rosato, 2005: Towards the development of a decision support system for water resource management, *Environmental Modelling & Software, Volume 20, Issue 2, February 2005, Pages 203–214, doi:10.1016/j.envsoft.2003.12.019*

Nese J.M., 1989: Quantifying Local Predictabili1y in Phase Space, *Elsevier Science Publishers B.V., Physica D 35 (1989) 237-250*

Nowak, K., J. Prairie, B. Rajagopalan, and U. Lall , 2010: A Non-parametric Stochastic Approach for Multisite Disaggregation of Annual to Daily Streamflow, *Water Resour. Res., 46.*

Nowak, K. C. , 2011 : Stochastic Streamflow Simulation at Interdecadal Times Scales and Implications for Water Resources Management in the Colorado River Basin, *Civil, Environmental, and Architectural Engineering Ph.D. Thesis, University of Colorado, Boulder, CO.*

Nowak, K., M. Hoerling, B. Rajagopalan, E. Zagona, 2012: Colorado River Basin Hydroclimatic Variability, *J. Climate.*

Nowak, K., B. Rajagopalan and E. Zagona 2011: Wavelet Auto-Regressive Method (WARM) for multi-site streamflow simulation of data with non-stationary spectra, *J. Hydrology, 410 (1-2) 1-12.*

O'Connell, P.E., 1971: A simple stochastic modeling of Hurst's law. In Mathematical Models in Hydrology, *Warsaw Symposium, (IAHS Publ.100, 1974), 1, pp.169-187*

Oseledec VI, 1968: A Multiplicative ergodic theorem. Lyapunov characteristic numbers for dynamical systems. *Trudy Mosk Mat Obsc 19:197; Moscow Math Soc 19: 197*

Packard N.H., J. P. Crutchfield, J.D. Farmer, and R. S. Shaw, 1980: Geometry from a timeseries, *The American Physical Society, Volume 45, Number 9, Pages 712-716*

Peterson T. J. and A. W. Western, 2014: Multiple hydrological attractors under stochastic daily forcing: 1. Can multiple attractors exist? , *Water Resour. Res., 50, 3010-3029, doi: 10.1002/2012WR013004*

Porporato A. and L. Ridolfi, 1996: Clues to the existence of deterministic chaos in river flow, *International Journal of Modern Physics B 10:1821-1862*

Porporato A. and L. Ridolfi, 1997: Nonlinear analysis of river flow time sequences, *Water Resour. Res., 33, NO. 6, Pages 1353-1367*

Prairie, J. and R. Callejo, 2005: Natural Flow and Salt Computation Methods, *United States Bureau the Interior, Salt Lake City, UT*

Prairie, J., Rajagopalan, B., Fulp, T., and Zagona, E. (2006). "Modified K-NN Model for Stochastic Streamflow Simulation." *J. Hydrol. Eng., 11(4), 371–378.*

Prairie J., K.Nowak, B.Rajagopalan, U.Lall, and T.Fulp, 2008: A stochastic nonparametric approach for streamflow generation combining observational and paleo reconstructed data, *WATER RESOUR. RES., VOL. 44, W06423, doi:10.1029/2007WR006684*

Raff D., Brekke L., Werner K., Wood A., and White K., 2013: Short Term Water Management Decisions: User Needs for Improved Climate, Weather, and Hydrologic Information, *United States Army Corps of Engineers*

Rajagopalan B., and U. Lall, 1998: Low Frequency Variability in Western U.S. Precipitation, *J. of Hydrology, 210, 51-67*

Rajagopalan,B., and Lall,U. 1999: A k–nearest-neighbor simulator for daily precipitation and other weather variables, *Water Resour. Res., 35, NO. 10, 3089–3101*

Rajagopalan, B., E. Cook, U. Lall, and B. K. Ray 2000: Spatiotemporal Variability of ENSO and SST teleconnections to summer drought over the United States during the twentieth century, *J. Clim, 13, 4244– 4255.*

Rajagopalan, B., K. Nowak, J. Prairie, M. Hoerling, B. Harding, J. Barsugli, A. Ray, and B. U.Lall, 2009): Water supply risk on the Colorado River: Can management mitigate?, *Water Resour. Res., 45*

Rajagopalan B., J. Salas and U. Lall, 2010: Stochastic methods for modeling precipitation and streamflow, in Advances in Data-based Approaches for Hydrologic Modeling and Forecasting, Ed by B. Sivakumar and R. Berndtsson, *World Scientific, Singapore*

Rajagopalan B., S. T. Erkyihun, E. Zagona, U. Lall and K. Nowak, 2015: A Nonlinear Dynamical Systems based Modeling Approach for Stochastic Simulation of Stream flow and Understanding Predictability, *Journal of Geophysical Research, submitted*

Read, L. K., and R. M. Vogel, 2015: Reliability, return periods, and risk under nonstationarity, *Water Resour. Res.,51, doi:10.1002/2015WR017089*

Reckhow KH, 994: Importance of scientific uncertainty in decision-making. *Environ Manage 18:161–166*

Reclamation, 2012: Colorado River Basin Water Supply and Demand Study, *U.S. Department of the Interior, Bureau of Reclamation*

Redmond, K. T., and R. W. Koch, 1991: Surface climate and streamflow variability in the western United States and their relationship to large-scale circulation indexes. *Water Resour. Res., 27, 2381–2399.*

Regonda S., B. Rajagopalan, U. Lall, M. Clark and Y. Moon, 2005: Local polynomial method for ensemble forecast of time series, Nonlinear Processes in Geophysics, *Special issue on "Nonlinear Deterministic Dynamics in Hydrologic Systems: Present Activities and Future Challenges", 12, 397-406*

Regonda, S.K., Rajagopalan, B., Clark, M. and Zagona, E., 2006: A multimodel ensemble forecast framework: Application to spring seasonal flows in the Gunnison River Basin. *Water Resour. Res., 42: doi: 10.1029/2005WR004653. issn: 0043-1397*

Regonda, S., E. Zagona and B. Rajagopalan, 2011: Prototype Decision Support System for Operations on the Gunnison Basin with Improved Forecasts, *J. of Water Resources Planning and Management, 137 (5).*

Ropelewski, C.F. and M.S. Halpert, 1986: North American Precipitation And Temperature Patterns Associated With The El Niño / Southern Oscillation. *Monthly Weather Review, 114(2):2352-2362.*

Ropelewski, C.F. and M.S. Halpert, 1989: Precipitation Patterns Associated With The High Index Phase Of The Southern Oscillation. *J. Of Clim. 2:268-284.*

Sangayomi T. B., U. Lall, and H. D. I. Abarbanel, 1996: Nonlinear dynamics of the Great Salt Lake: Dimension estimation, *Water Resour. Res., 32, Pages 149-159*

Salas, J.D., J.W. Delleur, V. Yevjevich and W.L. Lane, 1980: Applied Modeling of Hydrological Timeseries, *Water Resources Publication.*

Schreiber T. and P. Grassberger, 1991: A simple noise-reduction method for real data, *Physics Letters A 160 (1991) 411—418*

Schreiber T. and H. Kantz, 1996: Observing and predicting chaotic signals: Is 2% noise too much? in Y.A. Kravtsov and J.B. Kadtke, eds., Predictability of Complex Dynamical Systems, *Springer, New York*

Schuster, R.J. 1989 "The Colorado River Simulation System." Hydraulic Engineering, *ASCE New York, NY, M. Ports, Ed. 473-478*

Sharma, A., D.G. Tarboton, and U. Lall, 1997: Streamflow simulation: a nonparametric approach, *Water Resour. Res., 33(2), 291-308*

Sivakumar B., K-K. Phoon, S-Y. Liong and C-Y. Liaw, 1999b: Comment on "Nonlinear analysis of river flow time sequences" by A. Porporato and L. Ridolfi, *Water. Resour. Res., 35, 895–97*

Steinman B.A, M.E. Mann, S.K. Miller, 2015: Atlantic and Pacific multidecadal oscillations and North Hemisphere temperatures, *Science Vol 347 ISSUE 6225*

Switanek M.B., and P.A. Troch, 2011 : Decadal prediction of Colorado River Streamflow anomaloies using ocean-atmosphere teleconnection, *Geophysical Research Letters, 38,L23404, doi: 101029/2011GL049644*

Takens F, 1981: Detecting strange attractors in turbulence. In Dynamical Systems and Turbulence, Warwick 1980, eds. D Rand and LS Young, *Lecture Notes in Mathematics 898* (*Springer, Berlin), 366*

Thomas, B. E., 2007: Climatic fluctuations and forecasting of streamflow in the Lower Colorado River basin. *J. Amer. Water Resour. Assoc., 43, 1550–1569.*

Thomas H. A. and Fiering, M. B., 1962: Mathematical synthesis of streamflow sequences for the analysis of River Basin by simulation. *In design of water resources systems (A. Mass et al., eds.), pp 459-493, Cambridge, Massachusetts, Harvard University Press*

Thomson A. M., R.A. Brown, N.J. Rosenberg, R.C.Izaurralde, D.M. Legler and R.Srinivasan, 2003: Simulated Impacts of El Nino Southern Oscillation on United States water Resources. *J. Amer. Water Resour. Assoc.*

Timilsena, J., T. Piechota, G. Tootle, and A. Singh, 2009: Associations of interdecadal/interannual climate variability and long-term Colorado River basin streamflow. *J. Hydrology, 365,289–301, doi:10.1016/j.jhydrol.2008.11.035*

Tootle, G. A., T. C. Piechota, and A. Singh, 2005: Coupled oceanic–atmospheric variability and U.S. streamflow. *Water Resour. Res., 41, W12408, doi: 10.1029/2005WR004381.*

Torrence C. and G.P. Compo, 1998: A Practical Guide to Wavelet Analysis. *Bull. Amer. Meteor. Soc., 79, 61-78*

Towler,E., B. Rajagopalan, C. Seidel, and R. S. Summers, 2009: Simulating Ensembles of Source Water Quality Using a K-Nearest Neighbor Resampling Approach, Environ. *Sci. Technol., 43, 1407–1411*

Tsonis A. A., 1992: Chaos: From Theory to Applications, *Springer, NewYork.*

U.S. Bureau of Reclamation, 2012: Colorado River Basin Water Supply and Demand Study, *U.S. Dep. of Inter., Washington, D.C.*

United States Department of the Interior, 2001: Record of Decision Colorado River Interim Surplus Guidelines Final Environmental Impact Statement, *Bureau of Reclamation, Boulder City*

Vogel R.M., A.L.Shallcross, 1996: The moving blocks bootstrap versus parametric time series models, *WATER RESOUR. RES., VOL. 32, NO. 6, PAGES 1875–1882,*

Walker WE, Harremoes P, Rotmans J, Van de Sluis JP, Van Asselt MBA, Janssen P, Krayer von Krauss MP, 2003: Defining uncertainty, a conceptual basis for uncertainty management in model-based decision support. *Integrated Assessment 4(1):5–17*

Wagener, T., Liu, Y., Stewart, S., Hartmann, H., and Mahmoud, M. 2006. Imagine –scenario development for environmental impact assessment studies. In: Voinov,A., Jakeman, A., Rizzoli, A. (Eds.). Proceedings of the iEMSs Third BiennialMeeting: "Summit on Environmental Modelling and Software*". International Environmental Modelling and Software Society, Burlington, USA, July 2006. CD ROM. Internet: http://www.iemss.org/iemss2006/sessions/all.html*

Wei. W.W.S., 2006: Time Series Analysis, *Temple University, Addison-Wesley*

Wilks, D. S., 1995: Statistical methods in the atmospheric sciences: Chapter 8 in Wilks, D. S., Timeseries, *xi, 467 pp., Academic Press, San Diego.*

Wolf A., J.B. Swift, H. L. Swinney and J. A. Vastano, 1985: Determining Lyapunov Exponents from a Time Series, *Elsevier Science Publishers*

Woodhouse C. A., S T. Gray, and D.M. Meko, 2006: Updated streamflow reconstructions for the Upper Colorado River Basin, *Water Resour. Res., 42, W05415, doi: 10.1029/2005WR004455*

Vera, C., M. Barange, O.P. Dube, L. Goddard, D. Griggs, N. Kobysheva, E. Odada, S. Parey, J. Polovina, G. Poveda, B. Seguin, and K. Trenberth, 2010: Needs assessment for climate information on decadal time scales and longer. *Science direct, Procedia Environmental Sciences 1 (2010) 275–286, doi:10.1016/j.proenv.2010.09.017*

Vogel R.M., A.L.Shallcross, 1996: The moving blocks bootstrap versus parametric time series models, *Water Resour. Res.,. 32, NO. 6, PAGES 1875–1882*

Yates .D, S. Gangopadhyay, B.Rajagopalan, and K. Strzepek, 2003: A technique for generating regional climate scenarios using a nearest-neighbor algorithm, *Water Resour. Res., 39, NO. 7, 1199, doi: 10.1029/2002WR001769*

Yohe G., Andronova, N. Schlesinger M., 2004: Climate: to hedge or not against an uncertain climate future?, *Science, 306 (2004), pp. 416–417*

Zagona, E.A., Fulp, T.J., Shane, R., Magee, T.M. and Goranflo, H.M. 2001: "RiverWare: A Generalized Tool for Complex Reservoir System Modeling." *Journal of the American Water Resources Association, 37(4), 913-929.*

Zhang, Y., J.M. Wallace, D.S. Battisti, 1997: ENSO-like interdecadal variability: 1900-93. *J. Climate, 10, 1004-1020*

Zucchini, W, MacDonald, I.L, 2009: Hidden Markov Models for Time Series An Introduction Using R, *CRC Press.*